Dipl.-Ing. Thomas Tanzer, BSc

Noise and Loss Reduction of Power Transformers by Classification of Electrical Steel Coils

DOCTORAL THESIS

to achieve the university degree of

Doktor der technischen Wissenschaften

submitted to

Graz University of Technology

Supervisor

Prof. Dr.-Ing. Annette Muetze

Electric Drives and Machines Institute

Graz University of Technology, Austria

External Examiner

Prof. Dr. Andy Knight

Department of Electrical and Computer Engineering

University of Calgary, Canada

Graz, August 2018

Keywords

Core noise, grain-oriented electrical steel, magnetostriction strain, magnetostrictive properties, measurement system, model transformers, piezoelectric acceleration transducers, power transformers, specific losses, steel coils, no-load losses, no-load noise, vibration velocity.

Contents

Contents

Affidavit

I declare that I have authored this thesis independently, that I have not used other than the declared sources/resources, and that I have explicitly indicated all material which has been quoted either literally or by content from the sources used. The text document uploaded to TUGRAZonline is identical to the present doctoral thesis.

_____   _____

             Date   Signature

Abstract

This work presents a new method for measuring the magnetostriction and specific losses of grain-oriented electrical steel (GOES) coils of up to 6,000 kg. Since power transformer (PT) core manufacturers are mainly supplied with complete rolled steel coils, a fast incoming goods inspection is desirable. The proposed method identifies the specific losses of the entire steel coil, as delivered. In addition, the measurement of magnetostriction of the coiled material, which allows the main property for PT no-load noise to be classified. The structure and setup of the developed coil measurement system (CMS) is shown, the measurement technique and necessary requirements are explained. Exemplary results of specific power losses and magnetostriction of steel coils are provided, and the reproducibility of the results is shown.

The main source of a PT's no-load noise is the magnetostrictive vibration of the magnetic core, which is built with stacked GOES sheets. The CMS allows differences in the GOES materials' magnetostriction to be identified. Based on these differences in the steel coils' magnetostriction, two studies with model transformers (MTs) and PTs are provided, showing initial findings of the relationship between the steel coils' magnetostriction and no-load noise. Both studies comprise a correlation and performance analyses. In addition, the GOES certificate B8 value, which is a predictor for noise, is compared to the steel coils' magnetostriction, and a relationship to the no-load noise of PTs is shown.

Two additional studies investigate the relationship between the experimentally determined specific power losses of steel coils and the no-load losses of transformers. First, MT cores are built from a single steel coil, whereby each steel coil has different specific losses. The relation of the MTs' no-load losses is then investigated by comparison of experimentally determined specific losses by the CMS, single sheet measurements, and the steel coils certificate values. A second study extends the investigations to PTs. Therein, the relation between the no-load losses of each of the four PT units and the steel coils' specific losses is studied.

Zusammenfassung

In dieser Arbeit wird eine neue Messmethode vorgestellt, mit der die Magneto-striktion und die spezifischen Verluste von ganzen Stahl-Coils aus kornorientiertem Elektroblech, mit einem Gewicht von bis zu 6,000 kg, bestimmt werden können. Hersteller von Transformatorkernen werden hauptsächlich mit ganzen Stahl-Coils beliefert. Daher ist es notwendig, eine schnelle Wareneingangskontrolle der angelieferten Stahl-Coils durchzuführen. Mit Hilfe der vorgestellten Messmethode werden die spezifischen Verluste von ganzen Stahl-Coils bestimmt. Zusätzlich wird die Magnetostriktion an aufgewickeltem Stahl-Band gemessen, um eine Klassifizierung in Bezug auf das Leerlaufgeräusch von Transformatoren durchführen zu können. Die Struktur und der Aufbau des Coil Messsystems (CMS) werden erklärt, wobei ebenso auf die Messtechnik und notwendige Anforderungen eingegangen wird. Exemplarische Ergebnisse der gemessenen spezifischen Verluste und der Magnetostriktion sowie deren Reproduzierbarkeit werden dargestellt.

Das Leerlaufgeräusch von Leistungstransformatoren kann auf die magnetostrikti-ve Vibration des Transformatorkerns zurückgeführt werden. Mit dem oben beschriebenen Messsystem wurden Unterschiede in den magnetostriktiven Eigenschaften einzelner Stahl-Coils festgestellt. Basierend auf diesen Unterschieden werden Untersuchungen mit Modell- und Leistungstransformatoren präsentiert, die erste Ergebnisse des Zusammenhangs zwischen der Magnetostriktion von Stahl-Coils und dem Leerlaufgeräusch von Transformatoren aufzeigen. Zusätzlich beinhalten die Untersuchungen eine Analyse des geräuschrelevante Zertifikatwerts B8 von jedem Stahl-Coil.

Der Zusammenhang zwischen den experimentell bestimmten spezifischen Verlusten von Stahl-Coils und den Leerlaufverlusten von Modell- und Leistungstransformatoren wird in zwei weiteren Studien ermittelt. Dabei wird vor allem auf die Vorhersagekraft der Verlustwerte von Stahl-Coils, Single Sheet Messungen und dem Zertifikatswert in Bezug auf die Leerlaufverluste eingegangen.

Acknowledgements

First, I express my gratitude to Prof. Annette Muetze, head of the Electric Drives and Machines Institute at Graz University of Technology, Austria, for supervising and supporting this work. Her initiatives and professional expertise improved my work, and her enthusiasm helped to advance and complete this thesis.

I would like to thank Mr. Helmut Pregartner, Head of Noise and Mechanics R&D at Siemens AG, Transformers Weiz, for all I have learned from him and for his continuous help and support. His dedication and expertise have made a very valuable contribution to this work. I also want to thank Mr. Justin Case, Mr. Robert Labinsky, Mr. Markus Riedenbauer, and Mr. Michael Witlatschil for their fruitfull conversations and support.

My sincere thanks also go to Mr. Martin Stoessl, Mr. Gerald Leber, and again to Mr. Helmut Pregartner who have given me the opportunity to conduct this research and who made this thesis possible.

I would also like to thank my family and my loving, encouraging, and patient wife Eva, who always believed in me.

Chapter 1

Overview

1.1 Motivation

PTs are strategically important elements in the power grid. They are designed to transfer and distribute electrical energy within a single power grid or between different power grids in an effective and reliable way. Due to rising energy consumption levels, the energy supply networks are becoming even more expanded. Legislative regulations from governments along with increasing demands from substation holders force PT manufacturers to improve their products in order to meet the growing demands related to noise emissions and energy efficiency.

The core is the critical element in the overall design of a PT. The nominal flux density in the core and the selected core material determine the size of the transformer core. In turn, the size of the core determines the overall size of a PT, which influences the total manufacturing costs of a unit. The selected core material affects both the noise emission and the losses of a PT in no-load condition. Low noise and low losses of a PT in no-load condition are a significant concern of utility operators, as they are present even if no energy is transferred. Therefore, the design of PT cores is given great importance. In general, GOES is used as core material, with PT manufacturers being supplied with steel coils up to several tons from various core steel manufacturers. Out of such steel coils single steel sheets are cut and used to stack the transformer core.

The specific losses of GOES can be determined with internationally known and standardized measurements methods like the Epstein frame or single sheet tester. These methods were initially also used to measure magnetostrictive properties of GOES sheets which are known to have a strong relation to the no-load noise of PTs. Nevertheless, commonly employed standards require only the declaration

of the specific losses of GOES material at a specified flux density and excitation frequency. Core steel manufacturers provide the specific losses of each single steel coil as a certificate value. However, no values are available which describe the magnetostrictive performance of the GOES material. Therefore, PT manufacturers have to rely on empirical values from tested PTs in the test laboratory, to predict the no-load noise performance of the deployed GOES.

This work closes the omission in past literature by presenting and applying a patented measurement method were both the specific losses and the magnetostrictive properties of entire steel coils with a mass of up to several tons can be determined. Thereby, a new possibility is presented on how magnetostriction of such large coils can be measured. The determined GOES materials' properties are analyzed and their relationship to the no-load characteristic of transformers is investigated.

1.2 Objectives and Scope of Work

The main goal of this work is to classify core material regarding its no-load noise characteristics and specific losses, based on the measured magnetostrictive and magnetic properties of entire steel coils. The extensive knowledge of the core material is an opportunity to optimize the design of PTs and it is a significant chance to address future requirements regarding low noise emission and efficient energy transmission.

It is assumed that the performance of the no-load noise is mainly affected by the magnetostriction of each utilized steel coil. Therefore, one goal is to provide a representative magnetostriction value for all steel coils that are used within an PT core, based on the measured magnetostriction values of each single steel coil. In contrast to similar work reported in [1], this research shows a novel approach in the determination of the magnetostriction strain perpendicular to the rolling direction of GOES material of large test specimen. This work extends earlier results on the flux-dependency and harmonic composition of magnetostrictive properties, as presented in [2–5]. Furthermore, this work closes the omission in past literature by presenting the relation between the measured magnetostriction of steel coils and the core noise of oil-immersed transformers.

In addition, the specific losses of entire steel coils are determined in a quick incoming goods inspection. Thereby, this work expands upon the many works employing small sample sizes and using single sheet or Epstein frame measurements by instead performing measurements on very large specimens. Using the results

obtained during the incoming goods inspection the relationship between the steel coils' specific losses and the no-load losses of PTs is discussed.

1.3 Related Publications

The work presented in this thesis has resulted in the following journal and conference publications. The journal publications are extended versions of the conference publications.

Journal Publications

T. Tanzer, H. Pregartner, A. Muetze, and K. Krischan, "Experimental determination of specific power losses and magnetostriction strain of grain-oriented electrical steel coils," IEEE Transactions on Industry Applications, vol. 54, pp. 1235-1244, 2018.

T. Tanzer, H. Pregartner, M. Riedenbauer, R. Labinsky, M. Witlatschil, A. Muetze, and K. Krischan, "Magnetostriction of electrical steel and its relation to the no-load noise of power transformers," IEEE Transactions on Industry Applications - Accepted for publication, 2018.

Conference Publications

T. Tanzer, H. Pregartner, A. Muetze, and K. Krischan, "Experimental determination of specific power losses and magnetostriction of electrical steel coils," IEEE International Conference on Electrical Machines (ICEM), pp. 2230-2236, 2016.

T. Tanzer, H. Pregartner, R. Labinsky, M. Witlatschil, A. Muetze, and K. Krischan, "Magnetostriction and its relation to the no-load noise of power transformers," IEEE International Electric Machines and Drives Conference (IEMDC), pp. 1-6, 2017.

T. Tanzer, H. Pregartner, M. Riedenbauer, R. Labinsky, M. Witlatschil, A. Muetze, and K. Krischan, "Magnetic properties and their relation to the no-load noise and no- load losses of large power transformers," IEEE International Electric Machines and Drives Conference (IEMDC), pp. 1-6, 2017.

1.4 Structure of Thesis

The thesis is organized as follows: Chapter 2 gives an introduction to the rising demands on transformers and on the importance of the deployed core materials' magnetic properties to meet future requirements. In addition, the chapter presents a new patented measurement method that enables the determination of the magnetic properties of entire steel coils with a mass of up to 6,000 kg.

Chapters 3 and 4 provide the theoretical background of PTs including their design and the material utilized in PT cores. Chapter 4 presents the properties and development of ferromagnetic material within a PT core. The fundamental background on the losses of ferromagnetic material and how they can be measured with standardized measurement methods is presented in Chapter 5. The magnetostriction of ferromagnetic materials, their properties, and different measurement approaches are described in Chapter 6. Chapter 7 gives an overview of a transformer's noise sources and how the emitted noise of each source can be measured. Therein, the acoustic quantities are described and common measurement methods are presented. Chapter 8 discusses the losses produced by a PT. Subsequently, the difference between the specific losses of PTs and single sheet specimen, described by the building factor, is demonstrated.

The first part of Chapter 9 provides a literature study on the prediction of the no-load noise by measuring the core steels' magnetostriction. The second and third part present preliminary studies of measuring the magnetostriction on steel coils perpendicular to the rolling direction and the loss deviation within a steel coil.

Chapter 10 presents the specific requirements for the realization of the CMS. Additionally, the influence of a test specimen's properties on the measured specific power losses are discussed. Subsequently, the implementation of the CMS as well as selected experimental results are provided. The chapter closes with a classification of selected steel coils with the same material grade, classified by their specific losses and magnetostriction strain determined by the CMS.

Chapter 11 begins by analyzing the magnetostriction of steel coils, including their harmonic composition. Subsequently, the chapter shows an experimental study on MTs in which two steel coils were used to build eight MTs. This chapter extends the investigations with a study on PTs in which the PT cores were built out of several steel coils with different magnetostrictive properties. In addition, the chapter provides information on the design of the PT core and close with a correlation and performance

analysis of the no-load noise of the PTs and the magnetostriction of the deployed steel coils.

Chapter 12 analyses the relation between the specific losses of steel coils and no-load losses of transformers. This notably includes a comparison to the steel coils' certificate values and results obtained by single sheet tests. Sections 12.1 and 12.2 within Chapter 12 provide information on the electric circuit for energizing the transformers and close with a correlation analysis of the no-load losses of the transformers and the specific losses of the deployed steel coils.

Chapter 2

Introduction

2.1 Demands on Power Transformers

In recent decades, a general increase in noise levels has been observed in inhabited areas. These higher noise levels can be mainly attributed to the growth of the population and urbanization [6]. Overall noise pollution has already led governments to change legislation and to introduce noise limits. Likewise, the European Parliament has started to set up corresponding policies, as, for example, the European Directive 2002/49/EC [7].

These amendments to legislation also concern operators of PT substations as well as PT manufacturers. Areas with a high population density expand and move in closer proximity to PT substations. Substation holders must guarantee certain sound pressure levels on the substation borders, independent of the number of operated PTs and their excitation. For this reason, transformer manufacturers are increasingly confronted with demanding customer specifications for low noise PTs. These requirements are specifically related to the no-load noise of PTs as the latter is independent of the PT's load current and hence present day and night.

In addition, the efficiency of the energy transmission and the reduction of the operating costs are significant concerns for PT operators'. This importance is apparent in contracts between transformer manufacturers and customers as they usually include penalty costs if the no-load losses of a PT measured in the test laboratory exceed the customer's specification. Therefore, substation holders have a high interest in low no-load noise and low loss PTs.

2.2 Electrical Steel: Magnetic Properties and Their Measurement

Both, the no-load noise and no-load losses of a PT are principally determined by the magnetic properties of the grain-oriented electrical steel (GOES) used for manufacturing the PT core. In general, single GOES sheets are cut out of entire steel coils with a mass of up to 6,000 kg in slitting processes, where the steel coil is automatically rewound. The single slitted sheets are then stacked to a magnetic core.

Magnetostriction is known as the main source of a PT's no-load noise, also known as core noise. Various core steel suppliers have developed techniques which lead to individual magnetostrictive properties of the GOES, as it is recognized within this work. The IEC report [1] describes the possibilities for determining magnetostrictive properties of electrical steels with a single sheet tester and Epstein frame. However, preparing single sheet samples with the dimension of 500 mm x 500 mm out of large steel coils is time consuming and not practicable for transformer manufacturers. In addition, magnetostriction results of such small samples only represent random tests of the material.

The no-load losses are mainly determined by the specific losses of the GOES material. Core steel manufacturers use different manufacturing processes to provide several steel grades with different magnetic properties and geometric dimensions. Although several steel coils are used in manufacturing PT cores, Epstein frame and single sheet tester are the most common methods for the determination of the magnetic properties, and hence provide the basis for the design of PTs. Sample sizes as described in [8, 9] are small compared to steel coils of up to 6,000 kg.

Several standards describe how the magnetic properties of electrical steel sheets determined. IEC 62044-3 [10] provides a standard for determining the magnetic properties of a complete core composed of soft-magnetic materials. IEC 60404-2 [8] and IEC 60404-3 [9] are mainly used for quality verification and incoming goods inspection, whereas the primary focus of [10] is on partly finished products in a certain manufacturing step. Similar to the method described within this research, IEC 60404-4 [11] describes the determination of specific losses of a laminated ring test specimen, but under DC excitation.

Steel Coils' Certificate Values

Currently, core steel suppliers mark steel coils either with the description 'standard' or 'low-noise.' This allows only a rough selection of the material. In [12] the B8 value, also known as B800 value, is mentioned as a possible noise indicator. The B8 value is a certificate value and expresses the flux density value at a magnetic field strength of 800 A/m. Materials with increasing B8 values tend to have lower magnetostriction. Nevertheless, PT manufacturers have no detailed information on the magnetostrictive properties of the GOES at different flux densities as to select single steel coils for specific noise requirements of PTs. In addition, a steel coil's certificate also contains information about the specific losses. This value represents the magnetic losses of the material at a flux density of 1.7 T and a excitation frequency of 50 Hz. In-house investigations have shown that each core steel supplier has his own strategy how to determine the specific losses of a steel coil; thereby, the well known Epstein frame, single sheet tester or even inline measurement systems are used. With an inline measurement system the specific losses along the complete steel coil length are determined at a defined flux density and excitation frequency while the steel coil is rewound.

New Measurement System

The need for a fast determination of the magnetic properties of an entire steel coil and of better knowledge of deployed core material's magnetic and magnetostrictive characteristics led to the development of a coil measurement system (CMS) [13] based on the patent [14]. The developed CMS allows the determination of the specific losses and the magnetostriction of a steel coil up to 6,000 kg. Hereafter, this method is referred to as the Coil-Method.

Continuous measurements of steel coils' magnetostriction values have revealed that the magnetostrictive properties of different steel coils vary within the same steel grade [15, 16]. Consequently, knowledge of the noise behavior of the deployed GOES in PT cores plays an important role in the development of competitive low noise transformers.

This work presents how magnetostriction can be measured on entire steel coils and how it can be used to classify the material. With the novel coil measurement system, the flux dependent magnetostrictive properties of each delivered steel coil can be determined. Drawing from the experimental results determined with the CMS, this

work extends earlier results on the flux-dependency and harmonic composition of magnetostrictive properties, as presented in [2–5]. This work contributes to better understanding of the relationship between the measured magnetostriction of GOES and the core noise of oil-immersed PTs. In addition, this work presents how the specific losses of entire steel coils can be measured and how these results can be used to classify the material, for very large sample sizes.

2.3 Coil-Method

The patented Coil-Method [14] follows similar principles to those described in the standards [8–11]. Uniformly distributed turns of the primary winding around the circumference of a test specimen act as a magnetizing winding. A secondary winding with one turn acts as a measurement winding. The current and voltage of the primary winding and the voltage induced in the secondary winding are measured. Contrary to [8,9] but similar to [10,11], the test specimen's mass, which may be up to 6,000 kg, requires comparatively high excitation power. In addition, a measurement system measures the magnetostriction strain perpendicular to the rolling direction, also referred to as transverse direction (Fig. 2.1), of the coiled electrical steel at different flux densities.
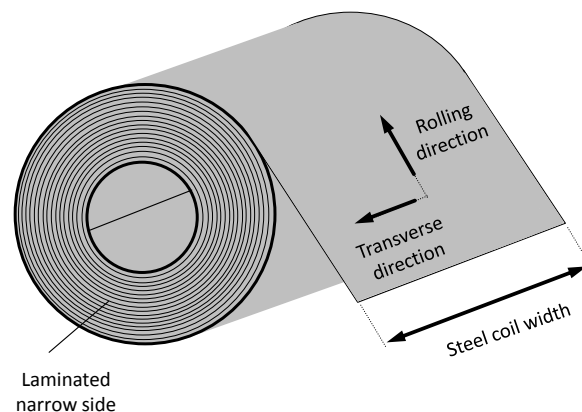
Figure 2.1: Rolling direction and transverse direction of a grain-oriented electrical steel coil.

The test specimen's mass and outer diameter are determined with two different systems; the width and the inner diameter of the steel coil are determined manually,

as described in detail in Section 10.3.6 (p. 59).

Figure 2.2 shows a block diagram of the CMS with the system's main components. This approach was realized as a CMS for entire steel coils.
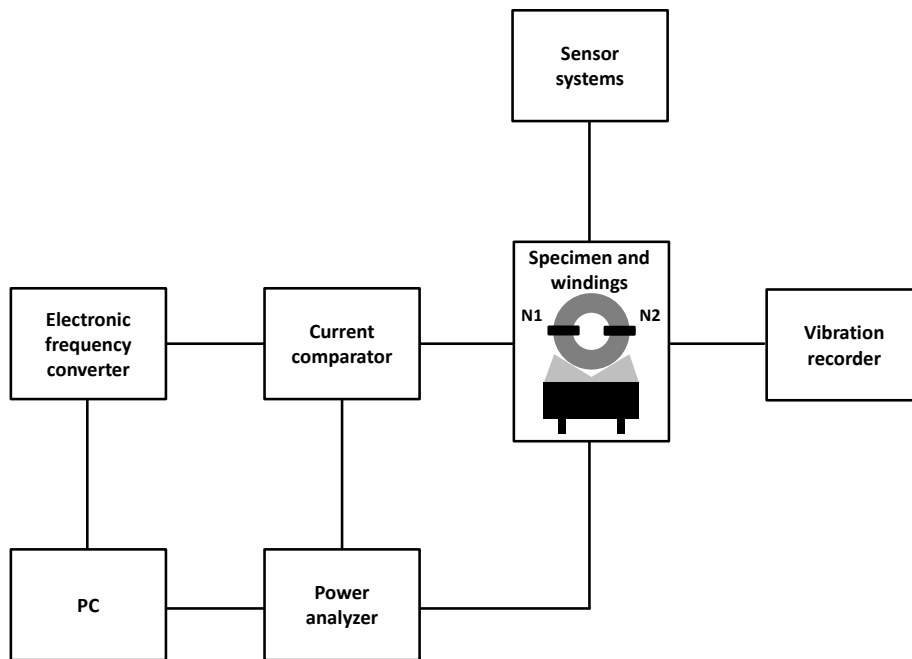
Figure 2.2: Block diagram of the CMS.

Chapter 3

Power Transformer

In the power grid transformers are important node points where electrical energy is transferred and distributed between different voltage systems in the same power grid or even between different power grids across countries. Thereby, highly efficient PTs are required to ensure low losses in the energy transmission between power plants and consumers. The most essential components of a PT, depicted in Fig. 3.1, are:
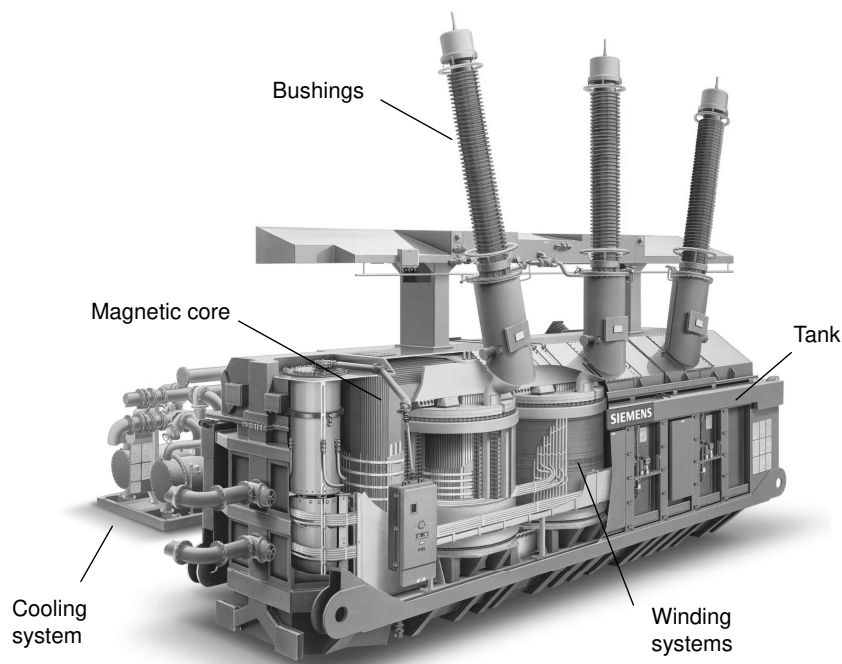
Figure 3.1: Illustration of an oil-immersed PT [17].

- The active part containing the winding systems and magnetic core,

- the isolation oil,

- bushings for the connection to the power grid designed for the low, medium, and high voltage system, and

- the tank and oil conservator.

The cooling system of a PT can be either mounted on the transformer tank or separated as an independent unit connected with pipes to the transformer tank. Oil-immersed PTs use mineral oil or esther oil as cooling medium. The oil circulates through the transformer's active part into the external radiators of the cooling system in which the generated heat is dissipated. Depending on the necessary heat rejection the cooling system can contain pumps and/or fans for forced oil and/or air cooling.

3.1 Power Transformer Core

The magnetic iron core is one element of the transformer's active part. The magnetic core conducts the magnetic flux between the winding systems. In general, the deployed core material determines the no-load characteristics of a transformer. The main no-load characteristics can be divided into (1) the no-load noise also designated as core noise, and (2) the no-load losses also known as core losses, summarizing from [18].

The transformer core is laminated and consists of a variety of single steel sheets. These single steel sheets are cut out of steel coils with a mass of up to several tons. Therefore, the heavy steel coils are automatically rewound in manufacturing lines where the steel band is slit, split and punched. With these processes, single core sheets with different geometries are obtained.

The single steel sheets are stacked together and form the laminated magnetic core. According to the state of the art, the step-lap technology with six steps is applied as stacking technology for the joints of the magnetic core. The vertical sections of the transformer core are the limbs (Fig. 3.2). The concentric windings are placed around the limbs except if the limb is used as an additional flux return limb. The horizontal
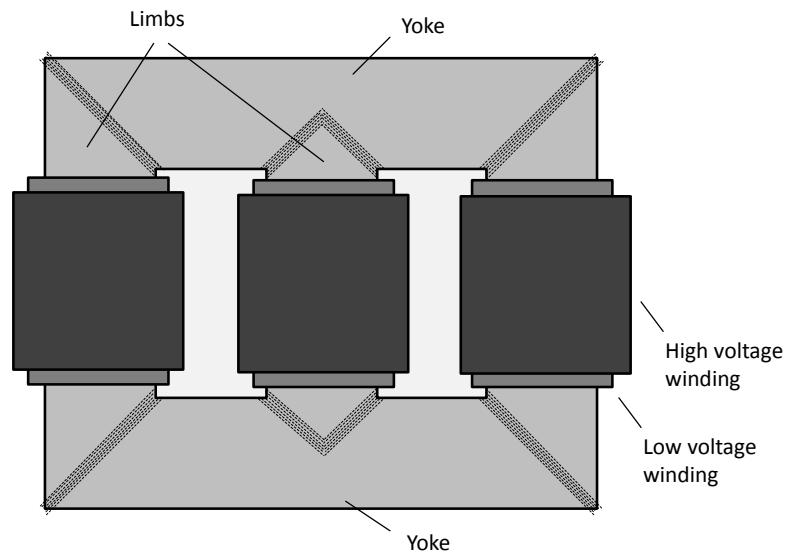
Figure 3.2: Illustration of a power transformer core with three limbs including concentrically wound low and high voltage windings.

sections at the top and bottom of the magnetic core are the lower and upper yoke to close the low reluctance path for the magnetic flux. A clamping frame is usually applied on the upper and lower yoke to support the stabilization of the stacked core.

3.2 Core Types

Generally, transformer cores can be categorized into one-phase (Fig. 3.3) and three-phase core designs (Fig. 3.4). In this work both, one-phase and three-phase transformers, are treated within the presented experimental studies.

The limbs of the transformer core are concentrically surrounded by the winding systems. Due to transport limitations the height of PTs can be restricted. Therefore, a core design with two additional flux-return limbs (Figs. 3.3 (a), (c) and 3.4 (b)) can be used where the cross-section of the upper and lower yoke may be reduced down to 50 %.
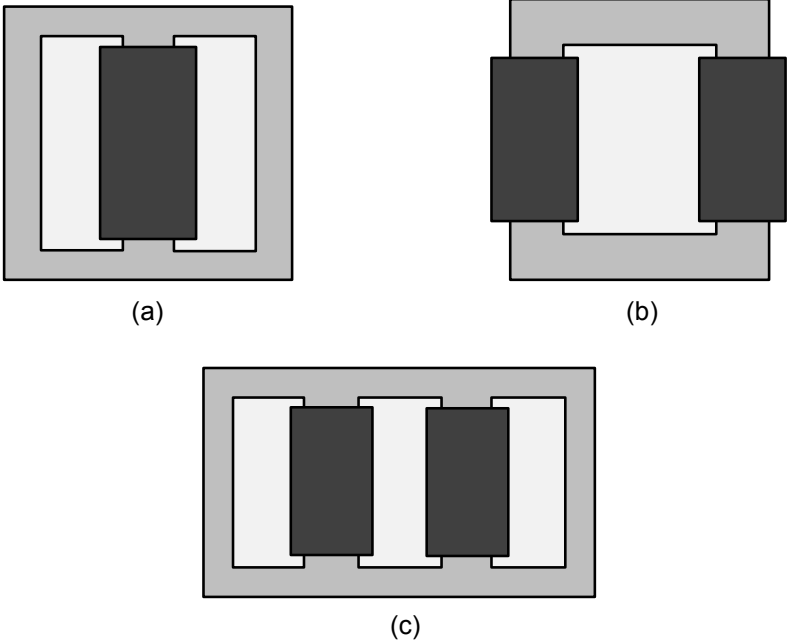
Figure 3.3: One phase transformer cores (a), (b), and (c) with schematically illustrated windings.
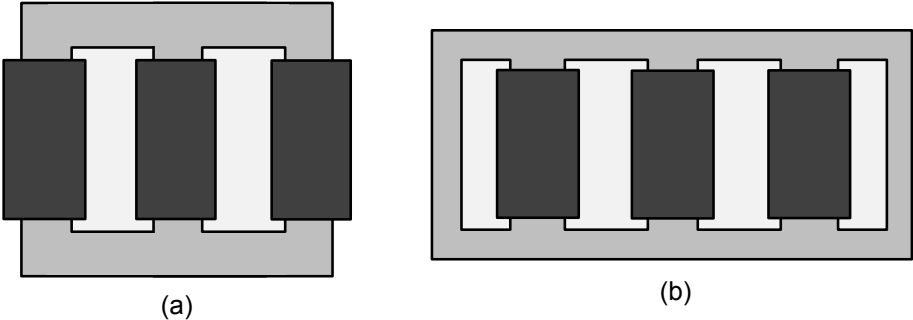
Figure 3.4: Three phase transformer cores (a) and (b) with schematically illustrated windings.

Chapter 4

Core Material

The transformer core leads the magnetic flux on a low-reluctance path to link the low and high voltage winding systems magnetically [19]. Grain-oriented electrical steel is used as core steel material which is a ferromagnetic alloy with approximately 3 % silicon. This chapter presents an overview of the ferromagnetic materials' properties, the development of electrical steel, and currently available steel grades.

4.1 Ferromagnetic Materials

Summarizing from [20, 21], ferromagnetic materials consist of a crystalline structure that can be described as a cubic-lattice (Fig. 4.1). In general, the body-cubic centered iron crystals have anisotropic magnetic properties. Iron crystals show the easiest direction of magnetization along the cube edge, described as [100] axis. Along the cube face diagonal, described as [110] axis, the magnetization is more difficult. The most difficult direction of magnetization is the cube volume diagonal axis [111].

Below the Curie temperature, magnetic materials consist of a variety of spontaneous magnetized elementary areas. These small regions with a different direction of magnetization are randomly distributed so that, viewed from the outside, the magnetic material has a non-magnetized state. Each of the elementary areas consists of several atoms whose magnetic moments, caused by the rotation of the atoms electrons, are aligned in parallel. These elementary areas are denoted as magnetic domains, illustrated in Fig. 4.2, paraphrasing from [21].

According to [20], the domain walls represent the boundaries between the magnetic domains of different magnetization where the direction of magnetization changes gradually the direction.
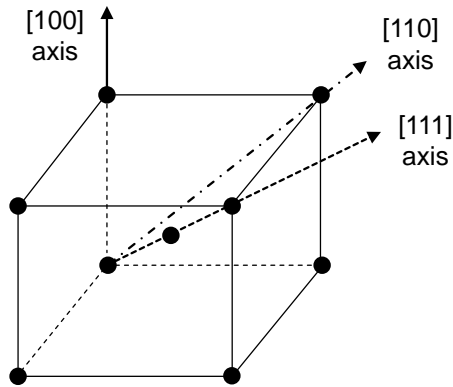
Figure 4.1: Directions of magnetization displayed on a body cubic iron crystal. [100] easy direction of magnetization, [110] medium direction of magnetization, and [111] hard direction of magnetization, based on [20].
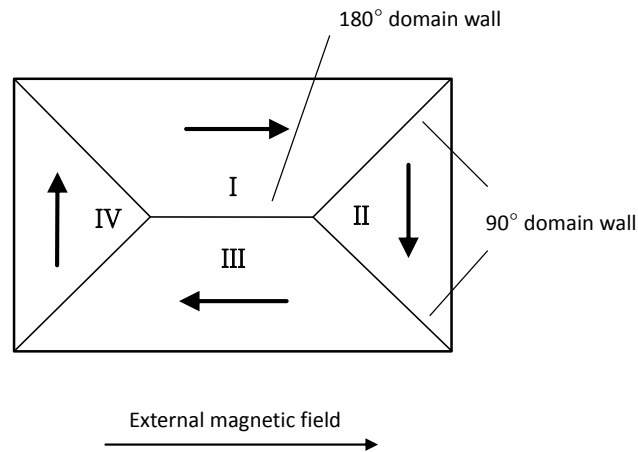
Figure 4.2: Magnetic domains with different direction of magnetization zoned by domain walls, based on [21].

The following paragraph outlines fundamental knowledge of domain walls as found in [21]. In general, domain walls are separated into 90° and 180° in reference to the direction of the external applied magnetic field as shown in Fig. 4.2. The 90°domain walls are the boundaries of the domains II and IV. The illustrated 180° domain wall is situated between domains I and III. Due to a applied magnetic field the domain walls are forced to move. An alternating magnetic field forces the domain walls to move with the magnetic fields frequency. Therefore, the mobility of the domain walls is an important property of ferromagnetic materials.

According to [22], the mobility of the domain walls correlates with the specific losses of the material.

4.2 Development of Electrical Steel

The performance of electrical steel improved in the last 100 years, as described in [20], due to (a) the addition of silicon (Si) in 1900, (b) the introduction of the Goss texture in 1934, and (c) the development of high permeability electrical steel (HiB) in 1974.

The following paragraph has been summarized as found in [21]. Depending on the amount of Si in the alloy the losses of the material change. In fact, the larger the silicon contents in the alloy, the lower the losses. With the introduction of the Goss texture a better orientation of the material grains was achieved. Due to a suitable combination of rolling and annealing steps the direction [100] in which the crystals of the material can be easily magnetized are aligned to the rolling direction and the (110) planes of the crystals are parallel to the surface of the electrical steel sheet (Fig.4.3). This grain texture leads to anisotropic magnetic properties in the material. In rolling direction the material, designated as conventional grain-oriented (CGO) material, achieves the highest permeability and lowest hysteresis losses. The mostly hot-rolled electrical steel was replaced by cold-rolled electrical steel after 1935 as cold-rolled electrical steel has a better uniformity, dimensional stability, and includes a smooth surface. These advantages allow a more compact stacking of single core sheets in the PT core.

The grain orientation of CGO material is not completely aligned in rolling direction but with a tilt angle of about 6° [20].

Paraphrasing from [19], in 1965 the manufacturing process of the CGO material was improved by a reduction of one cold rolling step and the use of aluminium
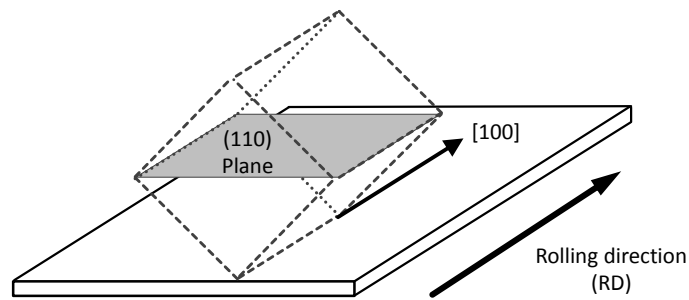
Figure 4.3: Goss texture - The crystals are aligned with their (110) plane parallel to the steel sheet and the crystals edge [100] is aligned in rolling direction, based on [20].

nitride as grain growth inhibitor. The resulted material has a more perfect grain orientation, compared to the CGO material, with a tilt angle of only 2-3°.

The developed highly grain-oriented material has a three times higher permeability above 1.7 T than the CGO material. Therefore, it is also designated as high-permeability (HiB) material. For low polarizations, HiB material can have even a worse permeability compared to CGO material, reviewing from [20].

In addition, a stress coating is applied to the HiB material leading to reduced magnetostriction due to the applied tensile stress by the coating, as discussed in [23, 24]. The typical coating with a thickness of $4\,\mu$m on both sides consists of a forsterite (Mg2SiO4) layer and a top layer out of aluminium orthophosphate [25].

In the production of HiB material additional domain refinement tools, such as laser scribing, chemical treatment, plasma jet irradiation or spark ablation are applied to reduce the domain wall spacing and hence reduce the materials' losses [20].

4.3 Steel Grades

The international IEC standard 60404-8-7 defines the latter described material classes CGO and HiB containing different nominal sheet thicknesses of 0.23 mm, 0.27 mm, 0.30 mm, and 0.35 mm. The standard contains general requirements on the material as for example the magnetic properties, the geometric characteristics, production tolerances, and inspection procedures. The designation of a steel grade's name depends on the specific total losses determined at a flux density of 1.7 T and an excitation frequency of 50 Hz. In addition, the thickness of the material and material

class are part of a steel grade's name, as described in [26]. For example, the designation M85-23P depicts the following information: the capital M displays the general affiliation to electrical steel; the specific total loss are 0.85 W/kg at 1.7 T and 50 Hz; the sheets thickness is 0.23 mm, and the capital letter P identifies the material class HiB.

Chapter 5

Losses of Ferromagnetic Materials

This chapter summarizes the most important basics of the losses of ferromagnetic materials, with primary reference to contents from textbooks such as [21,27]. Specifically the iron loss modelling is a content of many research activities which however is not the goal of this work. Rather, well-known standardized measurement methods are presented which are used to determine the losses of ferromagnetic materials.

5.1 Iron Losses

During each magnetization cycle in ferromagnetic materials a certain amount of electromagnetic energy is dissipated in the material as heat. The dissipated energy density per magnetization cycle and per volume unit

$$w_{\text{fe}} = \oint H dB \tag{5.1}$$

in mWs/m^3 is proportional to the area of the hysteresis loop. The specific iron losses of the material, often only referred to as specific losses, with the unit W/kg

$$P_{\text{fe}} = \frac{w_{\text{fe}} \cdot f}{\rho_{\text{fe}}} \tag{5.2}$$

can be calculated by the multiplication of the magnetization cycles per second (frequency) related to the material's density ρ_{fe}, summarizing from [27].

In every dynamic case, depending on the excitation frequency the iron losses

$$P_{\text{fe}} = P_{\text{h}} + P_{\text{w}} \tag{5.3}$$

consist of two main parts, the hysteresis losses P_{h} and the eddy current losses P_{w} [21].

5.2 Hysteresis Losses

In the static case, when the excitation frequency is close to zero, the area of the hysteresis loop is proportional to the hysteresis losses (Fig. 5.1) which is one part of the dissipated energy. In the dynamic case the width of the hysteresis loop rises due to additional losses caused by eddy currents [28].

The hysteresis losses

$$P_{\text{h}} = \frac{A_{\text{stat}} \cdot f}{\rho_{\text{fe}}} \tag{5.4}$$

can be calculated for a dynamic case with the excitation frequency and the area of the static hysteresis loop A_{stat} [29].
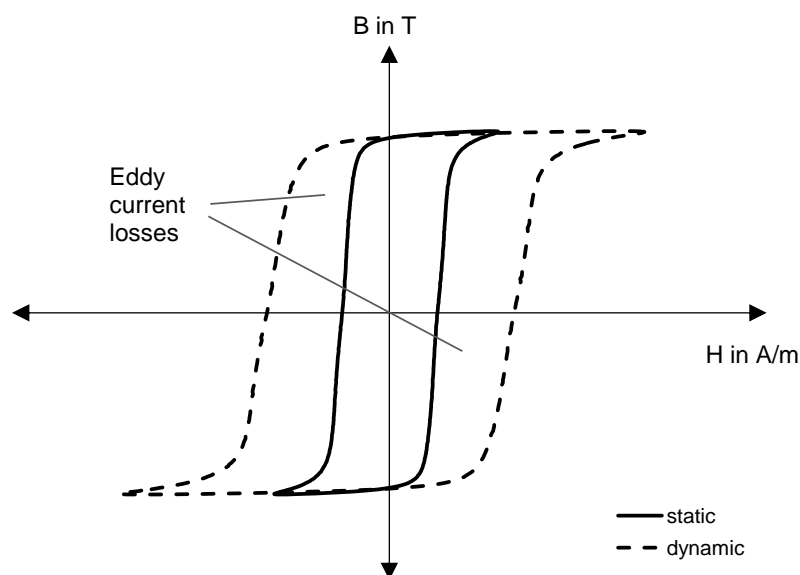
Figure 5.1: Schematic illustration of the static hysteresis loop ($f \to 0$) and dynamic hysteresis loop ($f > 0$), based on [28].

5.3 Eddy Current Losses

When ferromagnetic materials are exposed to alternating magnetic fields, voltages are induced in the material according to Faraday's law of induction. The induced
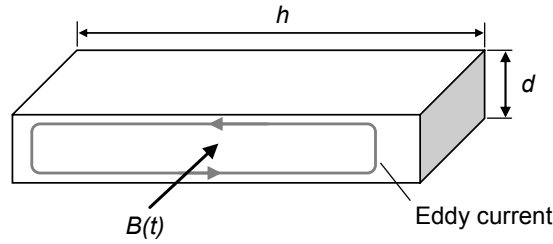
Figure 5.2: Induced eddy current in a electrical steel sheet with the thickness d and width h, adapted from [30].

voltage causes the flow of eddy currents in the ferromagnetic resistance paths and create additional thermal losses.

In general, the thermal loss

$$P_w = \frac{1}{T} \int_t^{t+T} \frac{\sigma \cdot d^2 \cdot V}{12} \left(\frac{dB}{dt}\right)^2 dt \tag{5.5}$$

caused by eddy currents can be calculated for any time dependent flux density with the thickness d of the electrical steel sheet, the specific conductivity of the material σ, and the material's volume V [29].

Based on the assumptions

- the shape of the magnetic flux is sinusoidal,

- homogeneously distributed in the steel sheet, and

- the steel sheets width h is larger than the sheets thickness d

summarized in [30], the eddy current losses can be calculated with

$$P_w \simeq \frac{1}{24} \cdot \omega^2 \cdot d^2 \cdot B^2 \cdot V \cdot \sigma. \tag{5.6}$$

5.4 Additional Losses

Summarizing from [21], comparisons between calculations and measurements revealed that an additional loss part contributes to the iron losses apart from the hysteresis losses and eddy current losses. The previous considerations assume a homogeneous distribution of the magnetization. In reality inhomogeneous distributions occur in electrical steel sheets. The movements of the domain walls change

the local magnetisation and hence lead to additional eddy currents in the area where the domain walls move. Therefore, the additional loss part is called the anomalous losses or anomalous eddy current losses. Compared to the classical eddy current losses the anomalous losses are independent of the steel sheets thickness but strongly dependent on the grain size.

Several approaches, as shown in [29], have been investigated to describe the anomalous eddy current losses. However, these additional losses are not discussed further in this work.

5.5 Measurement Methods

The most common methods to determine the specific losses of electrical steel are the standardized Epstein frame [8] and single sheet tester [9]. The standards IEC 60404-2 and IEC 60404-3 describe for the Epstein frame and single sheet tester the preparation of the test specimen, the measurement system specifications, and setup.

Within the Epstein frame (Fig. 5.3) several steel strips are stacked with a simple overlap technique (double-lapped joints) to a square magnetic frame that provides a closed path for the magnetic flux similar to a transformer core. The steel strip's geometry is defined within the standard by a width of $b = 30\,\text{mm} \pm 0.2\,\text{mm}$ and a length from $280\,\text{mm}$ up to $320\,\text{mm}$. Consequently, during a measurement, the specific losses of the stacked steel strips are determined.

Within a single sheet tester (Fig. 5.4) only one steel plate is used as specimen under test. The magnetic path is closed by placing a magnetic yoke on the test specimen. The specimen's geometry is defined by a minimum width of $60\,\%$ referencing the yoke's width and a minimum length of $500\,\text{mm}$.

The power supply within both measurement methods requires a stable voltage and frequency. It is required to induce voltages with a sinusoidal waveform with the form factor of $1.111 \pm 1\,\%$. This is a necessary requirement to achieve comparable and reproducible measurement results.
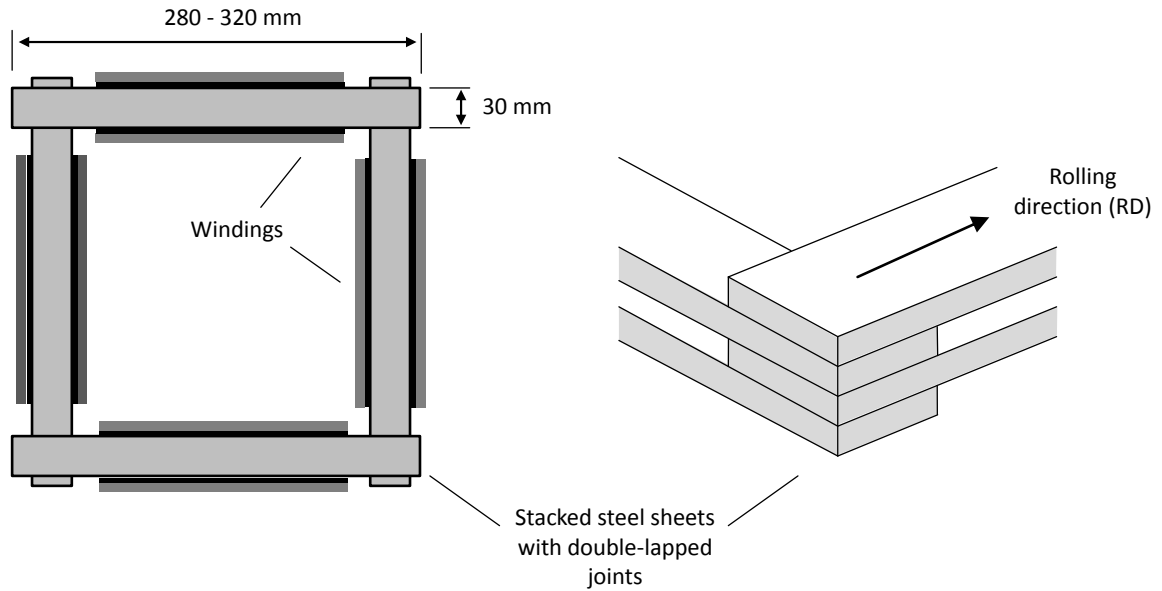
Figure 5.3: Illustration of the Epstein frame and the corner area with doubly-lapped joints, based on [8].
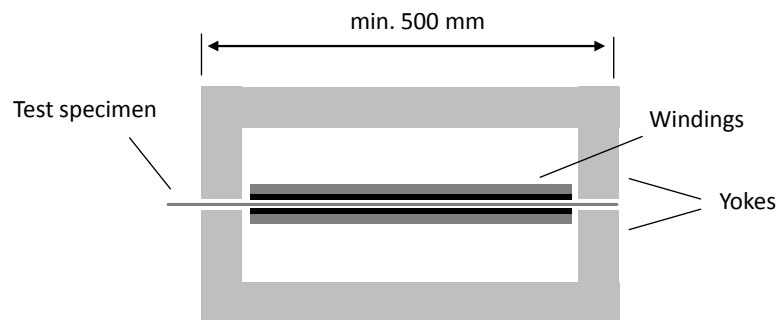
Figure 5.4: Single sheet tester with upper and lower yoke, based on [9].

Chapter 6

Magnetostriction of Ferromagnetic Materials

This chapter describes the basics to understand the origin of ferromagnetic materials' magnetostriction, and how it can be measured. The fundamentals of magnetostriction were mainly obtained from textbooks, such as [20, 21, 27]. Since this work presents a new method to measure magnetostriction, other published methods and their properties are summarized.

6.1 Fundamentals of Magnetostriction

Magnetostriction is a property of ferromagnetic materials and describes the change of the geometric dimensions caused by the alternating magnetic field. This effect is also known as Joule effect (Fig. 6.1) [20].

Depending on the direction of observation compared to the direction of the applied magnetic field, magnetostriction is designated as length, transverse or volume magnetostriction [21].

The following paragraph summarizes the origin of magnetostriction as found in [20]. Generally, magnetostriction can be described by the domain wall movements that occur with displacements of several μm. The dimensional change of the ferromagnetic materials results from the rotational movement of single magnetic domains, whereby the movements of the 90° domain walls contribute mainly to the magnetostriction. The external magnetic field causes the domains to rotate until they are aligned to the magnetic field's direction. This movement changes the strain inside the material's crystals that in turn causes the change of the material's dimen-
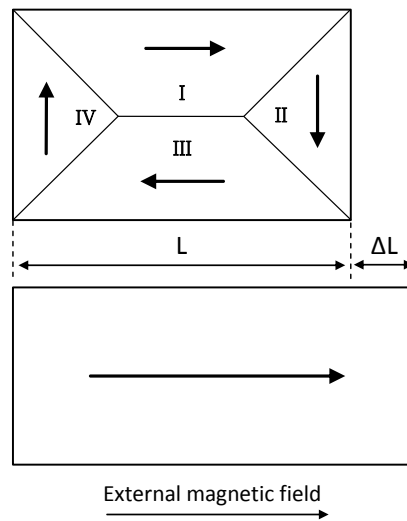
Figure 6.1: Change of the material's length due to movement of the 90° domain walls with reference to the applied external magnetic field, adapted from [20].

sion (Fig. 6.1). Since the 180° domain walls are already aligned in the direction of the magnetic field they do not contribute to the change of the material's dimensions.

[31] lists possibilities to reduce the 90° domain volumes with a focus on the material, the processing, and magnetization in order to finally reduce the magnetostriction.

6.2 Magnetostrictive Properties

Generally, the magnetostriction strain

$$\lambda = \frac{\Delta L}{L} \tag{6.1}$$

defined by the change in the length ΔL of the material, based on the material's initial length L, is the representative parameter for the magnetostriction. Nevertheless, depending on the measurement method, either the magnetostriction strain [32] or the acceleration of the vibrating material is determined [33] when it is exposed to an alternating magnetic field. Based on the physical relations,

$$s(t) = \int v(t)dt = \iint a(t)dtdt \tag{6.2}$$

the acceleration, velocity, or displacement can be used to describe magnetostriction.

Magnetostriction occurs with a fundamental frequency of twice the power frequency including harmonics at integer multiples of the fundamental frequency. In Fig. 6.2 the excitation voltage and the measured magnetostriction on a steel coil's narrow side is shown at a flux density of 1.7 T and 50 Hz.
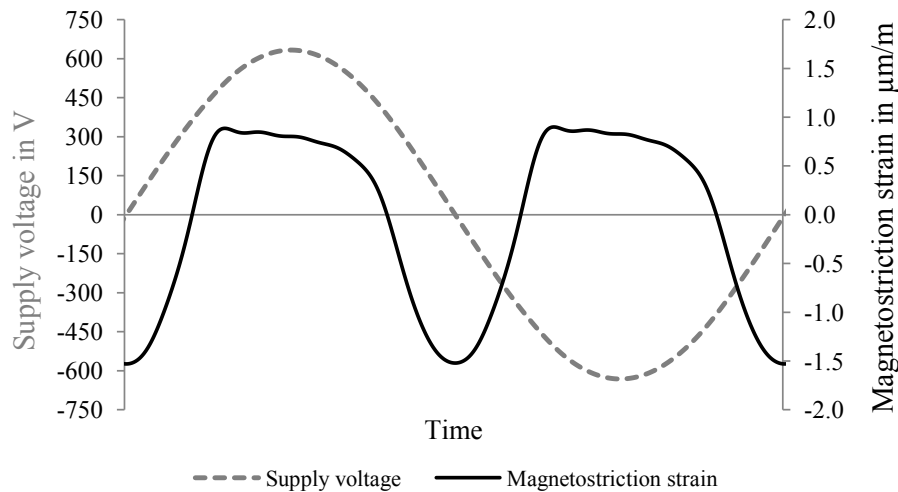
Figure 6.2: Measured magnetostriction at 1.7 T and 50 Hz occurs at twice the frequency of the excitation voltage's frequency including higher harmonics.

6.3 Measurement Methods

The magnetostriction of ferromagnetic materials occurs in the range of several μm. Therefore, its measurement requires a very sensitive measuring system whereby the applied sensing application should not influence the material's vibration by its weight and attachment. Hence, different approaches were developed based on the Joule effect, as described in [20]. These approaches can be divided into contact and non-contact methods wherein magnetostriction is usually measured in the direction of magnetization.

6.3.1 Overview: Contact and Non-Contact Methods

One of the first approaches to measure magnetostriction was realized with a phonograph pick-up positioned in the middle of the Epstein samples surface [34]. A similar

method was introduced by [35] where a piezoelectric element mechanically linked to a stylus was used as sensing device to determine magnetostriction of one lamination. These come with two main disadvantages: unidirectional sensitivity and the need of frequent calibration. In addition, strain gauges were used to measure magnetostriction, as presented in [36, 37], but with the disadvantages, summarized in [38], that the use of strain gauges is a time consuming procedure and that they are extremely sensitive to vertical vibrations. The use of piezoelectric acceleration transducers, as presented in [33, 39], come with the advantages of an easy set up and calibration, high resolution, and broad frequency range. Nevertheless, as piezoelectric acceleration transducers are directly mounted to the specimen, there mounting exerts stress on the specimen and, as a consequence, may influence the measurement of magnetostriction. Likewise more measurement methods such as capacitance displacement methods or linear variable differential transformer methods were used [1]. All of these methods have direct contact with the sample under test where the sensing system itself may influence the material's magnetostriction.

The development of non-contact methods was driven to solve the latter described problems. [40] introduced a novel method using a laser Doppler velocimeter which was one of the first methods with no direct contact with the sample including the advantages of high reproducibility and the possibility to measure very small displacements below $4 \cdot 10^{-8}$ m. The IEC report [1] provides possibilities of measuring magnetostrictive properties of electrical steel with the standardized devices, single sheet tester and Epstein frame. Optical methods are mainly applied on single sheet tester whereas accelerometers are applied on Epstein frame samples. Advantages and disadvantages of various developed magnetostriction measurement systems have been summarized in [38].

6.3.2 New Measurement Method

Within this work, a new measurement system, as proposed in [13], is presented where the magnetostriction of entire steel coils with a mass of up to 6,000 kg can be determined with piezoelectric acceleration transducers. The magnetostriction is thereby measured transverse to the rolling direction whereby the material is magnetized in rolling direction. Compared to a steel coil's mass the acceleration sensor's mass is negligibly low. In addition, the laminated narrow side of the steel coil provides a stable foundation for the transducers. Therefore, the exerted stress on the material under test due to the sensor's mass can be neglected.

Chapter 7

Transformer Noise

The overall noise emission of a transformer is a superposition of the noise from three main noise sources situated inside and outside of the transformer tank, as shown in Fig. 7.1. The noise created inside of the transformer tank can be mainly attributed to the active part of the transformer, containing the transformer core and the windings wound around the core limbs. Outside of the transformer the cooling system's pumps and fans generate noise due to their operation.

7.1 Noise Sources of Power Transformers

The load noise is determined by the magnetic stray field of all current carrying windings and the load-current in the windings. The superposition of the current carrying windings and the stray flux lead to axial and radial forces in the windings which predominantly determine the load noise. Therefore, the load noise, occurring at twice the power frequency, is also called winding noise, summarizing from [41].

In addition, the stray flux enters other iron parts such as magnetic tank shunts. As a consequence, magnetic forces arise and contribute to the winding noise with higher harmonics of the power frequency.

The noise created by the PT core, designated as core noise, is independent of the load current in the windings. Therefore, the core noise is also known as no-load noise. The alternating magnetic flux in the stacked magnetic core causes two different effects which both contribute to the so called core noise, as found in [42]:

- In the stacked transformer core the magnetic flux is forced to leave the steel sheets across small air gaps in the limb-yoke joints. Such transitions lead to compressive inter-laminar magnetic forces between the single steel sheets
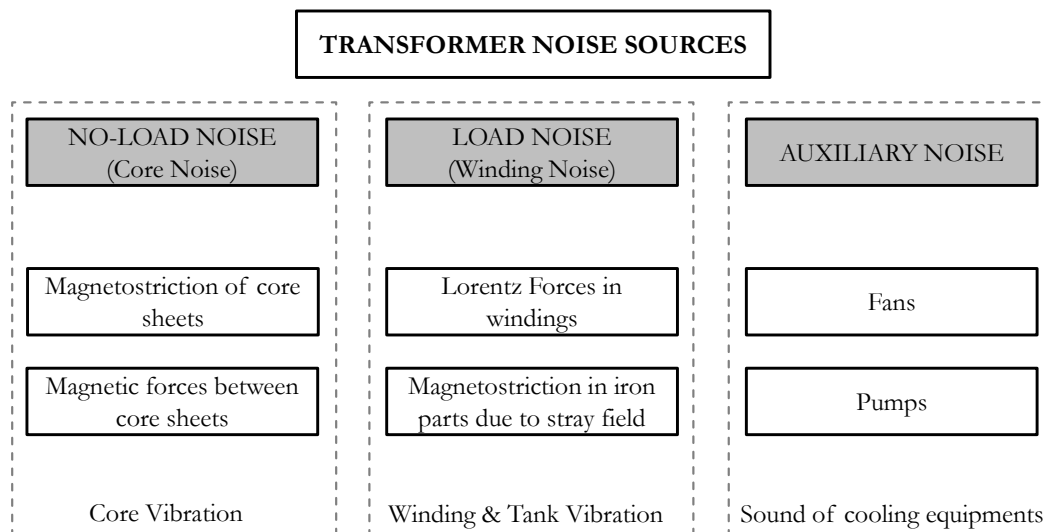
Figure 7.1: Noise sources of a power transformer.

because of the spatial change in permeability. These forces are proportional to the square of the magnetic flux density and occur mainly in the joint areas of the magnetic core.

- The second part known as the major contribution to the core noise is the magnetostriction. Magnetostriction is a property of ferromagnetic materials as described in Section 6 (p. 29). The alternating magnetic field causes small changes in the material's dimensions producing longitudinal vibrations of the core sheets. These changes, with a micrometer scale, alternate between compression and elongation of the single core sheets with even harmonics of the power frequency (100 Hz, 200 Hz, 300 Hz, ... at 50 Hz power frequency) because the change in the dimension of the material is not linearly proportional to the magnetic flux.

The vibrations of the active part are transferred through the isolation oil to the transformer tank where this structure born noise is radiated (Fig. 7.2) [43]. Most of the noise can be related to the vibrating yokes and joints because the limbs' vibrations are damped by the encircled windings [42].

Pumps and fans are often mounted outside of the transformer tank to dissipate heat created by losses in the core and windings. These auxiliary devices contribute
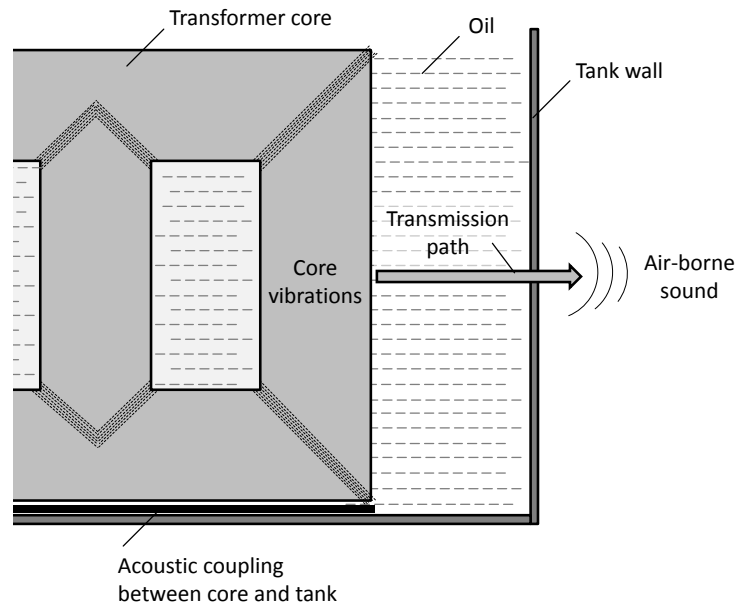
Figure 7.2: Illustration of the noise transmission path originating as transformer core vibrations transferred through the oil and radiated as air borne sound from the transformer tank walls, adapted from [43].

to the overall noise of a PT. Depending on the cooling system's design several fans and/or pumps are implemented which contribute to the overall noise level with their broadband noise in a frequency range from 500 Hz to 2000 Hz.

7.2 Acoustic Quantities

7.2.1 Sound Pressure

Vibrating solids such as transformers set the surrounding air particles in motion and lead to pressure variations which are superimposed on the static barometric pressure. This radiated acoustic energy from vibration solids generates sound. Audible sound can be described as such pressure variations in air or other elastic mediums in a frequency range from 20 Hz up to 20 kHz that can be detected by the human ear, reviewing from [44].

The sound pressure p expressed in pascal (Pa) is an important quantity that is usually measured in engineering acoustics, as the human's hearing mechanism responds sensitive to pressure variations [45]. It is defined as the root-mean square

(RMS) of sound pressure variations over a certain time period. The sound pressure is a scalar quantity and location dependent [44]. As the human ear can detect sound pressure in a wide range from the auditory threshold of p_0=20·10^{-6} N/m^2 up to the pain barrier of 200 N/m^2 the sound pressure is described internationally in decibels [46].

The sound pressure level is calculated as follows with the RMS sound pressure in reference to the auditory threshold p_0.

$$L_\mathrm{P} = 20 \cdot \log \frac{p}{p_0} \tag{7.1}$$

7.2.2 Sound Intensity

The following paragraph reviews the particle velocity u, as found in [44]. The particle velocity is the second important quantity in engineering acoustics and describes the oscillation velocity of the particles in elastic mediums as for example in air. The particle velocity is a location dependent vector quantity and hence describes in which direction the sound wave propagates.

The sound intensity I of a stationary sound source is calculated by the time-averaged product of the instantaneous sound pressure and corresponding particle velocity at the same time

$$\vec{I} = \overline{p(t) \cdot \vec{u}(t)}. \tag{7.2}$$

It describes the sound energy flow through a surface element per unit area in unit time. The sound intensity, expressed in W/m^2, is a vector quantity which has the same direction as the particle velocity [47].

The sound intensity level

$$L_I = 10 \cdot \log \frac{|\vec{I}|}{I_0} \tag{7.3}$$

is calculated with the reference sound intensity I_0=1·10^{-12} W/m^2.

7.2.3 Sound Power

The sound power describes the acoustic energy radiated from a certain sound source. In engineering acoustics the sound power is an important descriptor of a sound source and is used for sound emission ratings and comparisons between sound sources because it is a location independent quantity, summarizing from [44].

The sound power

$$W = \int_S \vec{I} \cdot d\vec{S} \tag{7.4}$$

of a sound source can be described by the sound power travelling through a surface *S*. Generally it can be calculated by integration of the sound intensity above the surface *S* [46].

The ISO standard 3746 defines the determination of the enveloping surface *S* in m^2 which is surrounding the sound source. Noise measurements on transformer tank covers are usually not accessible due to high voltages. Therefore, the actual standards define approaches how to calculate the enveloping surface, designated as measurement surface, by the measurement distance, the height of the principal radiating surface of the transformer, and the length of the measurement path around the transformer, paraphrased from [48].

The sound power level

$$L_W = 10 \cdot \log \frac{W}{W_0} \tag{7.5}$$

is calculated with the reference sound power $W_0 = I_0 \cdot 1\text{m}^2 = 10^{-12}$ Watt [48].

The relationship between the sound intensity and the sound pressure has been summarized from [46]. For the propagation of plane waves the sound intensity

$$I = \frac{p_{\text{eff}}^2}{\rho_0 \cdot c} \tag{7.6}$$

can be calculated by the sound pressure including the density ρ_0, and the speed of sound in the elastic medium. Therefore, the sound power can be also expressed by only measuring the sound pressure on a defined measurement surface around the sound source.

7.2.4 A-Weighting

The human ear has a frequency depending sensitivity to sound. The highest sensitivity is given around 2-3 kHz. Below and above 2-3 kHz the sensitivity is reduced. The A-weighting function $A(f)$, described in IEC 61672-1 approximates this sensitivity (Fig. 7.3).

$$A(f) = 2 + 20 \cdot \log \frac{12200^2 \cdot f^4}{(f^2 + 20.6^2) + \sqrt{(f^2 + 107.7^2) \cdot (f^2 + 737.9^2)) + (f^2 + 12200^2)}}$$
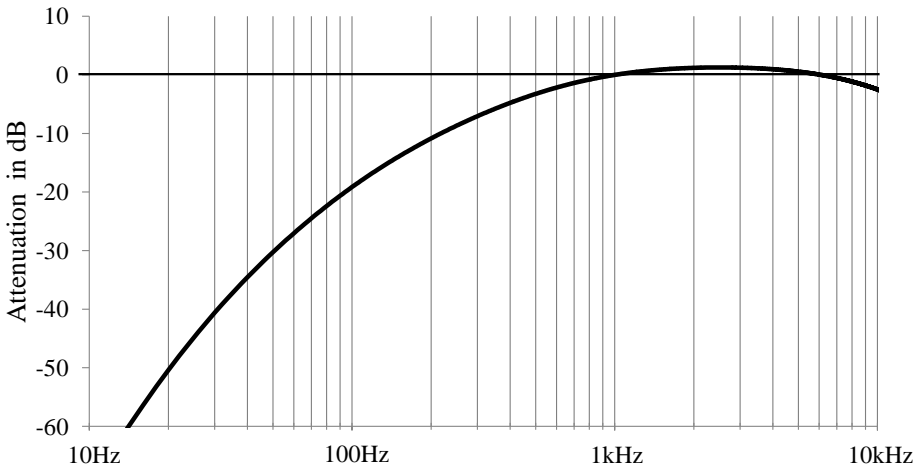
Figure 7.3: A-weighting function to approximate the human ears sensitivity; according to IEC 61672-1.

$$(7.7)$$

7.3 Determination of Sound Power Levels

In general, three main sources of sound contribute to the overall sound of a PT. Each of these sources radiate sound to the surrounding air which can be expressed by a sound power level. The emitted sound of each sound source is determined independently from each other during defined test laboratory measurements according to IEC 60076-10 [48] and IEEE Std. C57.12.90 [49].

Usually the sound power level of the PT in no-load condition is determined at rated voltage with a sinusoidal waveform and rated frequency at an untapped winding, as described in [48]. During no-load condition the energized winding draws only a small magnetization current to build up the mutual flux in the magnetic core between the interlinked windings [42].

According to [48] the sound power level of the transformer in load condition is determined during one winding is short-circuited and the other winding is carrying the rated current at rated frequency. The tap-changer position should be on principal tapping. The voltage required to drive the rated current in this condition is considerable lower than the rated voltage. As a result the core noise is negligible due to the low flux density in the core.

The sound level of the cooling devices shall be determined with all implemented cooling devices, such as pumps and fans, which are necessary to operate the PT at rated power.

It is common that purchasers define within their PT specification additional excitation conditions where sound levels have to be determined and guaranteed. The overall sound power of a PT can be calculated by the logarithmic sum

$$L_W = 10 \cdot \log(10^{\frac{L_{W1}}{10}} + 10^{\frac{L_{W2}}{10}} + 10^{\frac{L_{W3}}{10}}) \tag{7.8}$$

of the sound power levels of all three noise sources.

7.4 Measurement Methods

The sound pressure or sound intensity method can be used to determine the sound power. Both methods are discussed, as they were both applied in the experimental studies to measure the sound of the transformers. The core noise of the MTs was determined with the sound pressure method. Noise measurements on the PTs were carried out with the sound intensity method. It is important for both, the sound

pressure and sound intensity, to refer the individual sound level to a certain measurement distance to the PT which defines the measurement area. This measurement distance is defined by the standards IEC [48] and ANSI [49].

Sound Pressure Method

The sound pressure method uses one single pressure microphone to determine the sound pressure. Indoor measurements in a test laboratory differ from ideal free field conditions. Hence, the measured sound pressure may be affected by reflections and background noise. Therefore, generally, two corrections have to be applied to correct these influences: (1) the correction of the background noise, and (2) the correction for sound reflections due to indoor measurements.

Sound Intensity Method

The following paragraph reviews the the sound intensity method as found in [47]. The sound intensity method uses two single pressure microphones (Fig. 7.4) arranged in a defined distance to each other. This distance Δr is provided by a spacer and defines the measurable frequency range of the intensity probe. The particle velocity

$$u = -\frac{1}{\rho} \int \frac{p_B - p_A}{\Delta r} dt \qquad (7.9)$$

is related to the pressure gradient which can be approximated by the measured sound pressures p_A and p_B of the two closely spaced microphones and the density of air ρ. This method already considers the background noise and reflections.
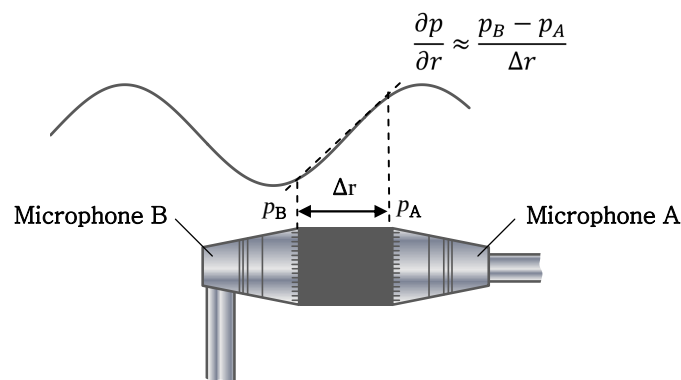
Figure 7.4: Intensity probe built with two pressure microphones, adapted from [50].

Chapter 8

Transformer Losses

The total losses of a PT can be separated into the no-load losses, mainly produced in the transformer core, and the load losses, caused by the current flow in the transformer windings. Hence, the no-load losses are designated as core losses and the load losses as winding losses. Operators of PTs specify these losses as for example the no-load losses are constantly arising operating costs independent of the transformer's load. PT manufacturers have to guarantee the specified losses during acceptance tests in the test laboratory as they are included into operators' investment appraisals.

8.1 No-Load Losses

The no-load losses of a PT, generally determined at the specified rated voltage and rated frequency, are mainly produced in the transformer core. The losses can be explained by the dissipated energy in the PT core due to the alternating magnetic flux in the core material caused by the excitation current in no-load condition. This magnetization current amounts to only a few percent of the nominal current. The core losses itself can be described by the core materials' hysteresis loss and the eddy current loss as described in Section 5 (p. 23). In addition, minor losses for example due to the low excitation current in the windings contribute to the no-load losses [19].

The no-load losses are determined by energizing any winding system of the PT when the other windings are open-circuited [49]. In the test laboratory it is convenient to energize the low-voltage or tertiary-voltage winding instead of the high-voltage winding as it is difficult to provide such high voltage levels as on substations.

Sections 12.1 (p. 96) and 12.2 (p. 101), which show experimental studies, detail the electric circuits for energizing the transformers under test.

The no-load losses are sensitive to the waveform distortion as well as the frequency [49]. Therefore, international standards define tolerances for the supply frequency and wave form distortion of the supply voltage.

8.2 Building Factor

The specific no-load losses of a PT $P_{s,PT}$ in W/kg are usually higher than the specific losses P_s in W/kg of electrical steel determined with an Epstein frame or single sheet tester. In Fig. 8.1 the difference in the specific losses of a single sheet test, a three-phase MT, and a one-phase PT are displayed, each using the steel grade M85-23P5. The difference of the specific losses, described by the building factor

$$BF = \frac{P_{s,PT}}{P_s} \tag{8.1}$$

is mainly attributed, as described in [19,42,51], to the additional losses created in the transformer joint areas, where the magnetic flux is forced to leave the direction of grain orientation and additionally has to overcome small air gaps. When the magnetic flux enters again the steel sheets the occurring eddy currents cause additional losses in the joint areas.
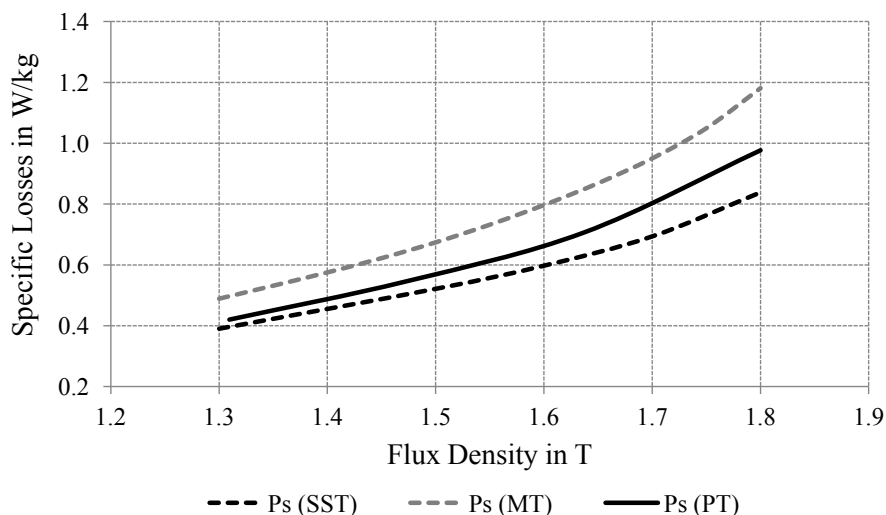
Figure 8.1: Specific losses of a single sheet test with 0.5 kg, a three-phase MT with 917.5 kg, and a one-phase PT with a weight of 40,000 kg.

The building factor depends also on the flux density, core material grade, and core type [42]. In each core type different flux distributions arise due to the different structure and amount of joint areas between the limbs and yokes. Therefore, differences in the PT no-load losses occur. [51] describes additional influences such as burrs of the core sheets produced by cutting or material stress due to the stacking of the single core sheets that may also contribute to a higher building factor.

8.3 Load Losses

The load losses of a PT are generated by the load current flow in the windings. The losses consist of I^2R loss in the windings due to the ohmic resistance of the windings and stray losses due to the windings leakage field. The leakage field induces eddy currents in adjacent iron parts such as the tank walls, core clampings or the magnetic shields leading to temperature rise in the material, paraphrasing from [42].

Based on [52], the following sentences describe the determination of the load losses. The load losses are determined by energizing the high voltage winding by the short-circuit voltage to generate a current flow in the high voltage winding and short-circuited low voltage winding corresponding to the nominal current of the transformer. The measured effective power in this condition is equivalent to the load losses.

Chapter 9

Preliminary Studies

This chapter presents a literature study of the main causes of PTs' no-load noise and the opportunity to predict the no-load noise performance by measuring the core steels' magnetostriction. A feasibility study investigates the measurement of magnetostriction on steel coils perpendicular to the rolling direction and includes the analysis of the Young's modulus, and the measurement of the magnetostriction strain on both narrow sides of the steel coil. In addition, an analysis demonstrates how much the losses can deviate within one steel coil. For this purpose, single sheet specimen were extracted along a steel coil's length.

9.1 Measurable Parameters for No-Load Noise Performance Prediction

In general, no-load and load noise evidently depend on the transformer design and load. The no-load noise of PTs, however, is present even at night, at low load.

As described in Section 7.1 (p. 33), two main causes for the no-load noise of PTs are differentiated between magnetostriction and the magnetic forces between individual core sheets [5]. The effect of the two sources of the no-load noise has been explained, e.g., in [19, 42]. According to [42, 43], magnetostriction is the main reason for the no-load noise, whereas [5] reviews the differing understandings of the contributions of the two sources. Further analysis of the extent to which magnetostriction contributes to the no-load noise of the PT exceeds the scope of this work.

In contrast to the magnetic forces, magnetostriction can be measured before PT cores are built. Consequently, the measurement of the magnetostrictive properties of steel coils is a unique opportunity to estimate a PT's no-load noise.

9.2 Measurement of Magnetostriction Perpendicular to Rolling Direction

In general, magnetostriction is measured in the rolling direction, as discussed in Section 6.3 (p. 31). Several investigations have been carried out in which magnetostriction was measured at different angles to the rolling direction on the test specimen [53, 54] and also directly on PT cores [55]. On steel coils, the magnetostriction cannot be measured in rolling direction of the material because of the coils' toroidal geometry. Thus, a different approach must be found in order to determine the magnetostriction on entire steel coils. Delivered steels coils are wound mostly on carton cylinders on which the laminated narrow side of the steel coil in axial direction provides a sufficiently solid foundation to place appropriate sensors which measure the magnetostriction. It must be noted that in this case the magnetostriction perpendicular to the rolling direction is measured. Therefore, a feasibility study of the grain-oriented material and its elasticity properties was carried out. The Young's modulus

$$E = \frac{\sigma}{\epsilon} = \frac{F \cdot L_0}{A_0 \cdot \Delta L} \tag{9.1}$$

has been used to compare the materials' longitudinal (rolling direction) and transversal elasticity. Experimental studies of the Young's modulus of grain-oriented steel grades from different suppliers have been carried out, whereby σ denotes the tensile stress and ϵ the extensional strain. This ratio can also be described by the exciting force F, the cross sectional area A_0 on which the force is applied, the change in length of the object ΔL, and the original length L. The Young's modulus was determined to be 130-160 GN/m^2 in rolling direction and 250-320 GN/m^2 perpendicular to the rolling direction. These values were found to differ by a factor of two between both directions. Hence, at the same acting force on the material on the smaller side with the larger Young's modulus a smaller change in length occurs when compared to the rolling direction.

A feasibility study of the measurability of magnetostriction on the narrow side of steel coils with piezoelectric acceleration transducers was carried out. The study showed that the magnetostriction strain can be determined with piezoelectric acceleration transducers on the steel coil's narrow side with a sufficiently high signal to noise ratio (SNR) at flux densities between 1.0 T and 1.9 T. The measurement on both narrow sides of the steel coil was identified to be unnecessary, as the elongation and

compression of the material is symmetric to the centre of the steel coil. Figure 9.1 shows a exemplary measurement of the magnetostriction strain at 1.7 T at 50 Hz.
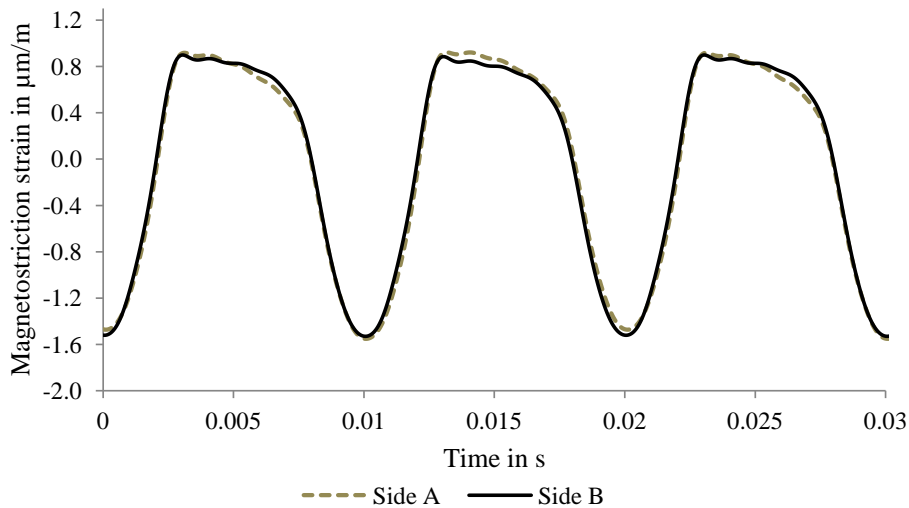
Figure 9.1: Compression and elongation of the steel coil measured on both narrow sides with piezoelectric acceleration transducers at 1.7 T at 50 Hz excitation frequency.

The measurement of magnetostriction in radial direction on the outer side of a steel coil was found insufficient due to undirected deflection. Section 10.3.7 (p. 60) offers more details on the determination of the magnetostriction strain.

9.3 Loss Deviation Within a Steel Coil

Due to the small sample size of Epstein and single sheet test specimen, only one section of an entire steel coil is tested with such a sample. To obtain representative specific losses of a steel coil, single sheet samples along the complete steel length and width were extracted out of a steel coil with the conventional grade M130-30S5 and a mass of 4,519 kg. Consequently, the heavy steel coil was rewound with special coilers. In-house investigations showed a deviation of up to 11 % in the specific losses along the complete steel band length of about 2,000 m. Therefore, single sheet test specimens were extracted across the total coil width of 1 m along the steel length at 20 m, 500 m, 1,000 m and 1,400 m. Table 9.1 depicts the minimum and maximum determined specific losses and length positions of the single sheet measurements.

Table 9.1: Deviation of specific losses within a steel coil of material grade M130-30S5 determined with single sheet tests.

P_s min	P_s max	P_s
[W/kg]	[W/kg]	[%]
(500 m)	(1,400 m)	(-)
1.1494	1.2798	11.4

These results illustrate that the use of the specific losses obtained by a single sheet tester is rather limited for the prediction of the no-load losses of PT cores. Furthermore, the following aspects have been observed:

- Since PT cores contain several steel coils, acceptance tests in the test laboratory determine the mean no-load losses of the PT.

- Single sheet tests cannot represent the mean magnetic losses of a steel coil because of the inhomogeneous distribution of the specific losses within the coil. Therefore, the mean magnetic losses of the deployed steel coils need to be obtained accurately to predict the PTs' no-load losses.

- The accurate determination of the mean magnetic losses of a complete steel coil could reduce the uncertainty in PT core designs.

As a result, the measurement of the specific losses of complete steel coils with a mass of up to 6,000 kg should increase the accuracy with which the specific losses of the deployed material are determined and hence allow better prediction of the no-load losses of PTs.

Chapter 10

Coil Measurement System

This chapter provides the specific requirements for the CMS and details its implementation. In addition, initial results of the measured magnetostriction strain and specific losses are provided.[1]

10.1 Specific Requirements for Coil Measurement System

10.1.1 Samples

The CMS has been designed and implemented for steel coils with the following minimum and maximum dimensions:

- width $0.30\,\text{m} \leq b \leq 1.3\,\text{m}$

- inner diameter $0.50\,\text{m} \leq D_i \leq 0.6\,\text{m}$

- outer diameter $0.62\,\text{m} \leq D_a \leq 1.30\,\text{m}$

- mass $500\,\text{kg} \leq m \leq 6{,}000\,\text{kg}$.

These specifications were determined by the delivered steel coils which hold iron fill factors (also referred to as stacking factor [57,58]) between $FF = 0.96$ and $FF = 0.99$.

In general, mother coils are differentiated from slitted steel coils. Mother coils, also referred to as master coils or parent coils, are steel coils with a mass between

---

[1]Selected results of this chapter have also been published in [13,56].

10,000 and 30,000 kg. Depending on the steel manufacturer's facilities, the steel coil's width can reach up to 1.6 m. The areas close to the material's edges are untreated and usually have worse magnetic properties than the material in the middle of the sheets. Typically, the width of the untreated border area of mother coils reaches up to 0.08 m per side. This is up to 10 % in reference to a steel coil width of 1.6 m. Usually, these areas with reduced quality are trimmed by the steel coil manufacturer to provide customers with steel coils ready for the cutting process. In addition, the heavy steel coils are fragmented in the slitting process to make them transportable. The steel coils' width is set depending on the customer's order. In addition, the standard IEC 60404-8-7 [26] includes regulations regarding the steel coils' mass, width, and inner diameter. Within the CMS, only steel coils with removed border areas and a maximum mass of up to 6,000 kg are analysed. The slitting degrades the magnetic properties of the material. This effect does not only occur during the slitting process for PT core sheets, but also when single sheet or Epstein test specimen are cut from coils. Because of the small ratio between burr and test specimen width for Epstein tests, the material must be stress annealed, to reduce the influence of the cutting process on the measured magnetic properties and better determine the properties of the original, uncut material. For single sheet test specimens or core sheets for PTs, this ratio is large and hence stress annealing may be neglected. The same conclusion can be drawn for the aforementioned steel coil test specimen.

The CMS's primary goal is to determine the average magnetic properties of the overall coil. The influence of the cutting process, as investigated in [38, 59], is subsequently considered in the design process.

10.1.2 Magnetic Field Excitation

The power source specifications include the maximum supply power for entire steel coils which depends on the measurement range to be covered and the steel coil geometry, mass and material grade. In addition, a sinusoidal output waveform of the excitation voltage with a low distortion is required. The number of turns of the primary winding and the magnetization current are related to the power supply voltage. Covering all flux densities that may occur at PT operation results in the following requirements:

- flux density $1.0\,\text{T} \leq B \leq 1.9\,\text{T}$ and

- frequency $50\,\text{Hz} \leq f \leq 60\,\text{Hz}$

To obtain a low distortion in the supply voltage, either a motor-generator set or an electronic frequency converter with a special output filter to obtain an extremely low total harmonic distortion (THD) can be used.

The following determines the required excitation voltage U

$$U = \frac{2\pi}{\sqrt{2}} \cdot N \cdot \hat{B} \cdot f \cdot A_{\text{fe}} \tag{10.1}$$

with the number of turns N of the primary winding, the peak flux density $\hat{B}$, the frequency f and the effective iron cross section A_{fe} of a test specimen. Section 10.1.6 provides the detailed determination of A_{fe}.

To prevent pre-magnetization from influencing the measurements, the measurement sequence must start at high flux densities. Hence, the sequence starts at $1.9\,\text{T}$ and ends at $1.0\,\text{T}$ for each supply frequency.

10.1.3 Windings

The incoming goods inspection requires fast mounting of the windings. To obtain a homogeneous flux distribution, the turns of the magnetizing winding should be distributed along the circumference of a test specimen [10, 11]. The cross section of the primary winding is related to the maximum current of the power source. For easy cabling, the windings should be flexible.

10.1.4 Handling of Specimen

A test specimen must be magnetized in a cabin to ensure protection against electric shocks. Steel coils of up to $6,000\,\text{kg}$ must be moved to a defined measurement position. Therefore, coil lift trucks or cranes generally provide the simple handling of the test specimens between the incoming goods department and their measurement position.

10.1.5 Electronic Devices

The incoming goods inspection frequently leads to a strong daily operation of the sensors and their cabling: hence, leading to the necessity for robustness and long-term stability of all additional electronic devices.

Because of the test specimen's weight, which may be up to 6,000 kg, primary currents must be determined with sufficient accuracy regarding both amplitude and phase.

10.1.6 Determination of a Specimen's Properties for Specific Loss Measurement

Similar to [8, 9], the properties of the test specimen, such as the geometry and mass, influence the voltage needed to obtain certain flux densities in the material. For rapid measurements, the mass and geometry of the test specimens must be measured automatically and accurately. To increase stability during transport, some steel coil suppliers wind steel bands on cardboard cylinders. Since these cylinders show a high variation in thickness, the sensors must detect the test specimen's inner diameter, neglecting the cardboard. Using the Coil-Method to obtain the specific power losses P_s, requires the mass m, the inner diameter D_i, and the outer diameter D_a, as well as the width of the steel coil b. Different sensor systems need to be used to obtain these properties for each test specimen. From these, the iron fill factor FF of a test specimen's geometry is determined with the density ρ_{fe} for electrical grain-oriented steel,

$$FF = \frac{1}{\rho_{fe}} \cdot \frac{m}{[(\frac{D_a}{2})^2 - (\frac{D_i}{2})^2]\pi b} \tag{10.2}$$

then, the effective iron cross section A_{fe} is calculated,

$$A_{fe} = \frac{D_a - D_i}{2} \cdot b \cdot FF. \tag{10.3}$$

10.1.7 Determination of Magnetostriction

For the determination of the magnetostriction, the specified measurement frequencies and comparability to PT sound emissions need to be met. From preliminary measurements, the frequency range was determined to be up to 1,000 Hz, which has also been discussed in [43]. From this, the requirements placed upon the frequency response of the strain measurement system are defined. The SNR gives an additional requirement at 1.0 T at 50 Hz. Preliminary measurements showed that the magnetostriction strain can be measured only transversely to the direction of rolling on the stable narrow side of the steel coil. This differs from the known non-contact methods

which use optical sensors or from contact methods with accelerometers which both are summarized in [1].

10.2 Influence of a Specimen's Properties on the Measured Specific Power Losses

The sensitivity of the measured specific losses towards uncertainties in the determination of the test specimen's mass m, inner diameter D_i, and outer diameter D_a is investigated as follows: Offset errors of $\pm 0.5\,\%$, $\pm 1\,\%$ and $\pm 2\,\%$ were added to the mass, inner and outer diameters. Based on these error affected values the calculated voltage (10.1) was evaluated using (10.1) - (10.3). Table 10.1 depicts the steel coils which were used for the present parameter study as well as for preliminary studies. First, the specific losses of the steel coils measured at certain excitation voltages were described with polynomials of degree six. Second, based on the voltage calculated with the offset errors added, the specific losses were interpolated between the measured specific losses with the help of the identified polynomials. These interpolated values, which consider the measurement uncertainties, were compared to the measured ones.

Table 10.1: Steel coils used for pilot investigations.

Test Specimen	Grade	Weight	Width	D_i	D_a
[-]	[-]	[kg]	[m]	[m]	[m]
Coil 01	M85-23P5	3760	0.945	0.528	0.982
Coil 02	M85-23P5	1380	1.205	0.530	0.684
Coil 03	M130-30S5	5045	0.955	0.526	1.081
Coil 04	M85-23P5	2539	1.000	0.524	0.841
Coil 05	M110-30P5	3152	1.015	0.524	0.894

The error of the measured specific losses

$$error_\% = \frac{P_{s,c} - P_s}{P_s} \cdot 100\,\%. \tag{10.4}$$

was determined from the losses $P_{s,c}$ calculated by the error affected voltage and the true measured specific losses P_s. Figs. 10.1-10.3 show the calculated errors of the

specific power losses in W/kg due to different errors in the determination of a test specimen's properties. The highest deviation occurs if the mass measurement includes errors (Fig. 10.1). The error increases with magnetic flux density as the specific power loss curves exhibit a higher gradient at high flux densities. Consequently, the same error has a larger effect. From this, the required accuracies of the respective sensors were derived. Section 10.3.6 (p. 59) details the determination of the test specimen's mass and geometry as well as the accuracies of the selected sensor systems to show that the specific power losses are determined with a maximum error of 1%.
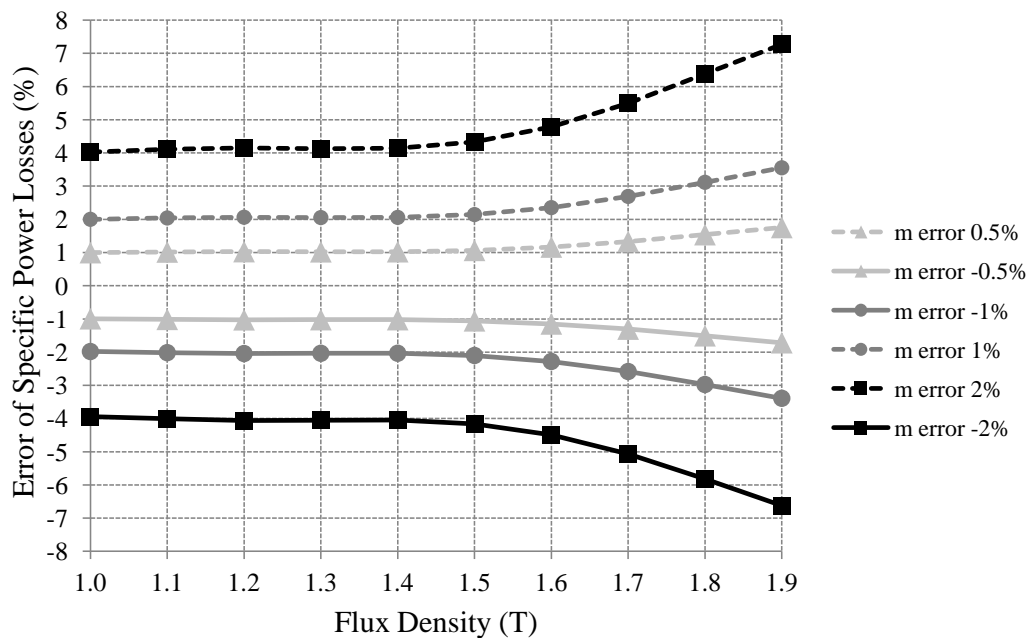

Figure 10.1: Error of determined specific power losses due to measurement error of test specimen mass.
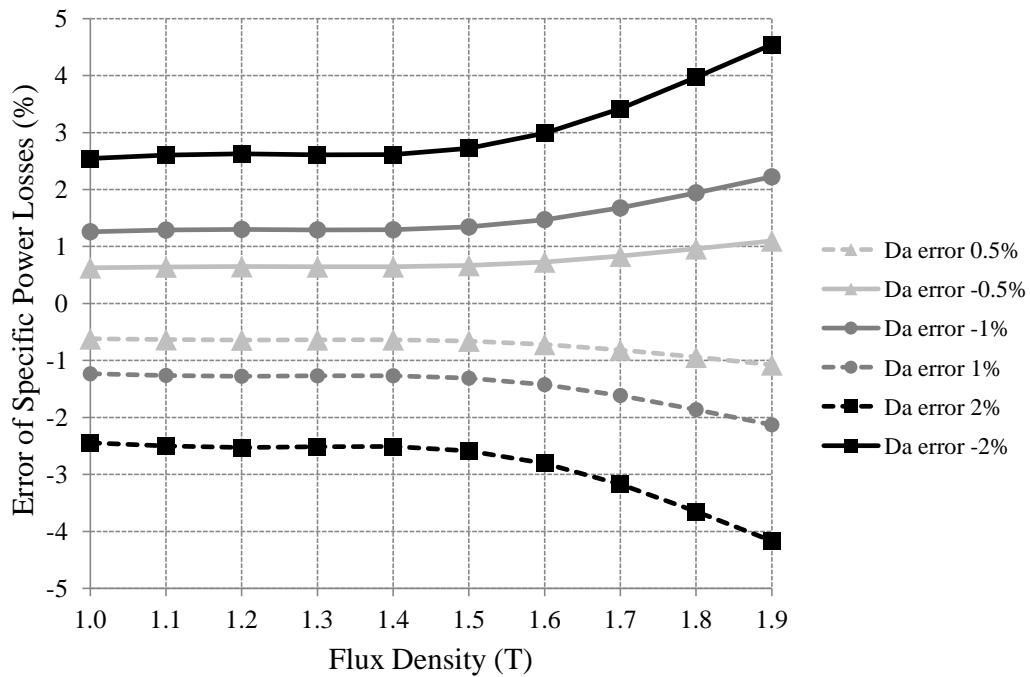
Figure 10.2: Error of determined specific power losses due to measurement error of test specimen outer diameter.
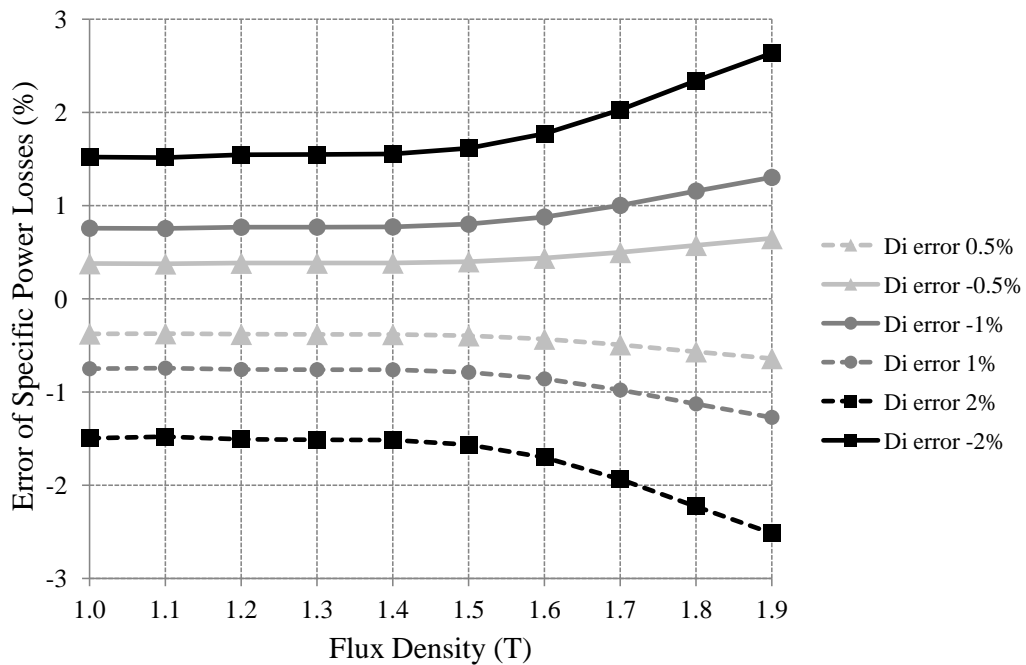

Figure 10.3: Error of determined specific power losses due to measurement error of test specimen inner diameter.

10.3 Implementation and Selected Results

10.3.1 Samples

Table 10.2 shows the steel coils used for the initial classification described in Section 10.4 (p. 62).

Table 10.2: Steel coils used for initial classification (Section 10.4).

Supplier/Coil	Grade	Weight	Width	D_i	D_a
[-]	[-]	[kg]	[m]	[m]	[m]
A / Coil 06	M105-30P5	2674	0.889	0.526	0.887
B / Coil 07	M105-30P5	2056	0.520	0.525	0.972
C / Coil 08	M105-30P5	3870	1.045	0.508	0.941
D / Coil 09	M105-30P5	5858	0.980	0.526	1.138
E / Coil 10	M105-30P5	5273	1.020	0.510	1.065
F / Coil 11	M105-30P5	2731	0.920	0.523	0.882

10.3.2 Magnetic Field Excitation

Preliminary tests were carried out with a 64 MVA high power generator and electronic frequency converter normally used as the power source for PT load and no-load tests. A low harmonic distortion of the voltage was identified to be the main focus of attention when selecting the power source. Indeed, Epstein, single sheet as well as PT tests are based on sinusoidal voltages with low harmonic distortion. In addition, the material's magnetostriction is affected by non-sinusoidal magnetic fields [60]. Accuracy, stability and resolution of the sinusoidal output waveform and its frequency are important for comparable and reproducible measurements [20]. An electric frequency converter (EFC) with an implemented smoothing filter proved sufficient for these aims and was selected as the power source.

The converter rating was estimated as follows: The steel grade M130-30S5 of the steel coils has a relative permeability of 1900 and 1.3 W/kg at 1.7 T. From this, 1.74 W/kg were computed over the flux density range of interest (1.0 T - 1.9 T) using linear regression for 1.9 T at 60 Hz. Multiplied by the maximum coil mass of 6,000 kg, the total necessary active power was determined to be 10.5 kW. The apparent power

of 0.52 MVA was determined assuming a power factor of $\cos\varphi = 0.02$. A safety factor of 15 % was added to account for the high non-linear load and expected high current peaks. This leads to a required apparent power of 0.6 MVA. Using (10.3) (p. 52), the minimum inner diameter of 0.5 m and maximum outer diameter of 1.3 m of a steel coil together with an iron fill factor of 0.97 and appropriate coil width give an effective iron cross section of $0.277\,\text{m}^2$. From (10.1) (p. 51), the maximum supply voltage of 0.84 kV at 60 Hz supply frequency and 1.9 T a maximum current of 0.71 kA is derived.

10.3.3 Windings

The winding arrangement is mounted within the CMS cabin. Between four to eight turns of the primary winding can be selected, depending on the test specimen's mass and geometry. The turns are distributed around the circumference of a test specimen (Fig. 10.4). The high currents required for the experimental investigation of the steel coils result in partially large current carrying components. The flux within the test specimen is determined from the voltage induced within one sensing turn (Fig. 10.4), which is arranged at maximum distance to the magnetizing winding to eliminate the impact of stray flux. An automatic system closes the primary and secondary winding around a test specimen in less than one minute.
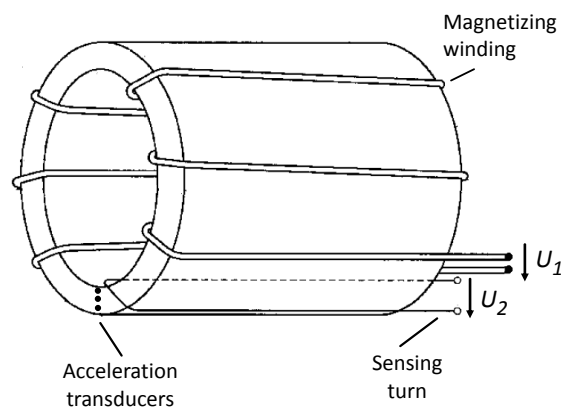
Figure 10.4: Placement of the three acceleration transducers on the laminated narrow side of a steel coil including the uniformly distributed turns of the primary winding and the sensing turn [14].

10.3.4 Handling of Specimen

To prevent complex handling sequences with heavy steel coils, a coil lift truck (Fig. 10.5) moves a test specimen into the CMS cabin. With a semi-automatic control of the coil lift truck and automatic mounting of the windings, the preparation time is approximately five minutes, whereas the complete measurement including the preparation can be realized within 15 minutes.
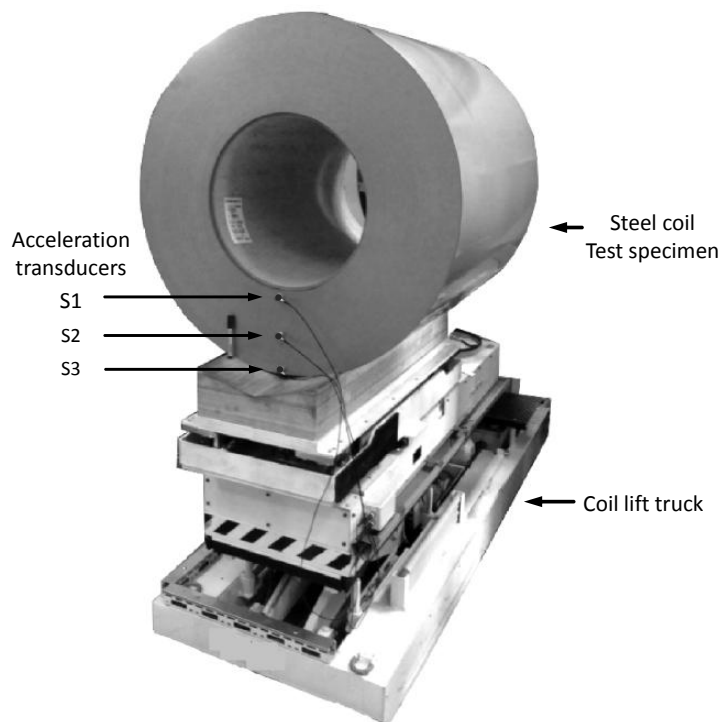
Figure 10.5: Handling of steel coils with a mass of up to 6,000 kg (inner diameter 0.51 m / width of 1.0 m) with rail-based coil lift truck.

10.3.5 Electronic Devices

The requirements of the current measurement can be met by the use of an current comparator with a active flux control [61]. The comparator used for the current measurement in the range of 1-200 % of the nominal current ensures an accuracy of +/-0.001 % of the amplitude and a maximum phase influence of +/-0.00083 degrees. In pre-tests, an SNR of 44 dB was identified with a current of eight A (RMS) at 50 Hz

supply frequency that corresponds to a flux density of 1.0 T at a steel coil with 3,000 kg. From this, currents can be determined with sufficient accuracy also in the lower measurement range.

The supply voltage, the current and the winding voltage on the secondary winding are measured with a power analyzer. The THD of the secondary voltage

$$THD_{U_2} = \frac{\sqrt{U_{h2}^2 + U_{h3}^2 + U_{h4}^2 + ... + U_{hn}^2}}{U_{h1}} \tag{10.5}$$

is determined from the amplitudes of the harmonics U_h, in which a THD $\leq 2\%$ can be met for excitations of up to 1.9 T. Hence, the need of a sinusoidal excitation voltage can be met, which is also known from [8,9] in which a form factor of $1.111 \pm 1\%$ is required.

10.3.6 Determination of a Test Specimen's Properties for Specific Loss Measurement

In the CMS cabin, the test specimen's properties mass and outer diameter are determined automatically. For the determination of a test specimen's mass, weighting cells are used with a composite error of $\leq \pm 0.012\%$ on the rated load of 5,000 kg. The outer diameter is measured with three distributed laser sensors at the circumference of the test specimen with a sensor accuracy of 0.11% of the full scale range of 0.7 m. The sensors' accuracies were determined from the overall measurement uncertainties, according to the sensors data sheets. The inner diameter and the steel coil width are determined manually.

The active power P_m in W is determined from the current I_1 and the voltage of the sensing turn U_2 (Fig. 10.6)

$$P_m = U_2 \cdot \frac{N_1}{N_2} \cdot s \cdot I_1 \cdot \cos\varphi \tag{10.6}$$

with the turn ratio of the primary and secondary winding N_1/N_2 and the transmission ration s of the current comparator. Using the secondary voltage eliminates the influence of the leakage inductance and any voltage drop associated with current flow in the primary winding. Instead of a wattmeter as described in the standards [8] or [9], a power analyzer determines the active power, because of standby facility reasons and the benefits of data transmission.

From the mass m in kg and the measured losses P_{m} in W, the specific losses P_{s} in W/kg are determined [8, 9, 11].

$$P_{\mathrm{s}} = \frac{P_{\mathrm{m}}}{m} \tag{10.7}$$
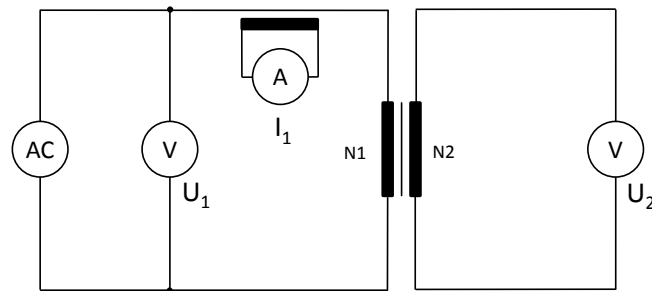
Figure 10.6: Electrical circuit of the Coil-Method.

10.3.7 Determination of Magnetostriction

Three sensors on one narrow side prove sufficient to obtain the mean acceleration measured at steady state flux density because of the toroidal shape of the steel coil test specimen. The sensors are distributed between the inner and the outer diameter on the narrow side in axial direction (Fig. 10.5). The mean acceleration from the three sensor signals is calculated and used for further analysis.

The selected piezoelectric acceleration transducers with a sensitivity of $52.3\,\mathrm{mV/ms^{-2}}$ ensure a good signal acquisition down to a flux density of $1.0\,\mathrm{T}$ as well as a high SNR because of an inherent noise lower than $50\,\mu\mathrm{V}$ between $1\,\mathrm{Hz}$ and $12.8\,\mathrm{kHz}$.

The acceleration signals recorded at each flux density are analyzed spectrally and processed with a frequency resolution of $2\,\mathrm{Hz}$ to determine the harmonics of the supply frequency. From the amplitudes of the harmonics, the peak deflections

$$\hat{s}_{\mathrm{h}} = \frac{\hat{a}_{\mathrm{h}}}{(2\pi f_{\mathrm{h}})^2} \tag{10.8}$$

at the harmonic nodes for each sensor signal are calculated [62].

The deflection time signal of each sensor is reconstructed containing the peak deflections and phase information of all harmonic frequencies from 0 Hz to 1,000 Hz.

$$s(t) = \sum_{h=1}^{20} s_{\mathrm{h}} = \sum_{h=1}^{20} \hat{s}_{\mathrm{h}} \cdot (-\cos(2\pi t + \frac{\pi}{180} \angle s_{\mathrm{h}})) \tag{10.9}$$

With the peak to peak deflection of each sensor, a mean peak to peak deflection is calculated. Scaled by half of the steel coil width b the peak to peak magnetostriction λ_{PP} in μm/m is obtained.

$$\lambda_{\mathrm{PP}} = \frac{2}{b} \cdot \frac{\sum_1^3 s_{\mathrm{pp,i}}}{3} \tag{10.10}$$

Different techniques have been developed in the past to measure magnetostriction in rolling direction, for example, with a Doppler vibrometer and displacement meter [2] or piezoelectric transducers [33,39] (see also Section 9.2). Measurement results of the presented Coil-Method were compared to results from previously proposed approaches. Therefore, the results from [2,33,39] have been converted to indicate the magnetostriction in μm/m. The distribution of the harmonic components of the magnetostriction has been evaluated at different flux densities. The frequency-domain analysis showed that the converted results and the proposed magnetostriction measurement with piezoelectric acceleration transducers are similar (Table 10.3). The 100 Hz harmonic was found to be the most dominant frequency component. With the 100 Hz component as the base line value, the 200 Hz component reaches only between 17-30 % and the 300 Hz harmonic 1-5 %.

Table 10.3: Harmonics of magnetostriction at 50 Hz with different measurement techniques.

Harmonic components	100 Hz	200 Hz	300 Hz
	[%]	[%]	[%]
Mapps & White (1984) at 1.5 T	100	20	5
Hirano (2003) at 1.5 T	100	26	1
Javorski (2012) at 1.7 T	100	17	3
CMS (2016) at 1.7 T	100	30	4

Figure 10.7 shows the measured harmonics of the normalized deflection of a steel coil, over the defined flux density range, at 50 Hz supply frequency. The slope of the

higher harmonic components changes with increasing flux density. Only the first and second harmonics of the magnetostriction strain increase continuously with increasing flux density.
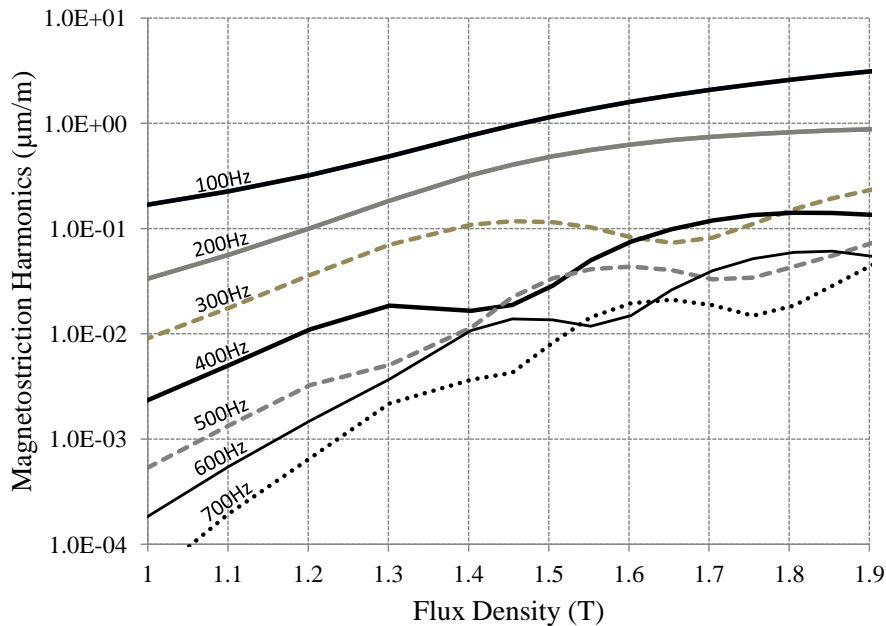
Figure 10.7: Harmonics of the magnetostriction in μm/m at 50 Hz on a test specimen with a mass of 3754 kg, a width of 0.945 m, and inner / outer diameters of 0.525 m / 0.982 m.

10.4 Initial Classification of Steel Coils and Measurement Reproducibility

The following Section discusses classifications of steel coils, according to the determined specific losses and magnetostriction strain. The reproducibility of the measured specific losses and magnetostriction strain with the proposed CMS, expressed by the standard deviation, is evaluated. For the verification, periodic measurements over a period of seven months were performed with steel coils nos. 1, 2 and 3 (Table 10.1) (p. 53).

10.4.1 Scaling of Steel Coils' Specific Losses

Figure 10.8 shows the determined specific losses of a steel coil, one extracted single sheet specimen and the specific no-load losses of a MT. The specific losses of electrical steel determined with a single sheet tester do not match with the specific losses of a transformer in no-load operation as described in Section 8.2 (p. 42). The higher specific losses of the steel coil may be attributed to the bending of the coiled electrical steel as described in [63]. The bending of the material causes tensile and compressive stress which in turn leads to higher losses, as discussed in [64, 65]. This thesis investigates the predictability of the PTs' no-load losses based on the mean specific losses measured for entire steel coils rather than to investigate the reason for the higher specific losses.
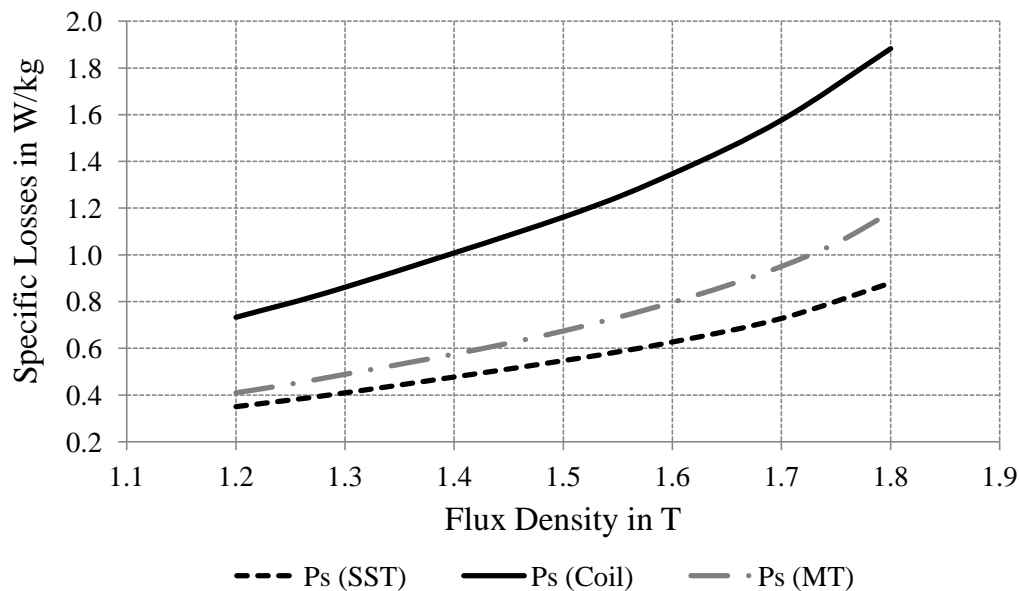
Figure 10.8: Specific losses of a steel coil, one extracted single sheet specimen, and the specific no-load losses of a MT.

Material rejections require measurements with standardized measurement methods including reference measurements on samples certificated from a metrology institute. The second confirms the correct functionality of the used measurement system. Hence, rejections of steel coils can only be based on measurements with standardized measurement methods, such as the single sheet tester or Epstein frame. The steel coils' certificate values are usually based on such standardized methods.

Likewise, comparisons to the steel coils' loss certificate value should be directly comparable during the incoming goods inspection to detect steel coils that are not conform with their certificate values. Therefore, the determined mean magnetic losses of entire steel coils are scaled to a statistical set of measurement values of a standardized single sheet tester.

The statistical scaling approach of the steel coils' specific losses

$$P_{s,scaled} = \frac{P_{h,Coil}}{c_h} + \frac{P_{w,Coil}}{c_w} \qquad (10.11)$$

is based on the measured specific losses of steel coils separated, according to Jordan [27], into the static hysteresis losses $P_{h,Coil}$ and dynamic eddy current losses $P_{w,Coil}$. The factors c_h and c_w obtained from many single sheet measurements determined in a specified time period depending on the material grade and supplier. Thus, the total average losses of a steel coil are transferred to the measurement range of standardized measurement methods.

Such a scaling to standardized measurement methods is required by the quality team which performs the incoming goods inspections. For all further comparisons the scaled specific losses of steel coils are used.

10.4.2 Specific Losses

Fig. 10.9 shows the measured specific loss curves of three different steel coils with the same steel grade. Each steel coil was delivered from a different supplier but all had the same specific loss certificate value. The measured loss curves are scaled with single sheet measurements to allow a comparison with the certification value. Material suppliers A and C from Table 10.2 (p. 56) show a deviation of 4.6 %.

The experimental variance was calculated with [66]

$$s^2 = \frac{1}{n-1} \cdot \sum_{i=1}^{n} (x_i - \bar{x})^2. \qquad (10.12)$$

A mean of all measured specific power losses was calculated for each supply frequency and flux. Using

$$s_{\%} = \frac{s}{\bar{x}} \cdot 100\,\% \qquad (10.13)$$

the relative standard deviation was calculated.
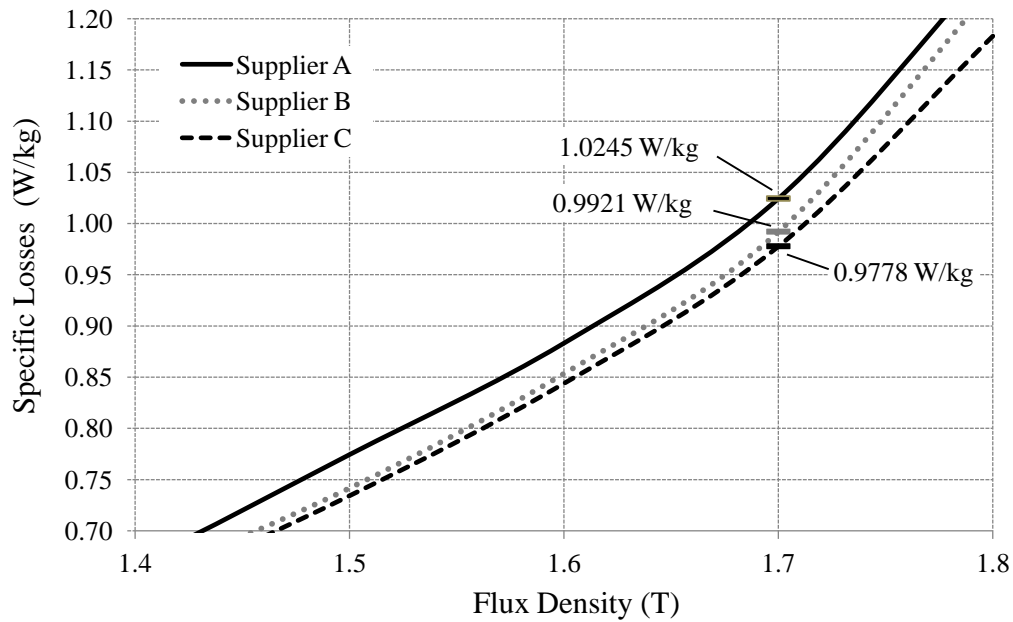
Figure 10.9: Classification of steel coils with same certificated loss values by specific losses determined with the CMS at 1.7 T and 50 Hz.

The reproducibility of the specific power losses P_s in W/kg was determined with a relative standard deviation lower than $s_\% = 1.0\,\%$. This evaluation was performed in a flux density range between 1.0 T and 1.9 T at the supply frequencies of 50 Hz and 60 Hz. Figure 10.10 shows the relative standard deviation of the coils nos. 1 to 3 listed in Table 10.1 (p. 53).

10.4.3 Magnetostriction Strain

Figure 10.11 depicts the measured magnetostriction at 50 Hz of three different steel coils. All three steel coils from the suppliers D, E and F have the same material grade (Table 10.2, p. 56). Each steel coil has a different magnetostriction characteristic.

Figure 10.12 shows the obtained relative standard deviation from the periodic magnetostriction measurements of steel coil nos. 1, 2 and 3 (Table 10.1, p. 53). Note that different paper types were used as electrical isolation between the acceleration transducers and the laminated narrow side of the steel coil. Nevertheless, a relative standard deviation below $s_\% = 3\,\%$ was achieved for the reproducibility over the

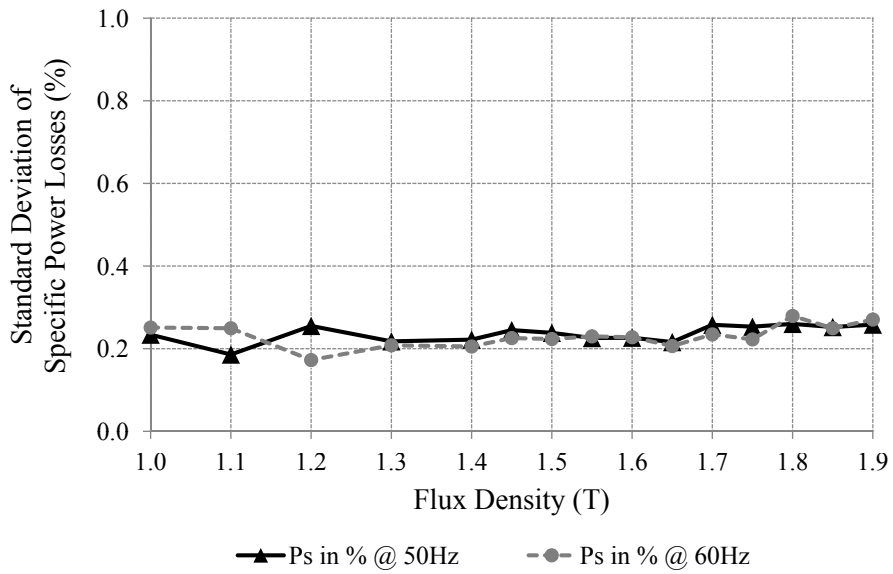Figure 10.10: Relative standard deviation $s_\%$ in measured specific power losses of steel coil nos. 1 to 3 (Table 10.1, p. 53).
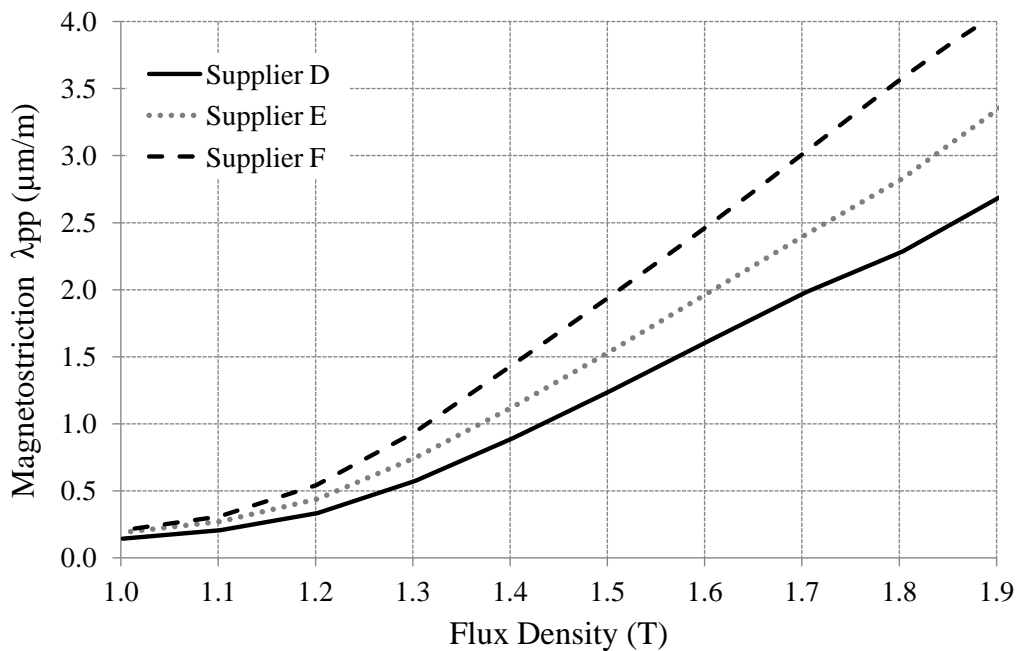
Figure 10.11: Classification of steel coils with same steel grade by magnetostriction levels.
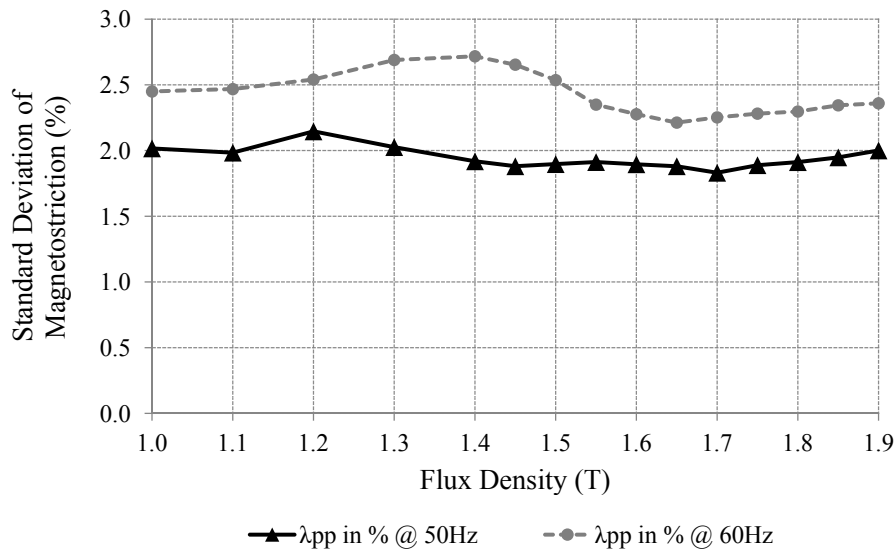
Figure 10.12: Relative standard deviation $s_{\%}$ in measured magnetostriction of steel coil nos. 1 to 3 (Table 10.1, p. 53).

large flux density range from 1.0 T to 1.9 T at 50 Hz and 60 Hz.

10.5 Summary of Coil Measurement System

The main conclusions can be summarized as follows:

- With the CMS each entire steel coil with a mass of up to 6,000 kg independent of its steel grade is investigated using a uniform and consistent approach.

- With this approach the specific losses and the magnetostriction perpendicular to the rolling direction are determined in the flux density range from 1.0 T to 1.9 T at 50 Hz and 60 Hz.

- Reproducibility studies resulted in relative standard deviations below 1 % for the specific losses and below 3 % for the magnetostriction strain.

- It is possible to classify entire steel coils according to their specific losses and magnetostriction strain for a future selective use in PT cores.

- The newly proposed system for the analysis of steel coils offers a unique possibility to identify low noise material before the core material is deployed in PT cores.

Chapter 11

Experimental Noise Studies

This chapter presents an analysis on the steel coils' magnetostrictive properties and how these properties physically relate to the emitted no-load noise of a transformer. The goal is to identify the magnetostrictive quantity to describe the no-load noise of a transformer. Two experimental studies on MTs and PTs provide results[1] of correlation and performance analyses between the steel coils' magnetostrictive properties and the no-load noise of transformers. These analyses should confirm the relation between the magnetostrictive quantity determined with the CMS and the transformers' no-load noise.

11.1 Analysis of Steel Coils' Magnetostriction

To examine the differences between the magnetostrictive characteristics more closely, two steel coils of the domain refined HiB steel grade M85-23P5 were analyzed. First, both magnetostrictive properties, the magnetostriction strain and the vibration velocity, were analyzed with respect to their harmonic content as well as the relationship between the flux density and magnetostriction. As per [4, 5] the vibration velocity has a better relation to the emitted sound of PTs. Also, [68] describes the velocity of a surface vibration as a useful measure for radiated noise.

The measured values were scaled to the width of each steel coil according to [13], to ensure comparability between steel coils with a different size. In addition, the results were compared to the steel coil's certificate value B8. The selected steel coils are further referred to as steel coils A and B. Table 11.1 displays the steel coils' properties and certificate values.

---

[1]Selected results of this chapter have also been published in [15, 16] and [67].

Table 11.1: Properties of steel coils A and B.

Steel Coil	Grade	Weight	Specific Losses (Certificate)	B8 (Certificate)
[-]	[-]	[kg]	[W/kg]	[T]
A	M85-23P5	5092	0.74	1.92
B	M85-23P5	4523	0.76	1.92

11.1.1 Magnetostriction Strain

With the CMS, the magnetostriction strain of both steel coils was measured with acceleration transducers at several flux densities. The measured acceleration was subjected to a Fast Fourier Transform (FFT) analysis. Based on the harmonics of the acceleration signal each harmonic of the magnetostriction strain was calculated with (10.8) (p. 60) at the harmonic frequency nodes.

The peak-to-peak magnetostriction strain was determined based on the reconstructed time signal with (10.9) (p. 61). Exemplarily, Fig. 11.1 shows the determined peak-to-peak magnetostriction strain of steel coils A and B at 50 Hz excitation. Over the measurement range from 1.1 T to 1.9 T, steel coil B shows less magnetostriction strain than steel coil A.

At 50 Hz excitation, the fundamental frequency of the magnetostriction is 100 Hz, also referred to as second harmonic in relation to the excitation frequency. Considering the harmonic content of the magnetostriction strain, only the second and third harmonic are dominant, as shown in Fig. 11.2, similar to what has been reported in [2, 33]. The harmonic spectrum at 1.7 T (Fig. 11.4), compared to 1.5 T (Fig. 11.3), shows an increase of the dominant second harmonic and the higher harmonics of the magnetostriction strain. With increasing flux density, the higher harmonics of the magnetostriction strain increase but have less effect on the total magnetostriction strain, as observed in the linear increase in Fig. 11.1. The noise of PTs increases almost with the square of the flux density. The magnetostriction strain shows a contrary trend, as it increases almost linear with increasing flux density.
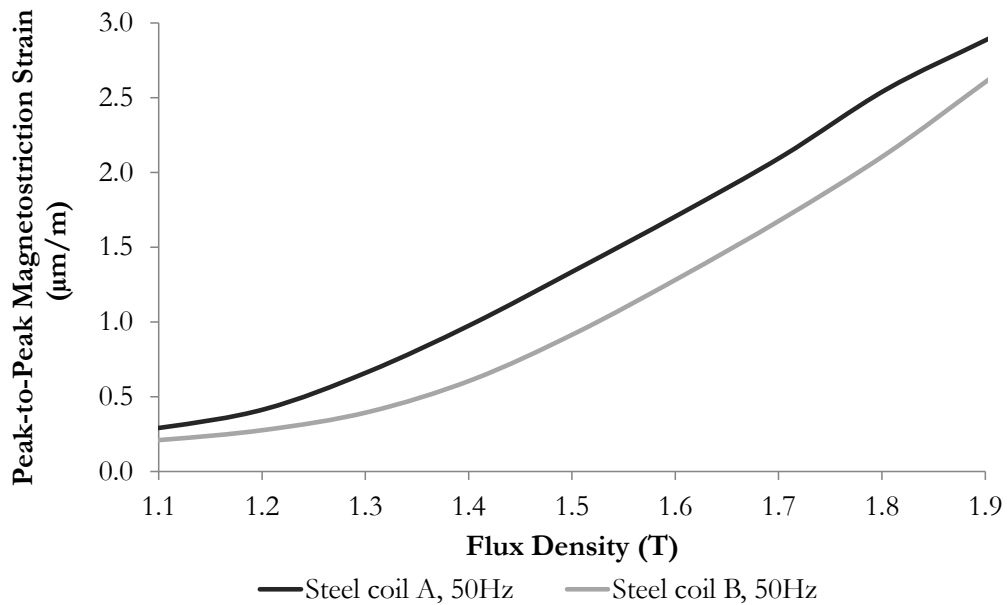
Figure 11.1: Peak-to-peak magnetostriction strain of steel coils A and B determined by the CMS at 50 Hz.

Figure 11.2: Measured harmonics of the magnetostriction strain of steel coils A and B at 1.3 T, determined with the CMS.
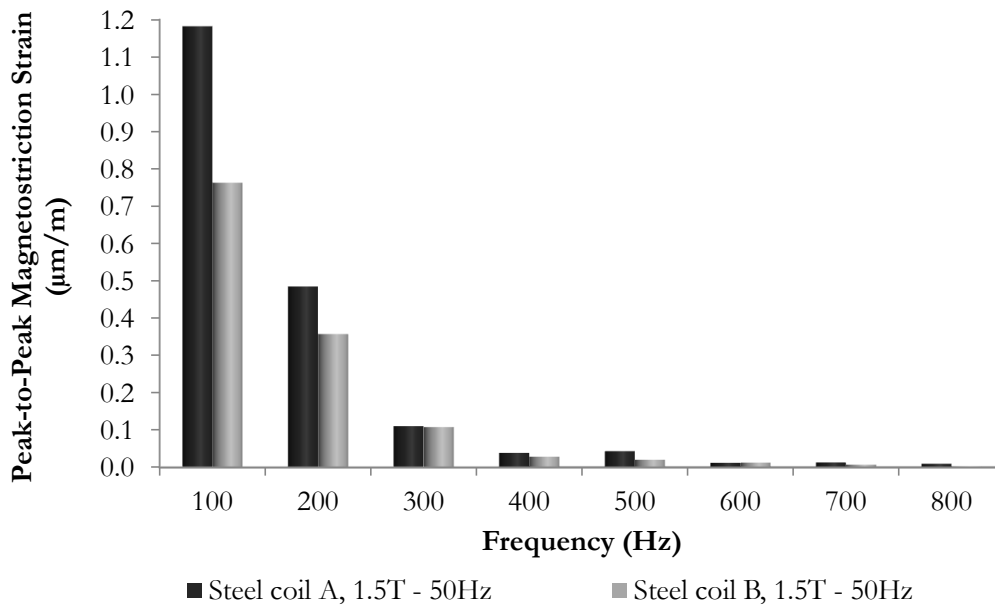
Figure 11.3: Measured harmonics of the magnetostriction strain of steel coils A and B at 1.5 T, determined with the CMS.
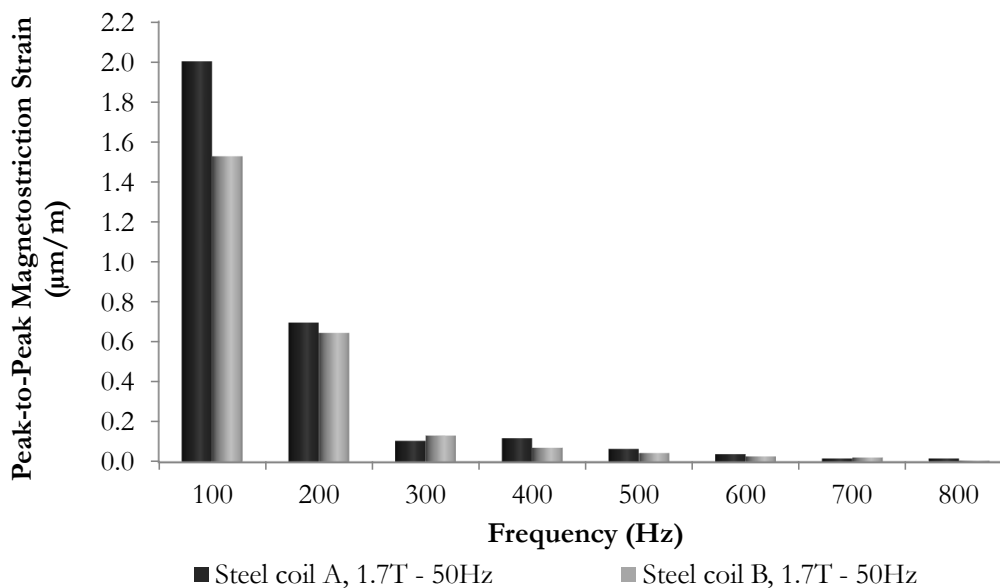
Figure 11.4: Measured harmonics of the magnetostriction strain of steel coils A and B at 1.7 T, determined with the CMS.

11.1.2 Vibration Velocity

In addition to the magnetostriction strain, also the vibration velocities of the steel coils were evaluated. Therefore, the harmonics of the vibration velocity have been calculated according to

$$\hat{v}_{\mathrm{h}} = \frac{\hat{a}_{\mathrm{h}}}{(2\pi f_{\mathrm{h}})} \tag{11.1}$$

and the peak-to-peak vibration velocity was determined based on the time signal of the vibration velocity, reconstructed similarly to (10.9) (p. 61). Similar to (6.1) (p. 30), the vibration velocity is scaled to the steel coil's width to obtain comparability with steel coils of different size.

Figure 11.5 presents the measured vibration velocities of steel coils A and B, where steel coil B outperforms steel coil A. The higher harmonics of the vibration velocity have a higher rise with increasing flux density compared to the magnetostriction strain. Figures 11.6, 11.7, and 11.8 depict the harmonic components at 1.3 T, 1.5 T, and 1.7 T. Table 11.2 shows the harmonic components of the magnetostriction strain in a percentage compared to the dominant second harmonic. The percentage of the higher harmonics of the vibration velocity are depicted in Table 11.3.
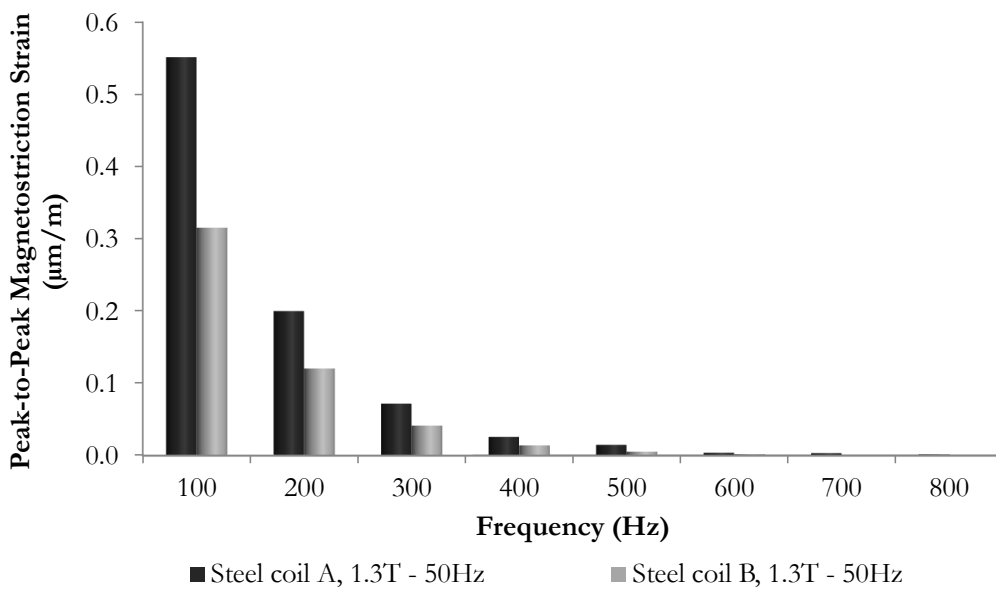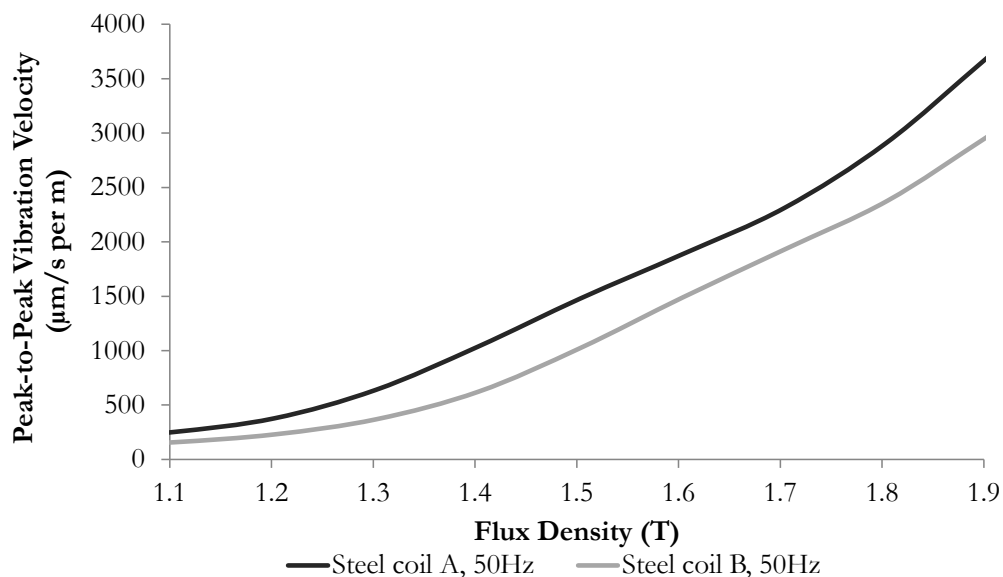

Figure 11.5: Measured peak-to-peak vibration velocity of the steel coils A and B, determined by the CMS at 50 Hz.
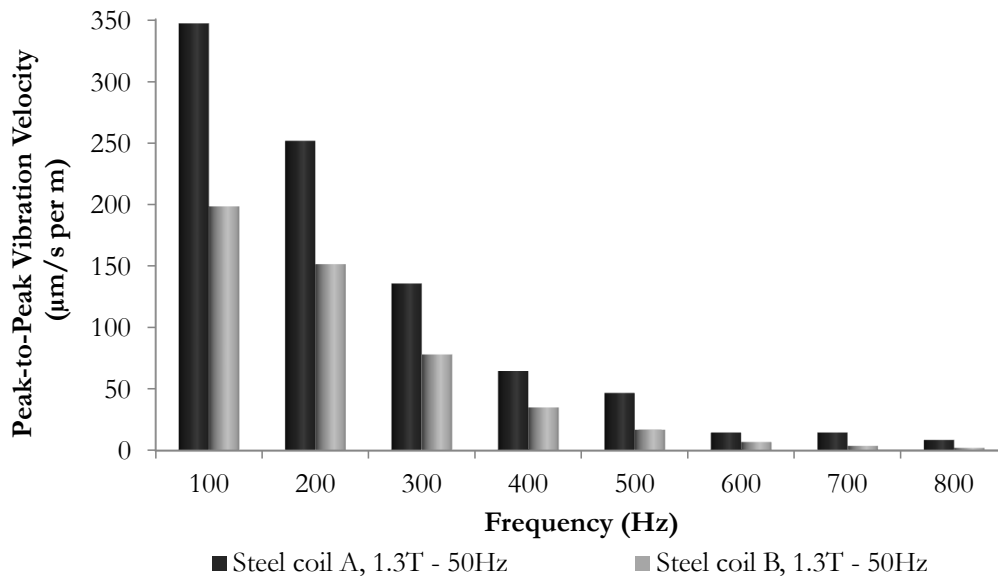
Figure 11.6: Measured harmonics of the vibration velocity of steel coils A and B at 1.3 T.

With increasing flux density the vibration velocity increases more strongly than the magnetostriction strain. This increase can be attributed to the greater increase of the higher harmonics. This tendency was also presented in [4], where it was concluded that this increase in the vibration velocity with increasing flux density can be attributed to the increase of the higher harmonics, which are responsible for the increase in noise in transformers. In general, the higher harmonics are radiated more efficiently and have, in addition, a greater effect on the human ear than low fundamental frequencies [69]. [4] suggests that the vibration velocity should be assessed with the A-weighting according to IEC 61672-1 [70] to emphasize the higher harmonics and to provide a suitable basis for comparisons with the noise of PTs.

Figures 11.9, 11.10, and 11.11 show the A-weighted harmonics at 1.3 T, 1.5 T, and 1.7 T illustrating the influence of the higher harmonics with increasing flux density. The total A-weighted vibration velocity of steel coils A and B is presented in Fig. 11.12 where steel coil B outperforms steel coil A. Above 1.6 T the rise in the A-weighted vibration velocity is higher compared to the non-frequency weighted vibration velocity. Figure 11.13 illustrates the difference between the A-weighted vibration velocity and the vibration velocity without frequency weighting between
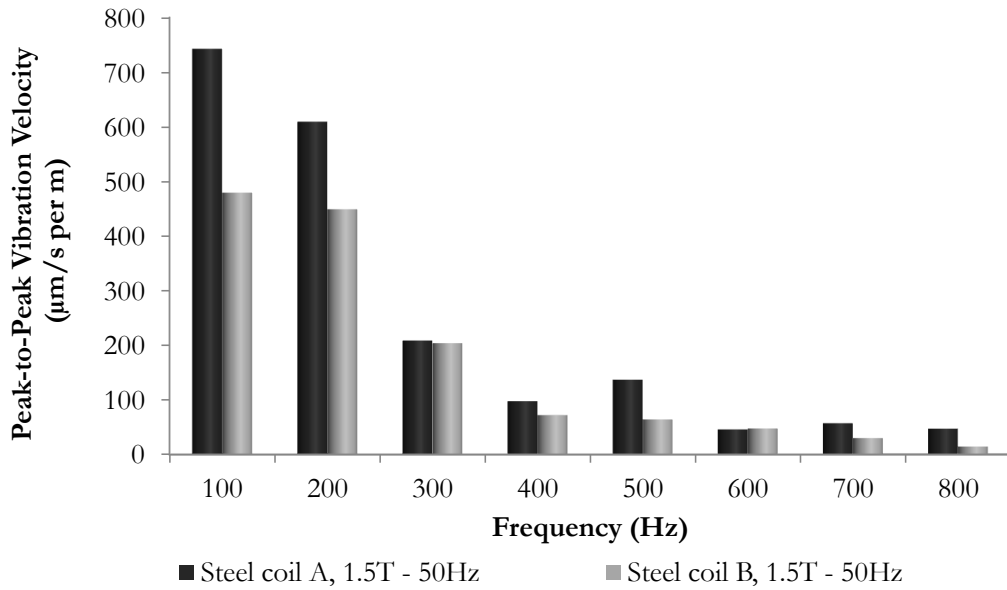
Figure 11.7: Measured harmonics of the vibration velocity of steel coils A and B at 1.5 T.
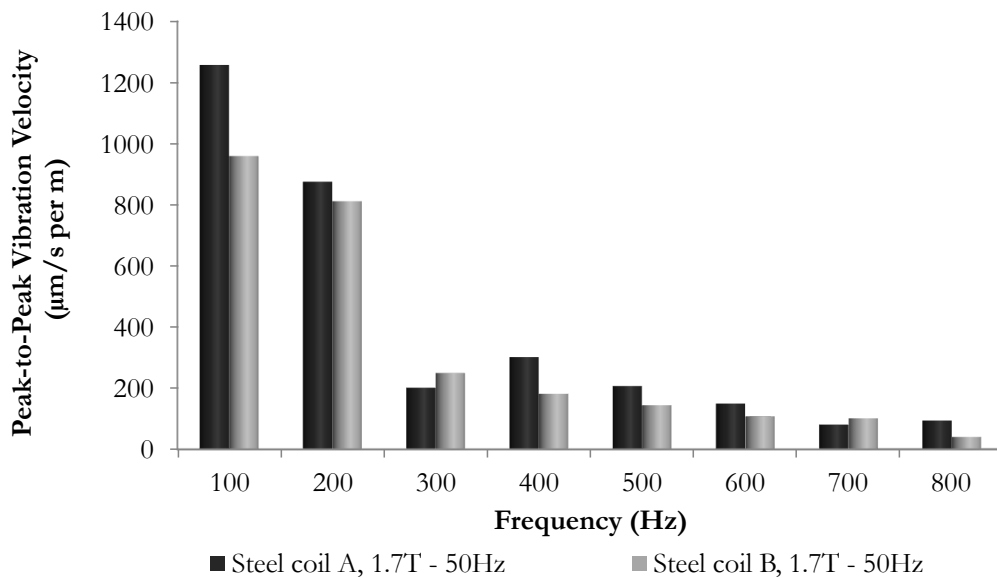
Figure 11.8: Measured harmonics of the vibration velocity of steel coils A and B at 1.7 T.

Table 11.2: Ratio of higher harmonics of the magnetostriction strain compared to the dominant second harmonic.

Frequency	1.3 T	1.5 T	1.7 T
100 Hz	100 %	100 %	100 %
200 Hz	38 %	47 %	35 %
300 Hz	13 %	14 %	5 %
400 Hz	4 %	4 %	6 %
500 Hz	2 %	3 %	3 %
600 Hz	1 %	2 %	2 %
700 Hz	0.3 %	1 %	1 %
800 Hz	0.1 %	0.4 %	0.9 %

Table 11.3: Ratio of higher harmonics of the vibration velocity compared to the dominant second harmonic.

Frequency	1.3 T	1.5 T	1.7 T
100 Hz	100 %	100 %	100 %
200 Hz	76 %	94 %	85 %
300 Hz	39 %	43 %	26 %
400 Hz	18 %	15 %	19 %
500 Hz	9 %	13 %	15 %
600 Hz	4 %	10 %	11 %
700 Hz	2 %	6 %	11 %
800 Hz	1 %	3 %	4 %

1.1 T and 1.9 T at 50 Hz excitation frequency.
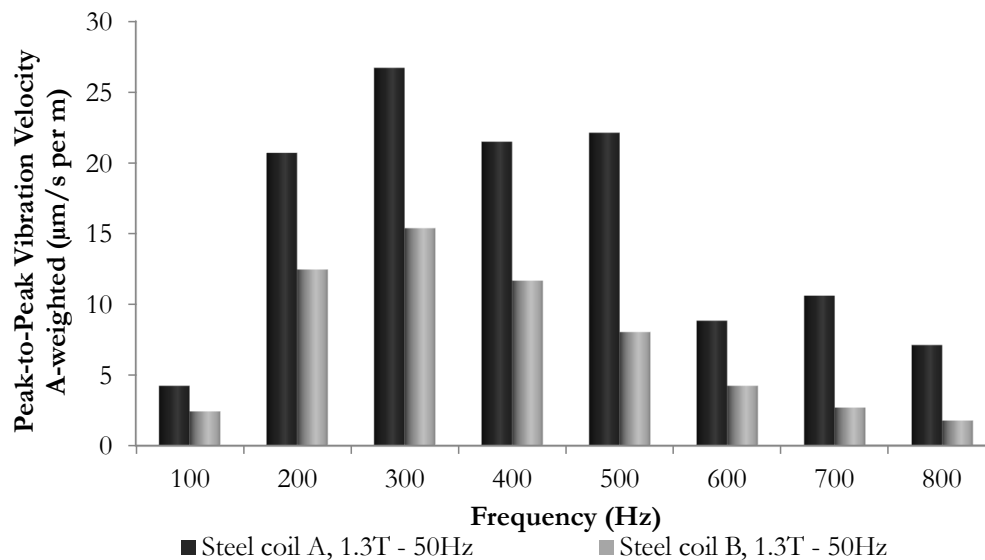
Figure 11.9: Measured A-weighted harmonics of the vibration velocity of steel coils A and B, determined by the CMS at 1.3 T .

11.1.3 Summary of Analyzed Magnetostrictive Properties

The measurement results obtained by the CMS can be summarized as follows:

- Steel coil B has lower magnetostriction strain and vibration velocity compared to steel coil A between 1.1 T and 1.9 T.

- With increasing flux density, the vibration velocity shows a greater increase than the measured magnetostriction strain. This behavior is also known from the noise behaviour of PTs.

- Although steel coils A and B have the same B8 value, the magnetostrictive properties differ.
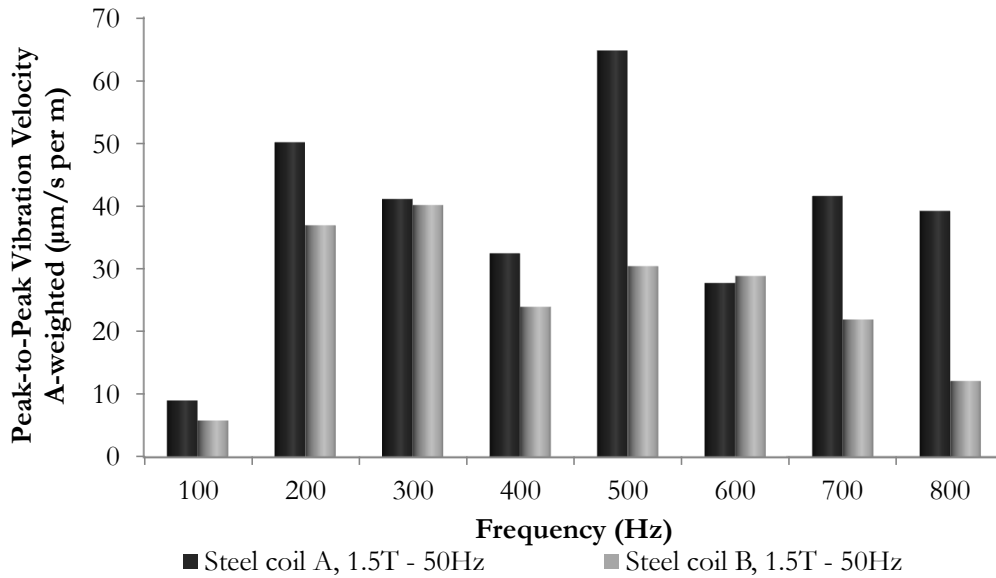
Figure 11.10: Measured A-weighted harmonics of the vibration velocity of steel coils A and B, determined by the CMS at 1.5 T .
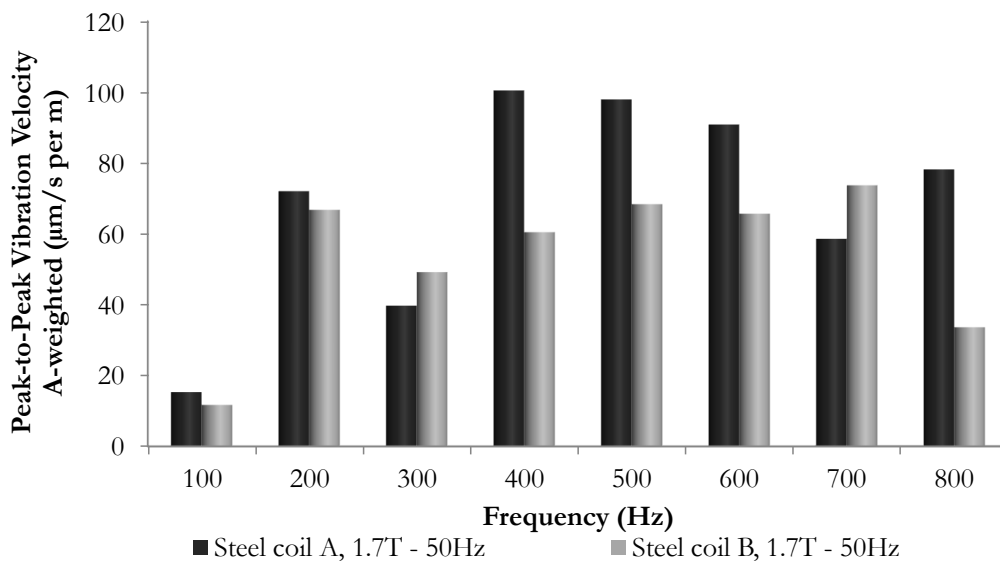
Figure 11.11: Measured A-weighted harmonics of the vibration velocity of steel coils A and B, determined by the CMS at 1.7 T .
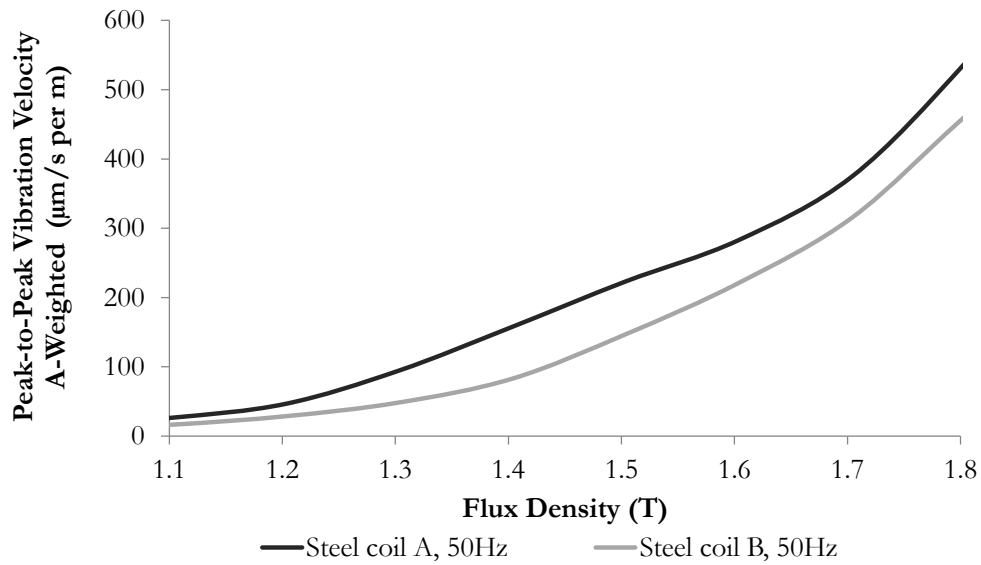
Figure 11.12: Measured A-weighted vibration velocity of steel coils A and B, determined by the CMS at different flux densities.
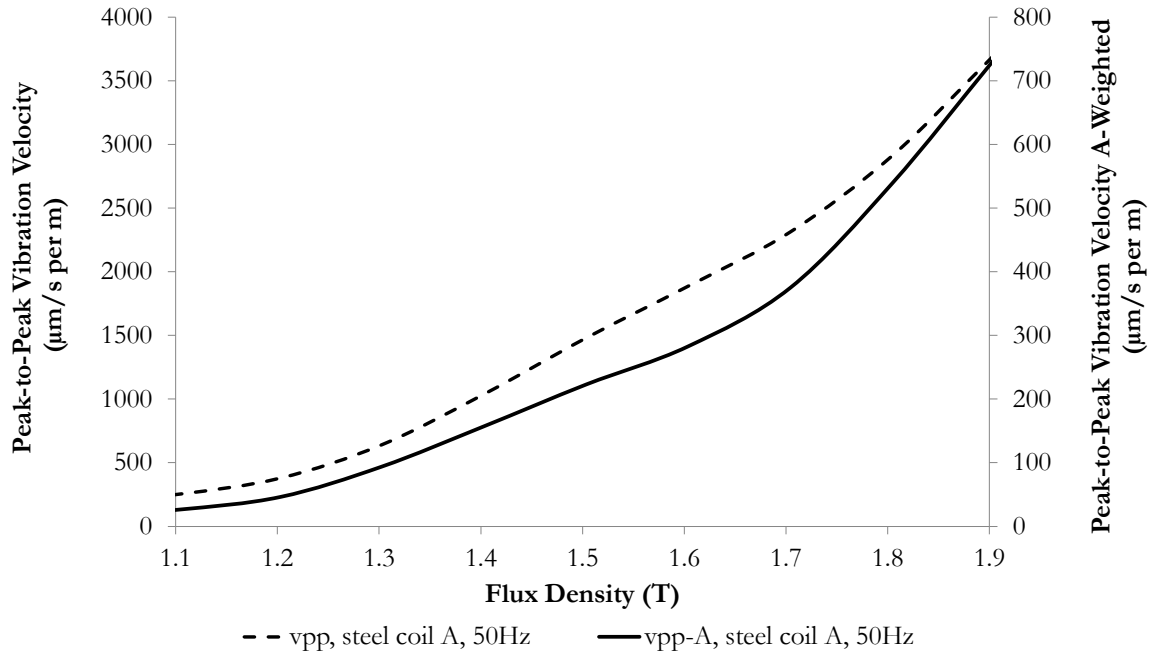
Figure 11.13: Measured peak-to-peak vibration velocity with and without frequency weighting.

These findings show that each steel coil has its own magnetostrictive characteristic. Despite the same B8 value, the steel coils have a different magnetostrictive performance. Based on these results, further studies on oil-immersed MTs and PTs were carried out. In these studies, the vibration velocity was analyzed since this had shown consistency with the findings reported in Section 11.1.2 (p. 73) and [4].

11.2 Study on Model Transformers

This Section reports on an experimental study on MTs, based on the findings in Section 11.1 (p. 69). With this aim, out of the steel coils A and B, respectively, four MT cores were built. This study should reveal a first correlation between the determined magnetostrictive properties of the steel coils and the no-load noise of the MTs measured in the test laboratory.

11.2.1 Design of Model Transformers

The MT cores were designed as three limb cores with one core step and a sheet width of 190 mm. For the stacking, the step-lap technology with six steps was used. The design weight of one MT core is 917 kg and the core has an effective core cross section of 3.5 dm^2. The geometry of the core with vertical step lap is shown in Fig. 11.14.
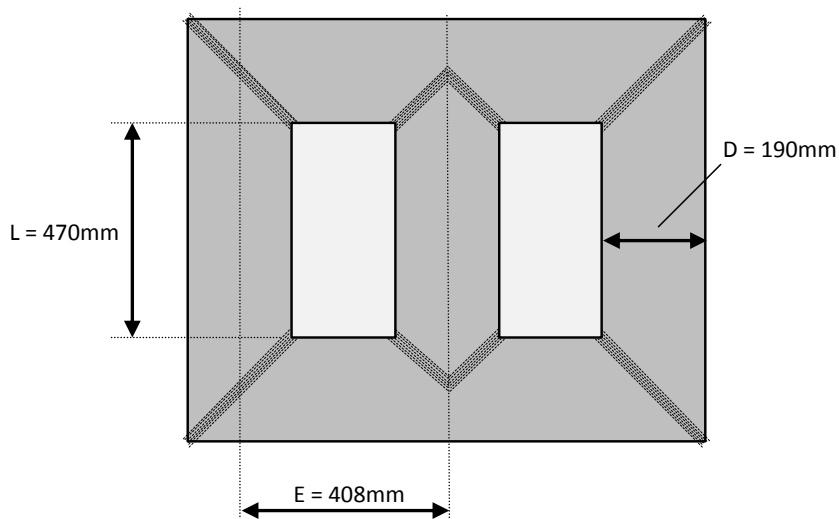
Figure 11.14: Sketch of the model transformer core design.

Every MT core was tested in uniform tanks with oil immersion, to cover the whole noise transmission path. The same clamping structure was used for each transformer core to overcome effects due to different clamping pressure distributions on each core. Preliminary analysis showed that it is necessary to provide a setup including the surrounding oil for all MTs to avoid effects which would lead to misinterpretations within the measured sound pressure. The active part of the MT core including the uniform tanks is shown in Fig. 11.15.

Figure 11.15: Model transformer core, active part, and uniform tank.

The three phase MTs were energized via a star (Y) connection whereby the star-point was connected to earth potential.

11.2.2 Correlation Analysis

Initially, each MT was tested at core excitations from 1.3 T to 1.8 T, whereas the sound pressure level was determined according to [48] with sound pressure microphones, positioned as shown in Fig. 11.16. The measured sound pressure levels $L_{p,i}$ of the four MTs, related to a certain steel coil, were averaged

$$\overline{L_p} = 10 \cdot \log(\frac{1}{4} \sum_{i=1}^{4} 10^{0.1 \cdot L_{p,i}}) \tag{11.2}$$

wherein, corrections for the background noise and reflections were considered.
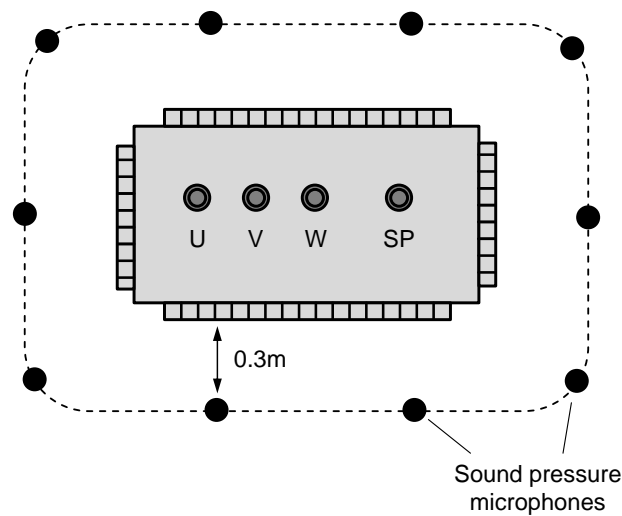
Figure 11.16: Top view - Position of sound pressure microphones around one MT during noise measurements in the test laboratory.

Consequently, the magnetostriction of the steel coils A and B in the MTs can be respectively related to an averaged A-weighted sound pressure level. This ensures a direct link between the magnetostriction of the deployed GOES material and the emitted no-load noise of the MTs.

To assess the relationship between the measured steel coils' vibration velocity determined by the CMS and the averaged sound pressure levels of the MTs, a correlation analysis was performed. Initially, no A-weighting was applied. The analysis resulted in correlation factors higher than 0.95 between flux densities of 1.3 T and 1.8 T. Figures 11.17 and 11.18 demonstrate the graphic interpretation of the strong correlation between the vibration velocity of steel coils A and B without A-weighting and the averaged sound pressure level of the MTs exemplary at 50 Hz and 60 Hz excitation frequency.

A strong dependency was also determined within the analysis of the measured peak-to-peak vibration velocity of steel coil B and the average sound pressure level of the four MTs, manufactured out of steel coil B, with a correlation factor above 0.95. Similar correlation factors were achieved with an additional A-weighting of the vibration velocity. Consequently, for all further investigations, only the A-weighted peak-to-peak vibration velocity is analyzed.
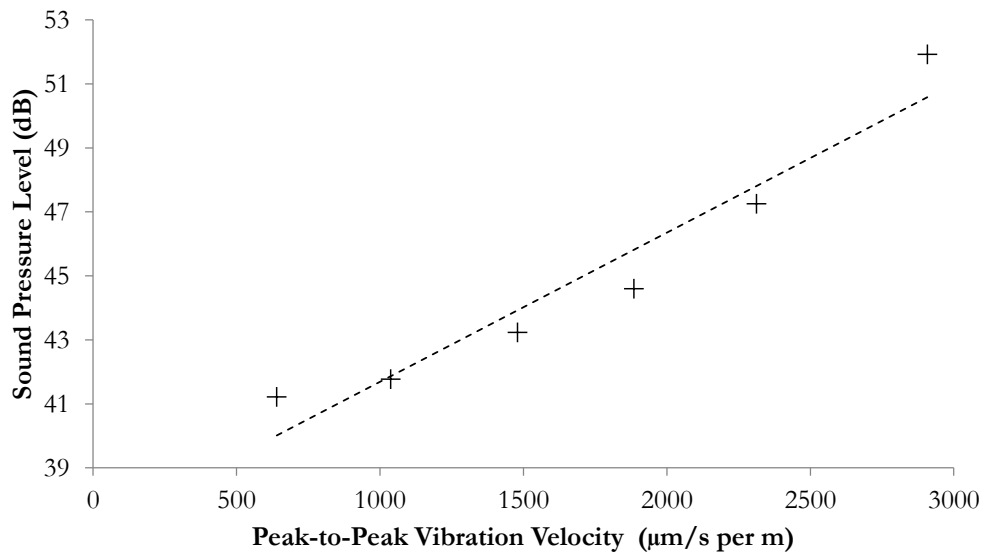
Figure 11.17: Correlation of the average sound pressure level and the vibration velocity of steel coil A (without A-weighting) at 50 Hz excitation frequency.
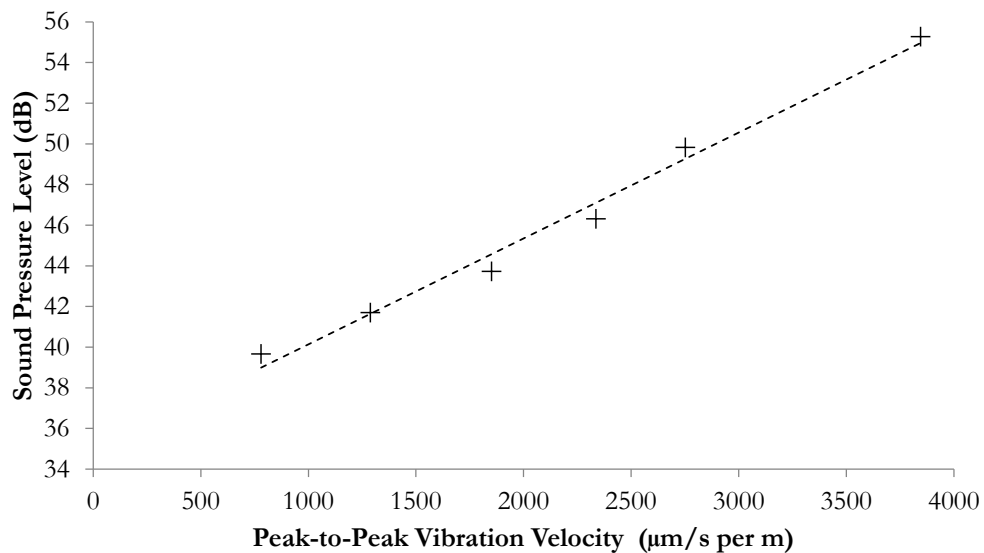
Figure 11.18: Correlation of the average sound pressure level and the vibration velocity of steel coil A (without A-weighting) at 60 Hz excitation frequency.

11.2.3 Performance Analysis

The relationship between the measured A-weighted vibration velocity of the steel coils and the measured sound pressure levels of the manufactured MTs were analyzed. It is expected that higher magnetostriction could lead to higher noise levels. Figures 11.19 and 11.20 show, the A-weighted vibration velocity of steel coils A and B at the excitation frequencies of 50 Hz and 60 Hz. Steel coil B has a lower vibration velocity compared to steel coil A. Figures 11.21 and 11.22 display that also the sound pressure level of the MTs manufactured out of steel coil B is lower compared to that of the MTs manufactured out of coil A. Thus, as expected the performance of the magnetostrictive vibration velocities of steel coils A and B is reflected in the no-load noise.

The trends of the sound pressure levels and the vibration velocity of steel coils A and B with rising flux densities differ. This is explained by the different structures of a steel coil and an MT core. The vibration velocities of steel coils A and B have a higher difference at an excitation frequency of 60 Hz (Fig. 11.20) compared to 50 Hz (Fig. 11.19) above 1.7 T. Similar behavior appeared between the averaged sound pressure levels of the MTs manufactured out of steel coils A and B (Figs. 11.21 and 11.22). This shows a similarity in the trend between the A-weighted vibration velocity and the no-load noise.

Compared to the B8 values (Table 11.1, p. 70) of the steel coils' certificate, the measured magnetostriction of steel coils A and B show a better indication of the no-load noise of the MTs.

11.2.4 Summary of Study on MTs

Four MTs were built out of two steel coils with the same noise relevant B8 certificate value but with different magnetostrictive performances. The study on MTs showed the following results:

- The determined steel coils' vibration velocities determined with the CMS shows a high correlation with the sound pressure levels of the MTs.

- It is possible to predict the MTs' no-load noise by the deployed steel coils' vibration velocity. The steel coils' magnetostrictive performance is reflected in
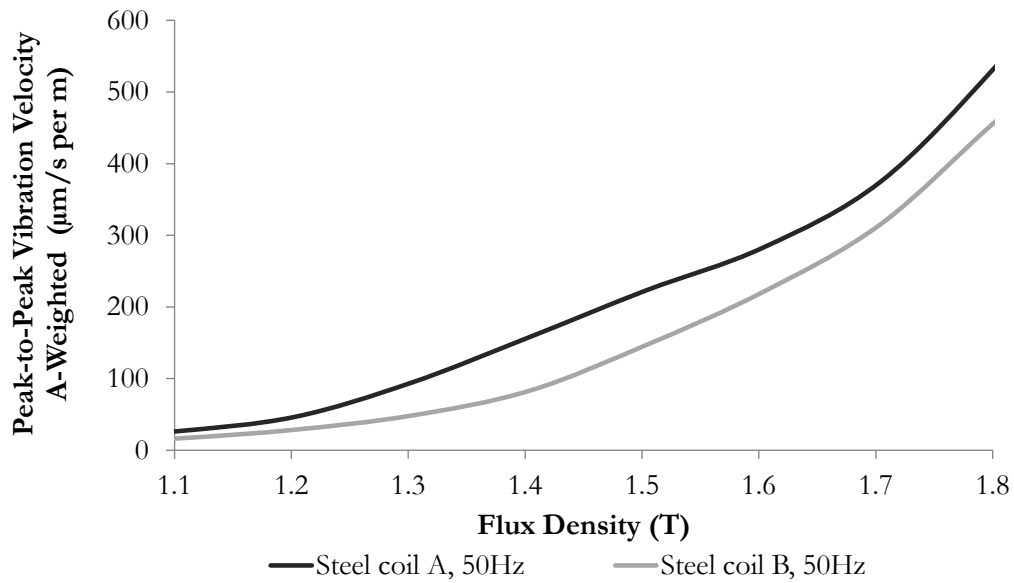
Figure 11.19: Measured A-weighted peak-to-peak vibration velocities of steel coils A and B at 50 Hz excitation frequency.
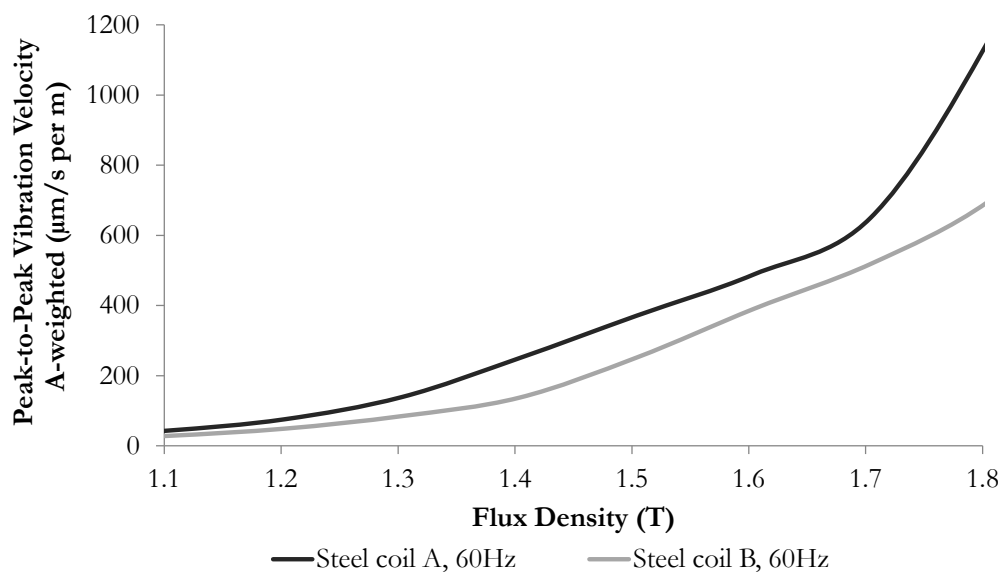
Figure 11.20: Measured A-weighted peak-to-peak vibration velocities of steel coils A and B at 60 Hz excitation frequency.
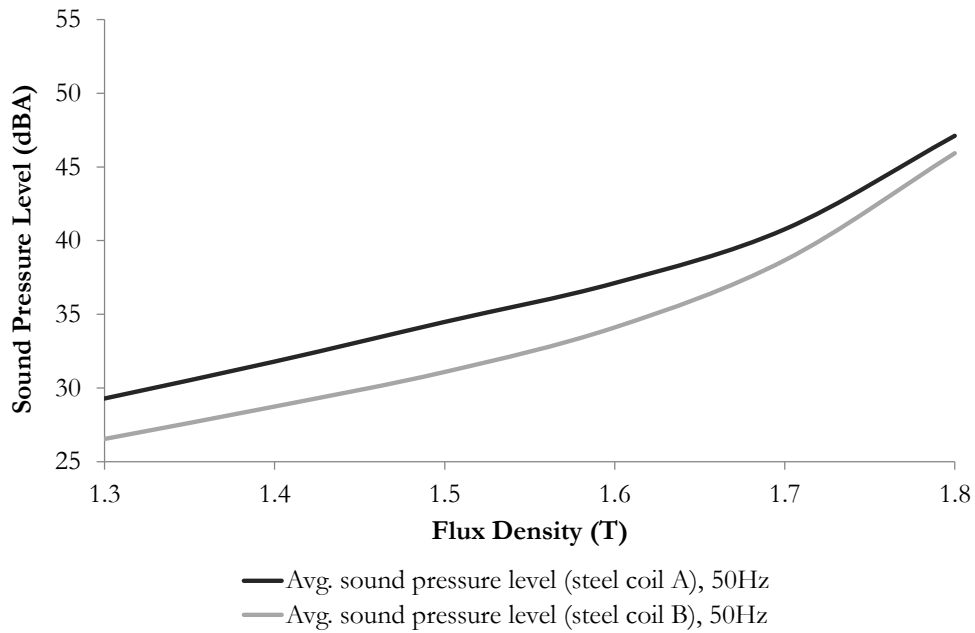
Figure 11.21: Measured A-weighted average sound pressure level of the MTs at 50 Hz excitation frequency.
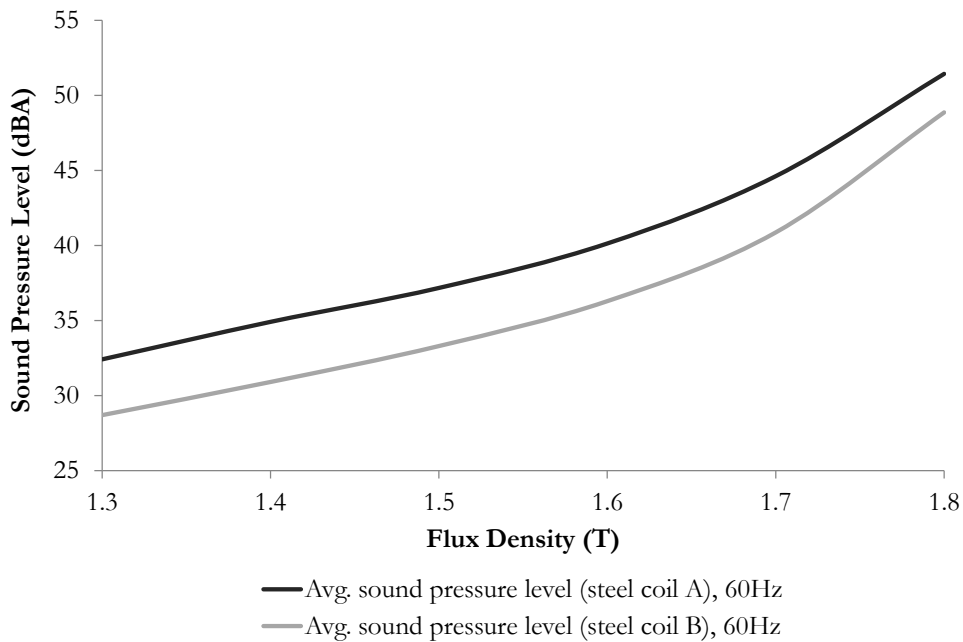
Figure 11.22: Measured A-weighted average sound pressure level of the MTs at 60 Hz excitation frequency.

the MTs' no-load noise. The steel coil with the lower vibration velocity also leads to a lower no-load noise, and vice versa.

- The noise relevant B8 values of the steel coils' certificate does not indicate the no-load noise correctly.

11.3 Study on Power Transformers

In addition to the experimental study on MTs, this Section analyses the no-load noise of four 400 kV one phase oil-immersed autotransformers with respect to the deployed steel coils' magnetostriction. During the study on MT cores, one steel coil could be used to realize even four MT cores; now, one PT core requires several steel coils to be built. To compare the different PT units, the measured A-weighted vibration velocities $v_{\mathrm{pp_A},i}$ of each steel coil were mass weighted with the steel coil's mass m_i for all N steel coils with the mass m_{N} deployed in one PT core.

$$v_{\mathrm{pp_A,total}} = \frac{\sum_i^N v_{\mathrm{pp_A},i} \cdot m_i}{m_{\mathrm{N}}} \tag{11.3}$$

This approach summarizes the performance of the steel coils deployed in one PT to an overall mass scaled value. For further analysis, each PT unit can be represented by a mass weighted vibration velocity. As described in Section 11.2.2 (p. 81), for all further investigations, only the A-weighted peak-to-peak vibration velocity is analyzed.

11.3.1 Design of Large Power Transformers

For each of the four 400 kV one phase oil-immersed autotransformers, a magnetic core with a design weight of 40,000 kg was built. The core steel material was defined as the domain refined HiB material M85-23P5. Out of the selected steel coils, transformer core sheet widths from 90 mm to 900 mm were cut to manufacture the PT cores. Depending on the mass and the width of the steel coils, a different number of steel coils was used to produce the single PT cores, as illustrated in Table 11.4. The nominal flux density of the PTs was designed with 1.64 T. Based on the measured magnetostriction, each steel coil was assigned to either the GOES materials A or B. The GOES materials A and B were deployed separately, each in two PT cores. The aim was to ensure a clear analysis between the measured magnetostrictive properties by the CMS and the determined sound power levels (SPL) of the PTs in the test

laboratory. In the following, the PT cores manufactured with the GOES material A are related to PT units 1 and 2, and the PT cores with the deployed GOES material B are linked to PT units 3 and 4.

The one phase PTs were energized via the tertiary voltage winding with an open high voltage winding.

Table 11.4: Overview of the deployed steel coils in PT units 1 to 4.

PT Unit	GOES Material	Number of Steel Coils
1	A	24
2	A	30
3	B	29
4	B	33

11.3.2 Correlation Analysis

This Section evaluates the correlation of the magnetostrictive properties of the deployed steel coils and the PTs' SPLs. Therefore, the SPLs of the PTs were measured in the test laboratory in no-load conditions at the flux densities 1.2 T, 1.47 T, 1.64 T, and 1.8 T with a sound intensity probe during walk around measurements, according to the standard IEC 60076-10 [48].

Generally, each single steel coil is measured within the CMS with a standard measurement sequence covering flux densities between 1.0 T and 1.9 T in 0.05 T steps. In order to provide comparable values to the measured SPLs at different core excitations, the measured vibration velocities of each steel coil were interpolated. Based on the interpolated values, the vibration velocities at 1.2 T, 1.47 T, 1.64 T, and 1.8 T were determined. Due to the fine flux density steps, an accurate determination of the vibration velocity at this certain flux densities is possible.

The performed correlation analysis resulted in correlation coefficients higher than 0.94 between each PT unit and the vibration velocity of the deployed steel coils (Table 11.5). The graphic interpretation of the relation between the mass weighted peak-to-peak vibration velocities and the PTs' SPLs is given, for example, for PT unit 1 and 4 in Figs. 11.23 and 11.24. Each data point represents a different core excitation
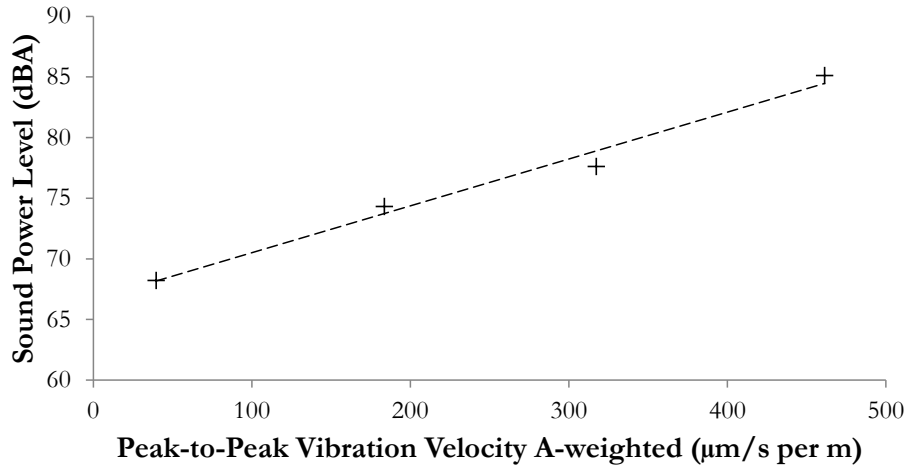
Figure 11.23: Correlation of measured mass weighted peak-to-peak vibration velocity (A-weighted) of the deployed steel coils and SPL of PT unit 1.
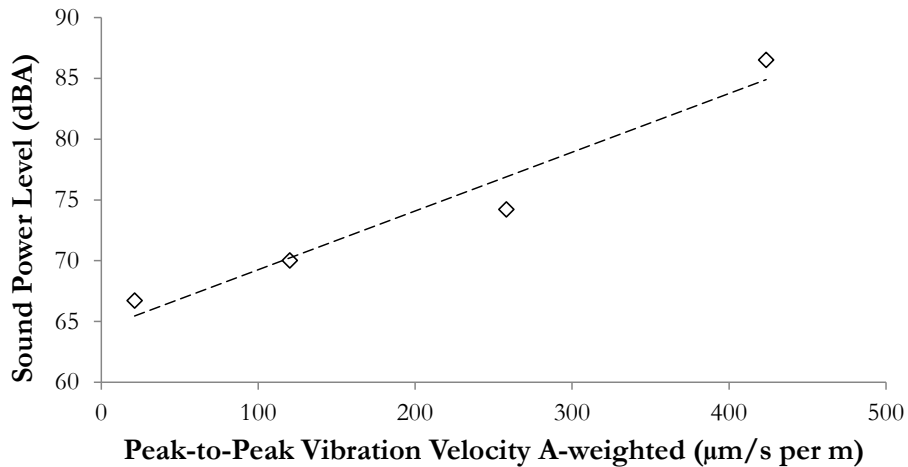
Figure 11.24: Correlation of measured mass weighted peak-to-peak vibration velocity (A-weighted) of the deployed steel coils and SPL of PT unit 4.

of the transformer.

Table 11.5: Correlation coefficients between measured vibration velocities and the PTs' SPLs.

PT Unit	Correlation Coefficient
1	0.992
2	0.990
3	0.941
4	0.974

11.3.3 Performance Analysis

Initially, only the performance differences between the magnetostrictive properties of materials A and B were evaluated. Figure 11.25 displays the A-weighted vibration velocity of the deployed steel coils in all four PT units. Ultimately, materials A and B clearly differ in the vibration velocity. The comparison of the steel coils' mass weighted vibration velocity identified material B as having less vibration velocity than material A. The mean deviation in the vibration velocity between materials A and B was determined to be 42.7 μm/s per m.

Comparing the steel coils of material A, manufactured in PT units 1 and 2, a similar performance was observed. The deviation of the vibration velocity was determined to be 3.3 μm/s per m. The steel coils of material B deployed in PT units 3 and 4 displayed with 8.0 μm/s per m a little higher deviation to each other.

Above 1.5 T the A-weighted vibration velocity of material B has a higher rise compared to material A. The vibration velocity of material A shows a linear increase between 1.2 T and 1.64 T. This behavior was expected to be also seen within the SPLs of the PT.

Figure 11.26 illustrates the core noise performances of the PT units. PT units 1 and 2 show a higher SPL up to 1.75 T than the PT units 3 and 4. This result coincides with the magnetostrictive performance of the mass weighted vibration velocity shown in Fig. 11.25. Considering only unit 3 and 4, a higher deviation in the SPL was determined, but with less than 1.5 dB(A). This is possible, due to the small deviation
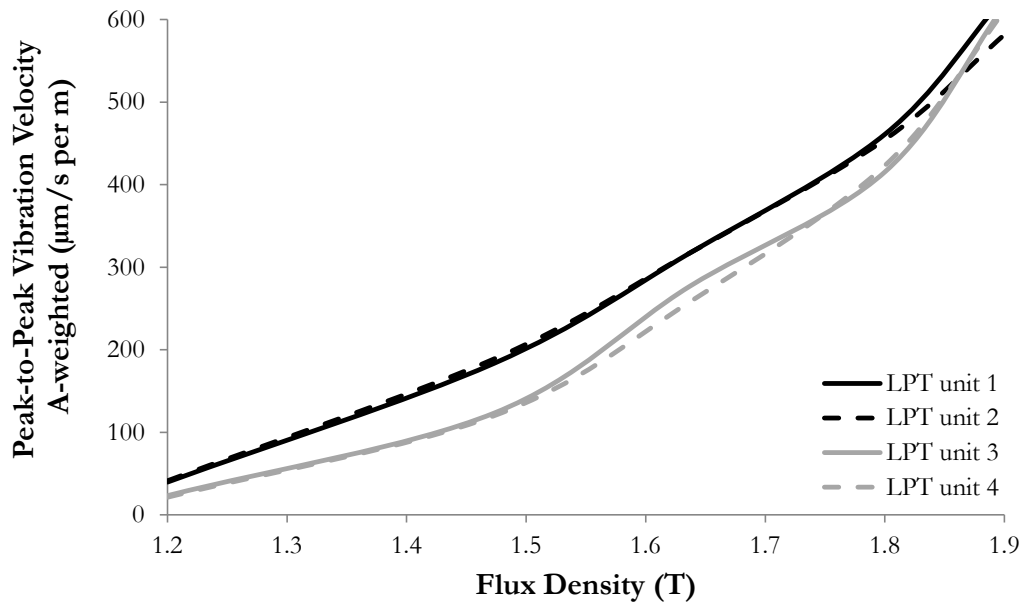
Figure 11.25: Mass weighted peak-to-peak vibration velocity (A-weighted) of the steel coils deployed in PT units.
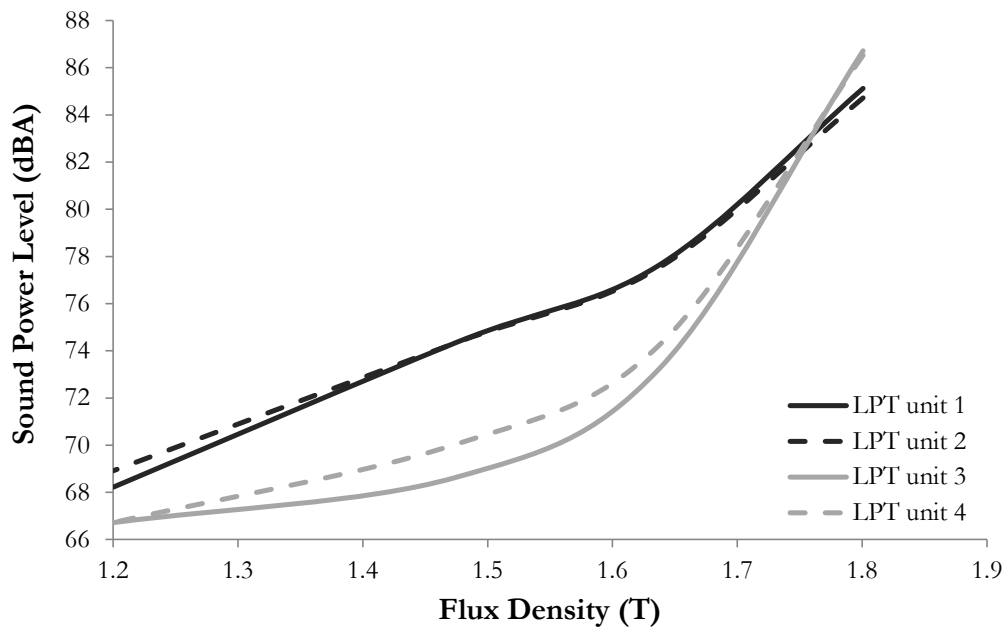
Figure 11.26: Sound power levels of the PT units 1 to 4.

between the steel coils' vibration velocity of material B, as described above. The highest deviation between the average SPLs of PT units 1 and 2 compared to units 3 and 4 was found to be at 1.473 T with 5.0 dB(A), where PT units 3 and 4 display very low SPL, compared to units 1 and 2.

Above 1.5 T, the trend of the SPLs of units 3 and 4 shows a higher rise. This tendency corresponds with the measured trend within the vibration velocity (Fig. 11.25). It appears that material B has been optimized for flux densities between 1.4 T and 1.5 T. The trend of the SPLs of PT units 1 and 2 relate to the trend of the measured vibration velocity. Both the vibration velocity and the SPLs have a linear increase between 1.2 T and 1.64 T.

For each PT, a mass weighted B8 value was calculated based on the certificate values of the deployed steel coils: PT units 1 and 2 deployed with material A have both a B8 value of 1.931 T, whereas the B8 value of PT units 3 and 4 resulted both in 1.924 T. Hence, PT units 1 and 2 were expected to have a lower core noise compared to units 3 and 4. Unfortunately, the investigations between the mass weighted B8 value and the no-load noise of the PTs did not confirm this relationship. Hence, vibration velocity is understood to be a better indicator of the no-load noise of the final transformers than the B8 value.

11.3.4 Summary of Study on PTs

Four PTs were built out of several steel coils. It was recognized that materials A and B clearly differ in the vibration velocity. Within the PT units 1 and 2 the material A with higher vibration velocities was deployed. The PT units 3 and 4 were manufactured with the material B that outperforms material A. The results of the analyses can be summarized as follows:

- The measured A-weighted vibration velocity shows a high correlation to the PTs' no-load noise.

- Material B with low vibration velocities led to low no-load noise of the PT units 3 and 4. Material A with higher vibration velocities compared to material B led to a higher no-load noise of PT 1 and 2.

- The steel coils' magnetostriction of material B was identified to be optimized for a flux density of 1.5 T. In addition, also the no-load noise of the PT showed a low noise emission at 1.5 T.

- The mass weighted B8 value of each PT showed no correct indication of the no-load noise. The vibration velocity is therefore understood to be a better indicator of the no-load noise of the final transformers.

Chapter 12

Experimental Loss Studies

Each single steel coil, delivered from a core steel manufacturer, is marked with a certificate containing the material's specific power losses at the flux density of 1.7 T and the excitation frequency of 50 Hz. Standardized Epstein frame [8] or single sheet tests [9] are usually performed to verify the material's specific losses. Therefore, specimens are extracted mostly at the beginning as well as at the end of the coiled GOES material. With the CMS, the specific power losses of each entire steel coil, to be used within a PT core, are determined. A quality check of the total GOES material planned to be deployed in a transformer core should allow a better predictability of the no-load losses. Within this chapter the following is investigated:

- With the CMS deviations in the specific losses of steel coils were determined. It is expected that low specific losses of steel coils lead to low no-load losses of transformers, and vice versa. If that proves true, it is possible to predict the no-load losses of transformers by the measured steel coils' specific losses.

- Core steel manufacturers provide a loss certificate value for each steel coil. The conformity between the steel coils' certificate values and the measured steel coils' specific losses is analyzed to reveal the certificates confidence.

- Parameters, such as the clamping pressure and the core mass, that may affect the validity of the results are also discussed within this chapter.

Two experimental studies with MTs and PTs are presented, where the relation between the steel coils' specific losses, determined with the CMS, and the no-load losses, measured with a power analyzer, is investigated.[1]

---

[1]Selected results of this chapter have also been published in [16].

12.1 Test Series of Eight Model Transformers

In this study eight MTs were built to investigate the conformity between the steel coils' specific losses determined with the CMS and the no-load losses of the MTs. The steel coils' certificate values and extracted single sheet measurements are included to evaluate which of these loss quantities results with the best prediction for the MTs' no-load losses. The selected MT cores were designed according to the design described in Section 11.2.1 (p. 80). The joints are manufactured with the step-lap technology of six steps which is also used in PTs.

The three phase MTs were energized via a simple star connection of a test winding with 17 turns per limb. The star-point was connected to earth potential. Figure 12.1 displays the electric circuit for the investigations on MTs with 1: test object, 2: current transducer, and 3: voltage divider.
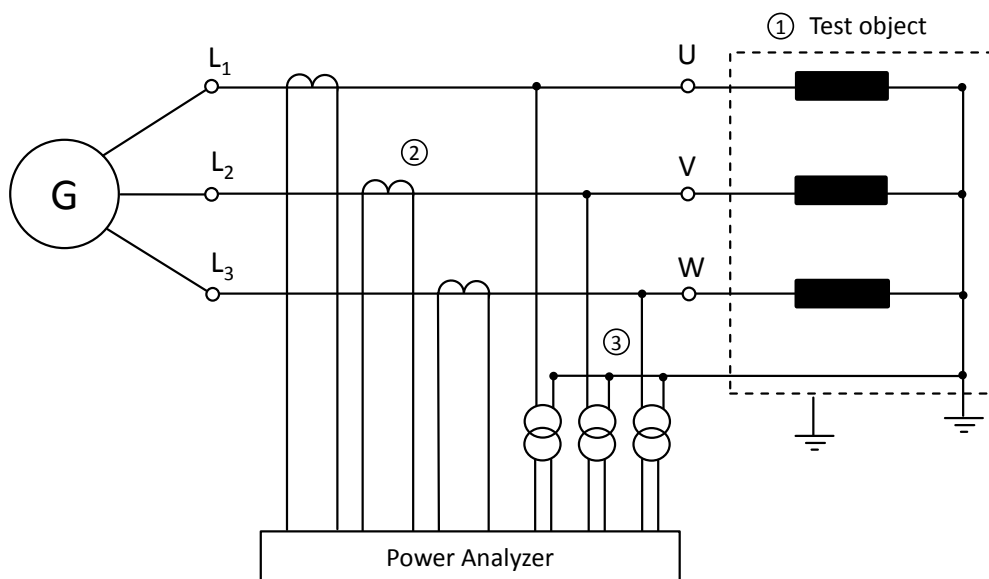
Figure 12.1: Electric circuit of the no-load investigations on MTs.

12.1.1 Selection of Steel Coils

Seven steel coils of the same steel grade M85-23P5 were selected according to their certificate value, determined by the steel coil manufacturer, and the steel coils' specific losses determined with the CMS just after their delivery.

Out of each steel coil two single sheet specimen were extracted at the steel coils beginning along the steel coils' width. The specific losses of both single sheet measurements were averaged to provide a representative value for one steel coil.
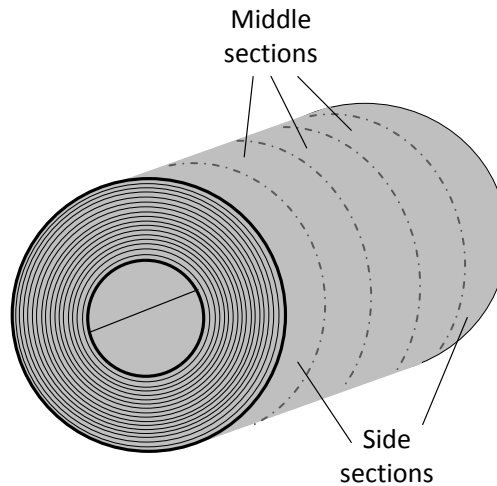
Figure 12.2: Middle and sides sections with a width of 190 mm as separated within the loss study on MTs.

Out of each steel coil the middle sections were used to manufacture the MT core. For comparison, an additional MT core was built using the side sections of a steel coil. On average, each steel coil was divided into five 190 mm wide sections. The sections near the steel coils' edge area are referred to as side sections, and the other as middle sections, as illustrated in Fig. 12.2.

The side sections may have a different texture compared to the middle sections: The coiled steel may contain a thinner rolled steel, caused by inhomogeneous pressure distributions when the steel passes the rolling processes, as presented in [71]. Due to the transport the steel coils' side sections may be also damaged. Therefore, the main focus of this investigation was laid on the middle sections of the steel coils. In Table 12.1 the steel coils' certificate values, the determined specific losses and the referencing coil sections are shown.

12.1.2 Influencing Parameters

It was recognized that the weight of the single MT cores differed with up to 8 kg to the design weight of 917 kg. This deviation can be attributed to the different thickness

Table 12.1: Selected steel coils of the HiB material M85-23P5 for the manufacturing of eight model transformer cores including the measured core weight.

Steel Coil	Certificate	Coil Measurement	Section	MT Core	Weight
[-]	[W/kg]	[W/kg]	[-]	[-]	kg
A	0.74	0.851	middle	1	913
B	0.74	0.817	middle	2	918
C	0.70	0.765	middle	3	918
D	0.80	0.830	middle	4	913
E	0.72	0.757	middle	5	909
F	0.72	0.801	middle	6	910
G	0.74	0.819	middle	7	915.5
G	0.74	0.819	side	8	917

of the core sheets used for stacking the MT cores. Lower core sheet thickness results within the same core stacking height in a higher *FF* and hence a higher effective iron cross section A_{fe}. It is necessary that differences of the effective iron cross section A_{fe} between single MTs are avoided, as they lead to a different flux density in the MT core at the same excitation voltage. Therefore, the weight of each MT core was determined during the manufacturing process before tanking. In Table 12.1 the measured weights of the eight MT cores is provided. Depending on the MT's core weight the excitation voltage was calculated according to (10.1)-(10.3) (pp. 51-52) in order to achieve the necessary average flux density in the MT core, and hence provide a sufficient basis for comparisons. Figure 12.3 shows the specific losses of the MTs with and without the corrected excitation voltage based on the measured mass of each MT. The uncorrected specific losses are based on the design weight of 917 kg. As a result, the specific losses were corrected by up to 3 %.

Before tanking the torsional moment of the clamping structure of each MT core was set to 28 Nm which corresponds to 0.3 N/mm^2. Although the pressure applied of the clamping system on the laminated MT core is perpendicular to the core sheets' surfaces, additional stress in the core sheets may lead to higher losses, as shown in [64, 65]. To exclude such additional influencing parameters, the same clamping pressure was applied on each MT core.
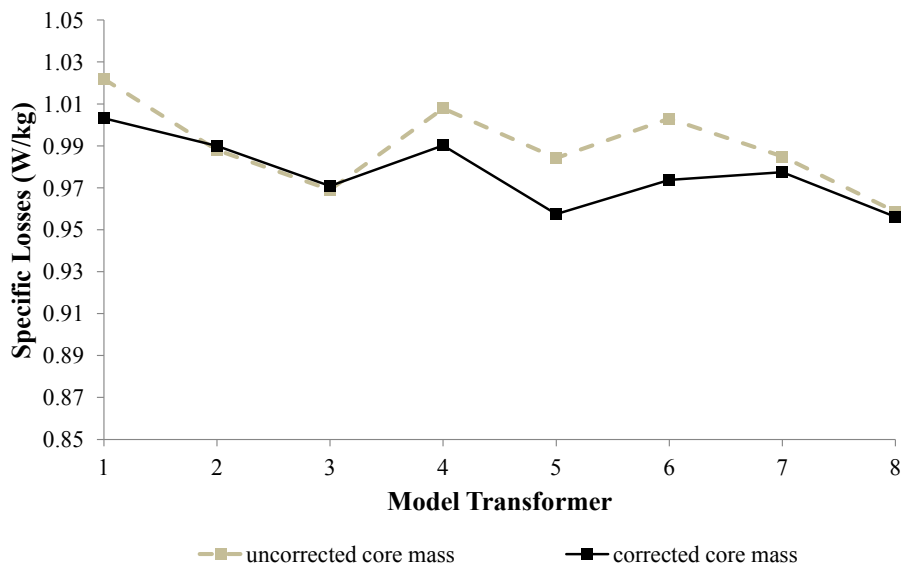
Figure 12.3: Specific losses of the MTs before and after the correction of the excitation voltage by the measured MTs' mass.

12.1.3 Correlation Analysis

Figure 12.4 shows the certificate values of the steel coils, the determined specific losses of the single sheet measurements, the coil measurements and the specific no-load losses of the MTs, at a flux density of 1.7 T, determined at 50 Hz. Generally, the certificates, the single sheets' values and the steel coils' specific losses seem to show a similar trend as the MTs' no-load losses. But, for example, the no-load losses of MT no. 1 could be predicted by the specific loss value of 0.85 W/kg, measured with the CMS; the specific loses of 0.80 W/kg, measured by a single sheet tester; or with the steel coil's certificate value of 0.74 W/kg. Indeed, this variation of about 13 % would include a uncertainty in the prediction of the no-load losses. Hence, the measurement method that predicts the no-load losses best, has to be identified. Therefore, a correlation analysis was carried out with the following results:

- The certificate values of the steel coils show a low conformity as the correlation factor is only 0.45. A forecast based on the certificate value would therefore lead to wrong loss predictions. The single sheet measurements provide a better relationship to the measured no-load losses of the MTs expressed by a correlation factor of 0.61. The best relationship to the MTs' no-load loss was
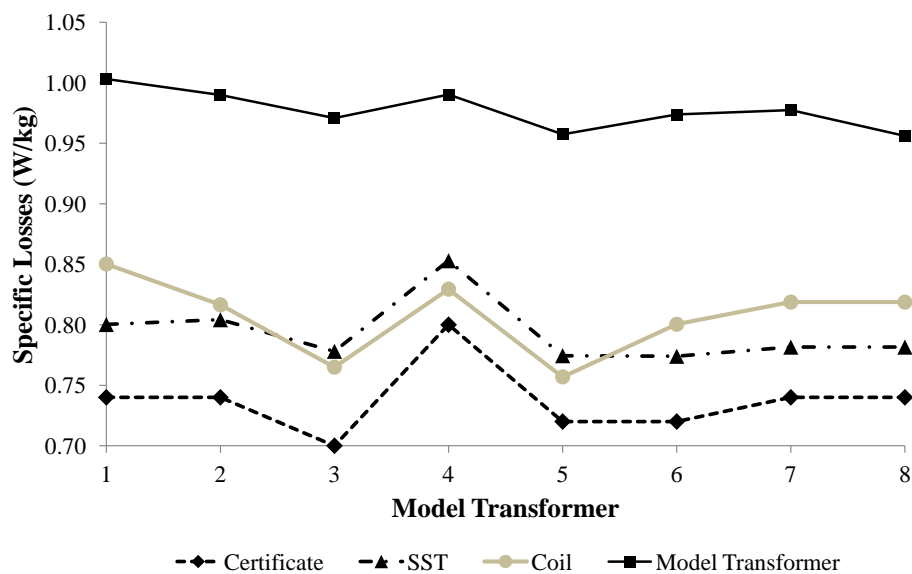
Figure 12.4: Specific losses of the single sheet measurements and coil measurements compared to the steel coils' certificate value and the specific no-load losses of the model transformers at 1.7 T and 50 Hz excitation frequency.

found to be by the determined specific losses of the steel coils with a correlation factor of 0.7.

- Steel coils with high specific losses also lead to high no-load losses in the MTs, and vice versa. Also the MTs with the highest losses (MT no. 1) and the lowest losses (MT no. 5) could only be predicted with the steel coils' specific losses rather than with the certificate values or the single sheet values. Compared to the single sheet specimen more material is under test within a coil measurement. This may be the reason that it results in a better consistency with the no-load losses of the MTs.

- Only MT no. eight had lower losses as expected, whereby in this case the side section of a steel coil was used to build the MT core. The better performance may be attributed to the possible thinner rolled electrical steel as described above. Thin steel would result into lower eddy current losses, and hence reduced overall iron losses. As the thickness was not measured, this explanation is only an assumption.

12.2 Specific Losses of Steel Coils Versus No-Load Losses of PTs

Building on the results of the previous study on MTs, the specific losses determined within the CMS are expected to be good predictive values for PTs' no-load losses. Different to the study on MTs, where one section of a steel coil was used to build the transformer core, now up to 33 steel coils with a different mass were used to build the magnetic core of one PT. Steel coils were assigned to either the GOES materials A or B depending on the measured magnetostriction, as presented in Section 11.3.1 (p. 87). The GOES materials A and B were deployed separately, each in two PT cores. In the following, the PT cores manufactured with the material A are related to PT units 1 and 2, and the PT cores with the deployed material B are referred to PT units 3 and 4. The specific losses of materials A and B determined with the CMS showed similar values. Therefore, it was expected that also the no-load losses of the four PT units are similar.

Figure 12.5 displays the electric circuit for the investigations on PTs.

12.2.1 Correlation Analysis

The mass weighted specific losses

$$P_{\text{s,total}} = \frac{\sum_i^N P_{\text{s,i}} \cdot m_{\text{i}}}{m_{\text{N}}} \tag{12.1}$$

for each PT were calculated with the specific losses of each steel coil $P_{s,i}$, its mass m_i for all N steel coils with the mass m_N deployed in one PT core, to apply a correlation analysis, in spite of the different mass of each steel coil.

In total four different flux densities were analyzed, related to 80 %, 90 %, 100 %, and 110 % rated voltage of the PT's nominal flux density of 1.64 T. At each flux density a correlation analysis was carried out. The accumulation of data points in Fig. 12.6 represents the specific losses and the no-load losses at a constant flux density of all four PT units.

The results illustrate a significant correlation between the specific losses of the steel coils and the PTs' losses in no-load condition. The specific power losses as well as the no-load losses of each PT unit cumulate at the respective excitations.
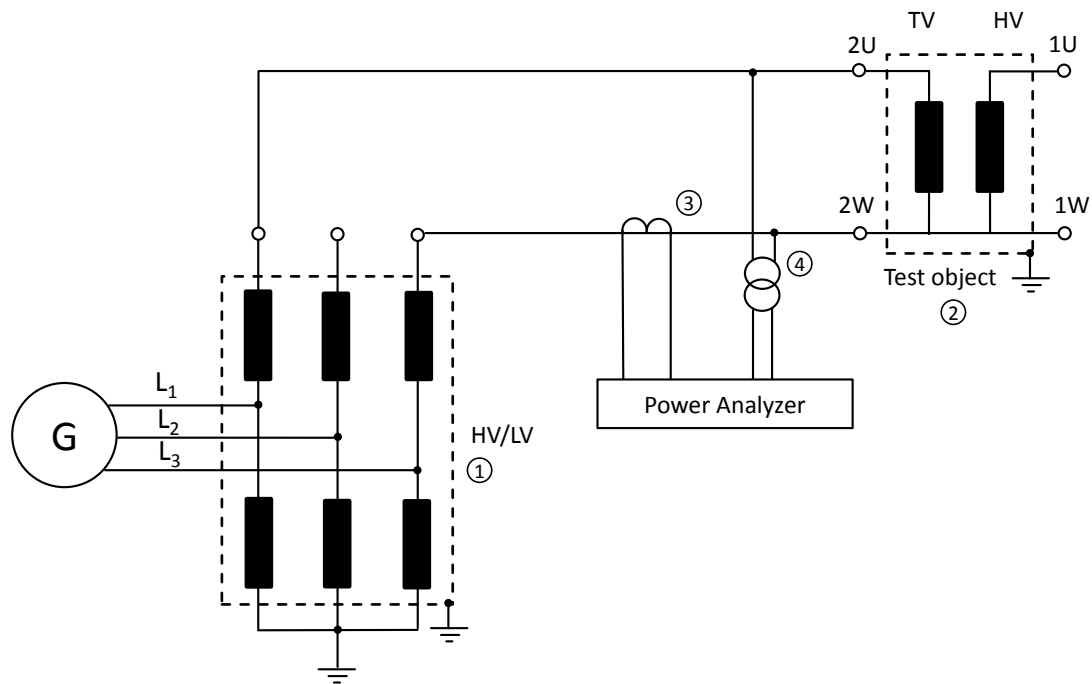
Figure 12.5: Electric circuit for energizing the PTs in no-load condition; 1: step-up transformer, 2: test object, 3: current transducer and 4: voltage divider.

Table 12.2 shows the relative deviations F_R

$$F_R = \left(\frac{P_{s,A}}{P_{s,B}} - 1\right) \cdot 100\% \tag{12.2}$$

between the specific losses of material A ($P_{s,A}$) and B ($P_{s,B}$) determined with the CMS and the PTs' no-load losses. For this evaluation, steel coils of material A, deployed in PT unit 1 and 2, were averaged as well as the no-load losses of PT unit 1 and 2. Similar to material A, the same procedure was applied for material B and the no-load losses of PT unit 3 and 4. As per Table 12.2, the deviation within the specific losses of materials A and B coincide with the deviation of the no-load losses of the PT units.

The good correspondence between the measured steel coils' specific losses and the PTs' no-load losses does not match the steel coils' certificate values. The mean certificated specific losses of material A was calculated to be 0.725 W/kg and of all material B 0.745 W/kg (Table 12.3). In contrast to the shown deviations in Table 12.2, a relative deviation of -2.8 % was calculated between the mass weighted certificate values linked to a flux density of 1.7 T. The inverse tendency and the higher deviation
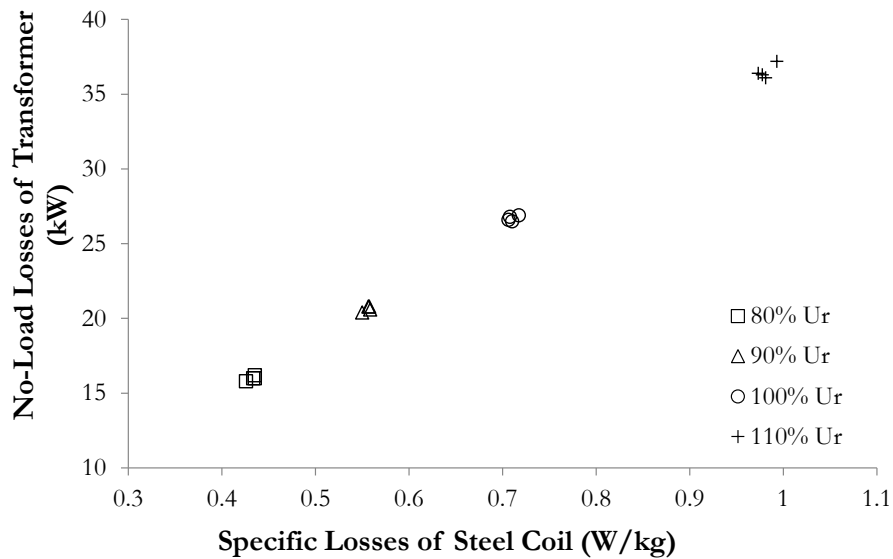
Figure 12.6: Correlation of measured no-load losses of PT units and the mass weighted specific losses of the deployed steel coils; U_r = rated voltage.

Table 12.2: Relative deviations of the specific losses of materials A and B and the PTs' no-load losses.

	80 % U_r	90 % U_r	100 % U_r	100 % U_r
	1.310 T	1.473	1.637 T	1.800 T
GOES coil's specific losses	-1.3 %	-0.7 %	0.4 %	0.4 %
No-load losses of PTs	-1.2 %	-0.5 %	0.4 %	1.7 %

between materials A and B of the certificate values, compared to the steel coils' specific losses, would have led to a wrong prediction of the PT no-load losses.

Table 12.3: Mass weighted certificate loss values of materials A and B.

	Material A	Material B
	1.7 T, 50 Hz	1.7 T, 50 Hz
Certificate losses	0.725 W/kg	0.745 W/kg

12.3 Results of Experimental No-Load Loss Studies

The two experimental studies with MTs and PTs, where the relation between the steel coils' specific losses and the no-load losses were investigated, resulted in the following:

- The steel coils' specific losses showed the highest correlation with the no-load losses of MTs and PTs, compared to the steel coils' certificate values and extracted single sheet values.

- Low measured specific losses of steel coils also resulted in low no-load losses in the MTs, and vice versa. The steel coils' specific losses predicted the MT with the highest and the lowest no-load losses correctly, rather than the certificate values or the single sheet values.

- The certificate values are not consistent with the transformers' no-load losses or the steel coils' specific losses. Hence, the steel coils' certificate values don't indicate the no-load losses of transformers correctly.

Chapter 13

Conclusions

13.1 General

The size of a PT core determines the overall costs of the entire PT. Consequently, the objective is to design and build compact transformer cores due to customer specifications and transport limitations. Such designs usually require a high core flux density, which causes higher no-load noise and no-load losses. However, customer specifications require low noise and low losses. Manufacturers have to meet customers' specifications of these values to avoid contractual penalties or even a rejection of manufactured transformers. Consequently, the no-load noise and no-load losses can be only reduced by the selected use of the GOES material. This requires a better knowledge of the GOES materials' magnetostriction and specific losses. Usually, only the certificate values, such as the specific losses at 1.7 T at 50 Hz and the noise relevant B8 value, are known. No additional information is provided by the core steel manufacturers. Therefore, transformer manufacturers have to rely on test laboratory measurements performed on formerly built transformers. Each core steel supplier has different manufacturing processes, and hence delivers different steel grades with individual magnetostrictive and magnetic properties. It is common that single sheet or Epstein frame measurements are randomly applied on selected steel coils to verify the specific losses of a delivered steel coil. Such extracted small sample sizes compared to a PT core with a core mass of up to 120 tons seems therefore not to be suitable to provide sufficient information on the PTs' no-load losses. In addition, the B8 value does not provide sufficient information about the noise performance at different flux densities. This demands a consistent inspection of each delivered steel coil to determine the magnetic and magnetostrictive properties.

13.2 Coil Measurement System

A coil measurement system for entire steel coils with a weight of up to 6,000 kg, was built to determine the specific losses and the magnetostriction. The measurement sequence from 1.0 T to 1.9 T at 50 Hz and 60 Hz covers the complete range of possible nominal flux densities and supply frequencies of PTs. Fast determination of a test specimen's mass, inner and outer diameters, and easy mounting of the windings are important to ensure a rapid incoming goods inspection, the measurement sequence defined above is being achieved within 15 minutes. The measurement of the magnetostriction with piezoelectric acceleration transducers in axial direction placed on the laminated narrow side of a steel coil was introduced. The measurement results of the proposed approach delivers similar results when compared to conventional methods, although the magnetostriction is measured perpendicular to the rolling direction.

The reproducibility and possibility of classifying steel coils by the specific losses and magnetostriction has been investigated. The main conclusions can be summarized as follows:

- Each steel coil independent of its steel grade is investigated using a uniform and consistent approach.

- In addition to the determination of the specific losses, the approach also includes the measurement of the magnetostriction perpendicular to the rolling direction.

- Reproducibility studies resulted in relative standard deviations of below 1 % for the specific losses and below 3 % for the magnetostriction strain.

- The measured steel coils can be classified within their steel grade according to the determined specific losses and magnetostrictive properties at certain flux densities which provides the possibility of a selective use in PT cores.

- A significant possibility, offered by the newly proposed system for the analysis of steel coils, is the identification of potential low noise material before the core material is deployed in PT cores.

13.3 Magnetostriction Versus No-Load Noise

The noise of PTs has recently become an increasingly important factor in the design process. Special attention has been paid to the noise emission of PTs in no-load condition, as this noise source is present also during low load conditions. Magnetostriction is designated as main source of a PT's no-load noise. Within this work the measured magnetostrictive properties of steel coils with a mass of up to 6,000 kg and the measured no-load noise of PTs have been investigated.

13.3.1 Analysis of Steel Coils' Magnetostriction

Initially, the measured magnetostrictive properties, the magnetostriction strain and the vibration velocity of two selected steel coils were investigated with a focus on their performance and trend at different flux densities. The analysis resulted with the following:

- Compared to a common low noise GOES material, a new material B was identified with even lower magnetostriction values.

- With respect to the trend of the magnetostrictive properties, the vibration velocity reveals a higher rise with increasing flux density, whereas the magnetostriction strain increase is nearly constant.

- With regard to the noise rise of PTs with increasing core flux density, the vibration velocity has a similar characteristic and hence, better physical relation to the emitted sound of PTs, which was also found in a previous publication [4].

13.3.2 Studies on MTs and PTs

Based on the magnetostrictive performance of the single steel coils, four MTs were built out of two analyzed steel coils, in order to determine a relationship to the no-load noise of the MTs. In addition, a second study was carried out with four large PTs, in which several steel coils were used to build a PT core. Within this study, steel coils were selected and ordered by the measured magnetostrictive vibration velocity. GOES material with higher vibration velocity, referred to as material A, was deployed in PT units 1 and 2, whereas the GOES material with lower vibration velocity, referred to as material B, was used to build the PT units 3 and 4. The main results of both studies can be summarized as follows:

- A strong correlation between the A-weighted magnetostrictive vibration velocities and the no-load noise of the MTs and PTs was determined.

- GOES material identified with less A-weighted magnetostrictive vibration velocity also resulted in a lower no-load noise within the transformers.

- The performance differences of the measured A-weighted magnetostrictive vibration velocities of the deployed steel coils are consistent within the no-load noise of the MTs and PTs.

- It was recognized that material B has optimized magnetostrictive properties around $1.5\,\mathrm{T}$ which caused lower no-load noise of the PTs at the same flux density.

- The B8 value cannot be used as a noise indicator in a comprehensive way for different GOES materials of the same steel grade.

Although the investigations were limited to a set of eight MTs and four PTs, the observed relationships between the magnetostrictive properties of GOES material and the no-load noise of PTs are significant. The achievements reveal a strong correlation between the measured magnetostrictive properties of steel coils and the PTs' no-load noise.

13.4 Specific Losses of Steel Coils Versus No-Load Losses

The steel coils' specific losses and their correlation to the no-load losses of transformers was examined within two experimental studies. The specific losses determined with a single sheet tester were generally lower than the no-load losses of the transformers. The higher losses can be mainly attributed to the PT joints. Similarly, the steel coils' specific losses are higher than those of single sheet values. The higher losses may be attributed to the bending of the coiled material as described in [63], which was not investigated within this work. The main objective was to investigate the relationship between the steel coils' specific losses and the no-load losses of PTs. The material is rejected if the measured steel coils' specific losses exceed the certificate value. A rejection of the material has to be based on measurements using standardized methods such as the single sheet tester. Therefore, the steel coils'

specific losses determined with the CMS were scaled to a statistical set of single sheet measurements. This enables a comparison to the steel coils' certificate value.

13.4.1 Study on MTs an PTs

The first study was performed on eight MTs. For seven MT cores only the middle sections of different steel coils were used. One MT core was built with the side sections of a steel coil. The study resulted in the following:

- The determined specific losses of the entire steel coils provide the highest correlation with the MTs' no-load losses, compared to single sheet tests of extracted samples and the certificate values of the steel coils.

- The MTs with the highest and lowest no-load losses were best described with the steel coils' specific losses rather than with the single sheet tests or certificate values. The no-load losses of the MTs can be predicted best by the steel coils' specific losses.

- The MT manufactured with the side section of a steel coil performed differently to the other seven units. First of all, only the entire steel coil was measured within the CMS rather than the different sections of the steel coil. The difference may be attributed to a thinner rolled steel due to inhomogeneous pressure distributions within the cold rolling processes.

Within a second study the no-load losses of four PTs with a core mass of 40,000 kg were investigated. In this study the specific losses of steel coils and the certificate values were compared to the no-load losses. The determined specific losses of the steel coils used for each PT were revealed to be similar whereas the certificates showed differing values. The study shows whether the no-load losses of the transformers correspond to the certificate values or the measured steel coils' specific losses. The results are the following:

- All four PTs showed similar no-load losses. This was expected as the determined steel coils' specific losses showed less deviation among each other.

- The mass weighted certificate values of the steel coils showed no correlation with the PTs' no-load losses as a contrary behaviour was determined.

- The specific loss values of the deployed steel coils in each PT were shown to have a better relationship to the no-load losses than the certificate values, when it comes to large PTs.

13.5 Implementation and Application

The measured specific losses and magnetostriction of each steel coil determined with the CMS show a relationship to the no-load losses and no-load noise of PTs. The designs of PTs can be improved by using these experimentally determined values. As a first approach, the classification of steel coils can be used. By classifying each steel coil the material can be used more selectively within PTs, within certain requirements. The classification approach could be applied as follows:

- Based on the measured magnetostrictive performance, each steel coil is assigned to a different noise performance class. For example, steel coils with low magnetostriction are related to class A that correspond to a 'low noise' performance. Steel coils with a average magnetostriction performance are related to class B that corresponds to 'standard noise'.

- Depending on the required no-load noise target of a PT's specification, either steel coils of class A or B are used to build the transformer core. This allows the realization of noise critical PTs with 'low noise' GOES material.

- As more experience is obtained, it might be possible, to jointly use steel coils of different classes, to reach certain noise targets.

- A similar classification approach could be implemented for the measured specific losses of steel coils.

Nomenclature

Abbreviations and Units

CGO   ...   Conventional grain-oriented
CMS   ...   Coil measurement system
dB   ...   Decibel
dBA   ...   A-weighted decibel
dyn   ...   dynamic
EFC   ...   Electronic frequency converter
FF   ...   Iron fill factor (stacking factor)
GOES...   Grain-oriented electrical steel
HiB   ...   High permeability
IEC   ...   International Electrotechnical Commission
IEEE   ...   Institute of Electrical and Electronics Engineers
MT   ...   Model transformer
PT   ...   Power transformer
RMS   ...   Root mean square
Si   ...   Silicon
SNR   ...   Signal-to-noise ratio
SPL   ...   Sound power level
SST   ...   Single sheet tester
stat   ...   static
THD   ...   Total harmonic distortion

Symbols

a	...	Acceleration
$A(f)$	...	A-weighting
A_{fe}	...	Effective iron cross-section
A_{stat}	...	Area of the hysteresis loop for the static case
b	...	Width of a steel coil
B	...	Magnetic flux density
$B8$	...	Flux density at magnetic field 800 A/m, 50 Hz
$B800$	...	Flux density at magnetic field 800 A/m, 50 Hz
BF	...	Building factor
c_{h}	...	Scaling factor for hysteresis losses
c_{w}	...	Scaling factor for eddy current losses
c	...	Speed of sound in a elastic medium
d	...	Thickness of steel sheet
D_{i}	...	Inner diameter
D_{a}	...	Outer diameter
E	...	Young's modulus
f	...	Frequency
F	...	Force
F_{R}	...	Relative deviation
h	...	Harmonic
H	...	Magnetic field strength
L	...	Initial length of the specimen
ΔL	...	Change of specimens length
L_{P}	...	Sound pressure level
L_{I}	...	Sound intensity level
L_{W}	...	Sound power level
m	...	Mass
m_{N}	...	Mass of N steel coils
m_{i}	...	Mass of steel coils i
N	...	Number of windings
p	...	Sound pressure
P_{fe}	...	Iron losses
P_{h}	...	Hysteresis losses

P_w	...	Eddy current losses
P_s	...	Specific iron losses
$P_\mathrm{s,c}$	...	Calculated losses by the error affected voltage
P_m	...	Measured active power
R	...	Resistance
s	...	Standard deviation
s^2	...	Experimental variance
s_pp	...	Peak-to-peak displacement
$s(t)$	...	Displacement over time
S	...	Measurement surface
T	...	Time period
u	...	Particle velocity
v	...	Vibration velocity
v_pp	...	Peak-to-peak vibration velocity
v_ppA	...	A-weighted peak-to-peak vibration velocity
w_fe	...	Dissipated energy density per magnetization cycle and per volume unit
W	...	Sound power
$\bar{x}$	...	Average value
x_i	...	Sample

ϵ	...	Tensile strain
λ	...	Magnetostriction strain
λ_pp	...	Peak to peak magnetostriction strain
ρ_0	...	Density in air
ρ_fe	...	Material density of iron
ρ_R	...	Specific resistance
σ	...	Tensile stress
σ_R	...	Specific conductivity of the material

Bibliography

[1] "Electrical steel - Methods of measurements of the magnetostriction characteristics by means of single sheet and Epstein test specimens," IEC TR 62581 Edition 1.0, August 2010.

[2] M. Hirano, Y. Ishihara, K. Harada, and T. Todaka, "A study on measurement of magnetostriction of silicon steel sheet by laser displacement meter," *Journal of Magnetism and Magnetic Materials*, vol. 254 - 255, pp. 43 – 46, 2003.

[3] H. Mogi, M. Yabumoto, M. Mizokami, and Y. Okazaki, "Harmonic analysis of AC magnetostriction measurements under non-sinusoidal excitation," *IEEE Transactions on Magnetics*, vol. 32, no. 5, pp. 4911–4913, 1996.

[4] E. Reiplinger, "Assessment of grain-oriented transformer sheets with respect to transformer noise," *Journal of Magnetism and Magnetic Materials*, vol. 21, no. 3, pp. 257 – 261, 1980.

[5] B. Weiser, H. Pfuetzner, and J. Anger, "Relevance of magnetostriction and forces for the generation of audible noise of transformer cores," *IEEE Transactions on Magnetics*, vol. 36, no. 5, pp. 3759–3777, 2000.

[6] L. Goines and L. Hagler, "Noise Pollution: A Modern Plague," *Southern Medical Journal*, vol. 100, no. 3, 2007.

[7] Europaeisches Parlament und der Rat der europaeischen Union, "Richtlinie 2002/49/EG Des Europaeischen Parlaments und des Rates vom 25. Juni 2002 ueber die Bewertung und Bekaempfung von Umgebungslaerm," 2002.

[8] *Magnetic materials - Part 2: Methods of measurement of the magnetic properties of electrical steel strip and sheet by means of an Epstein frame*. IEC 60404-2, 2008.

[9] *Magnetic materials - Part 3: Methods of measurement of the magnetic properties of electrical steel strip and sheet by means of a single sheet tester*. IEC 60404-3, 2010.

[10] *Kerne aus weichmagnetischen Materialien - Messverfahren - Eigenschaften im Leistungsapplikationsbereich.* DIN EN 62044-3, 2001.

[11] *Magnetische Werkstoffe - Teil 4: Verfahren zur Messung der magnetischen Eigenschaften von weichmagnetischen Werkstoffen im Gleichfeld.* DIN EN 60404-4, 2009.

[12] E. Dogan and B. Kekezoglu, "Power Transformer Noise, Noise Tests, and Example Test Results," *International Journal of Electrical, Computer, Energetic, Electronic and Communication Engineering*, vol. 10, no. 1, pp. 57 – 61, 2016.

[13] T. Tanzer, H. Pregartner, A. Muetze, and K. Krischan, "Experimental determination of specific power losses and magnetostriction strain of grain-oriented electrical steel coils," *IEEE Transactions on Industry Applications*, vol. 54, no. 2, pp. 1235–1244, 2018.

[14] Siemens Transformers Austria GmbH & Co KG, H. Pregartner, "WO 2011/012159 A1 - Method for classifying electrical sheet," Februar 2011.

[15] T. Tanzer, H. Pregartner, R. Labinsky, M. Witlatschil, A. Muetze, and K. Krischan, "Magnetostriction and its relation to the no-load noise of power transformers," in *IEEE International Electric Machines and Drives Conference (IEMDC)*, pp. 1–6, 2017.

[16] T. Tanzer, H. Pregartner, M. Riedenbauer, R. Labinsky, M. Witlatschil, A. Muetze, and K. Krischan, "Magnetic properties and their relation to the no-load noise and no-load losses of large power transformers," in *IEEE International Electric Machines and Drives Conference (IEMDC)*, pp. 1–6, 2017.

[17] M. R. GmbH, *Transformer 2020 - Design study into the transformer of the future.* Maschinenfabrik Reinhausen GmbH, 2016.

[18] K. Karsai, D. Kerényi, and L. Kiss, *Large Power Transformers.* Studies in electrical and electronic engineering, Elsevier, 1987.

[19] M. Heathcote, *J & P Transformer Book.* Elsevier Science, 2011.

[20] S. Tumanski, *Handbook of Magnetic Measurements.* CRC Press, 2011.

[21] C. Heck, *Magnetische Werkstoffe und ihre technische Anwendung.* Huethig, 1967.

[22] N. Engineers, *The Complete Technology Book on Steel and Steel Products (Fasteners, Seamless Tubes, Casting, Rolling of Flat Products & others)*. NIIR Project Consultancy Services, 2008.

[23] A. J. Moses, "Electrical steels: past, present and future developments," *IEE Proceedings A - Physical Science, Measurement and Instrumentation, Management and Education*, vol. 137, no. 5, pp. 233–245, 1990.

[24] A. J. Moses, S. M. Pegler, and J. E. Thompson, "Role of phosphate coating in determining the magnetic properties of goss-oriented silicon iron," *Proceedings of the Institution of Electrical Engineers*, vol. 119, no. 8, pp. 1222–1228, 1972.

[25] V. Goel, *Novel Coating Technologies for Electrical Steel*. PhD thesis, Cardiff University, 2016.

[26] *Magnetic materials - Part 8-7: Specifications for individual materials - Cold-rolled grain-oriented electrical steel strip and sheet delivered in the fully-processed state*. IEC 60404-7-8, 2008.

[27] R. Boll, *Weichmagnetische Werkstoffe*. Vakuumschmelze GmbH, Siemens Aktiengesellschaft, Berlin und München, 1990.

[28] ThyssenKrupp VDM, "Weichmagnetische Werkstoffe auf Ni-Fe-Basis," VDM Report 27, ThyssenKrupp VDM GmbH, 2003.

[29] Z. Neuschl, *Rechnerunterstuetzte experimentelle Verfahren zur Bestimmung der lastunabhaengigen Eisenverluste in permanentmagnetisch erregten elektrischen Maschinen mit Axialfluss*. PhD thesis, Technische Universitaet Cottbus, 2007.

[30] K. Kupfmueller, *Einfuehrung in die theoretische Elektrotechnik*. Springer Berlin Heidelberg, 1965.

[31] M. Yabumoto, S. Arai, a. M. M. R. Kawamata, and T. Kubota, "Recent development in grain-oriented electrical steel with low magnetostriction," *Journal of materials engineering and performance*, vol. 6, no. 6, pp. 713 – 721, 1997.

[32] N. Ekreem, A. Olabi, T. Prescott, A. Rafferty, and M. Hashmi, "An overview of magnetostriction, its use and methods to measure these properties," *Journal of Materials Processing Technology*, vol. 191, no. 13, pp. 96 – 101, 2007.

[33] M. Javorski, J. Slavic, and M. Boltezar, "Frequency characteristics of magnetostriction in electrical steel related to the structural vibrations," *IEEE Transactions on Magnetics*, vol. 48, no. 12, pp. 4727–4734, 2012.

[34] P. W. Neurath, "Magnetostriction and domain structure of materials for use in low-noise equipment," *Electrical Engineering*, vol. 73, no. 11, pp. 991–994, 1954.

[35] C. M. Brownsey and G. C. Maples, "Magnetostriction characteristics of 3.1 % grain-oriented silicon-iron transformer steel," *Proceedings of the Institution of Electrical Engineers*, vol. 113, no. 11, pp. 1859–1862, 1966.

[36] Goldman, J.E., "New techniques and results in the measurement of magnetostriction," *J. Phys. Radium*, vol. 12, no. 3, pp. 471–475, 1951.

[37] H. Takaki and T. Tsuji, "The measurement of magnetostriction by means of strain gauge," *Journal of the Physical Society of Japan*, vol. 11, no. 11, pp. 1153–1157, 1956.

[38] P. Klimczyk, *Novel Techniques for Characterisation and Control of Magnetostriction in G.O.S.S.* PhD thesis, Wolfson Centre for Magnetics, Cardiff School of Engineering, Cardiff University, 2012.

[39] D. J. Mapps and C. E. White, "Magnetostriction harmonics measurement using a double piezoelectric transducer technique," *Journal of Physics E: Scientific Instruments*, vol. 17, no. 6, pp. 472–479, 1984.

[40] T. Nakata, N. Takahashi, M. Nakano, K. Muramatsu, and P. Miyake, "Magnetostriction measurements with a laser doppler velocimeter," *IEEE Transactions on Magnetics*, vol. 30, no. 6, pp. 4563–4565, 1994.

[41] J. Harlow, *Electric Power Transformer Engineering*. The Electric Power Engineering Hbk, CRC Press, 2004.

[42] S. Kulkarni and S. Khaparde, *Transformer Engineering: Design and Practice*. Power engineering, CRC Press, 2004.

[43] M. Heckl and G. Mueller, *Taschenbuch der technischen Akustik*. Springer Berlin Heidelberg, 2013.

[44] *Power transformers - Part 10: Determination of sound levels - Application Guide*. IEC 60076-10, 2016.

[45] I.L. Ver, L.L. Beranek, ed., *Noise and Vibration Control Engineering - Principles and Application*. John Wiley & Sons, Inc., 2006.

[46] M. Moeser, *Technische Akustik*. VDI-Buch, Springer Berlin Heidelberg, 2012.

[47] W. Schirmer, *Technischer Laermschutz*. Springer, 2005.

[48] *Power transformers - Part 10: Determination of sound levels*. IEC 60076-10, 2016.

[49] *Standard Test Code for Liquid-Immersed Distribution, Power, and Regulating Transformers*. IEEE C.57.12.90, 2015.

[50] Bruel & Kjaer, "Sound intensity," September 1993. https://www.bksv.com/media/doc/br0476.pdf.

[51] R. Vecchio, B. Poulin, M. Feeney, P. Feghali, D. Shah, R. Ahuja, and D. Shah, *Transformer Design Principles: With Applications to Core-Form Power Transformers*. CRC Press, 2001.

[52] D. Kraaij, G. Schemel, and F. Wegscheider, *Die Pruefung von Leistungs-Transformatoren*. Buchverlag Elektrotechnik, 1983.

[53] Y. Zhang, Q. Li, D. Zhang, B. Bai, D. Xie, and C. S. Koh, "Magnetostriction of Silicon Steel Sheets Under Different Magnetization Conditions," *IEEE Transactions on Magnetics*, vol. 52, no. 3, pp. 1–4, 2016.

[54] M. Y. S. Arai, M. Mizokami, "Magnetostriction of grain oriented Si-Fe and its domain model," *PRZEGLAD ELEKTROTECHNICZNY Electrical Review R.87 No. 9b*, pp. 20–23, 2011.

[55] G. Shilyashki, H. Pfuetzner, J. Anger, K. Gramm, F. Hofbauer, V. Galabov, and E. Mulasalihovic, "Magnetostriction of Transformer Core Steel Considering Rotational Magnetization," *IEEE Transactions on Magnetics*, vol. 50, no. 1, pp. 1–15, 2014.

[56] T. Tanzer, H. Pregartner, A. Muetze, and K. Krischan, "Experimental determination of specific power losses and magnetostriction strain of grain-oriented electrical steel coils," in *IEEE International Conference on Electric Machines (ICEM)*, pp. 2230–2236, 2016.

[57] D. Zorbas, *Electric Machines: Principles, Applications, and Control Schematics*. Cengage Learning, 2014.

[58] U. Bakshi and M. Bakshi, *Electrical Machines I*. Technical Publications, 2010.

[59] M. Bali and A. Muetze, "Influences of CO2 Laser, FKL laser and mechanical cutting on the magnetic properties of electrical steel stheets," *IEEE Transactions on Industry Applications*, vol. 51, no. 6, pp. 4446–4454, 2015.

[60] S. Ghalamestani, L. Vandevelde, J. Dirckx, and J. Melkebeek, "Magnetostriction and the Influence of Higher Harmonics in the Magnetic Field," *IEEE Transactions on Magnetics*, vol. 48, no. 11, pp. 3981–3984, 2012.

[61] Haefely Hipotronics, *4761/4764 Current Comparators*, v05.18 ed. https://hubbellcdn.com/specsheet/HAEFELY_LL_4761-4764_SPEC.pdf.

[62] T. Kuttner, *Praxiswissen Schwingungsmesstechnik*. Springer Fachmedien Wiesbaden, 2015.

[63] H. Hagihara, Y. Takahashi, K. Fujiwara, Y. Ishihara, and T. Masuda, "Magnetic properties evaluation of grain-oriented electrical steel sheets under bending stress," *IEEE Transactions on Magnetics*, vol. 50, no. 4, pp. 1–4, 2014.

[64] A. Moses, "Effects of applied stress on the magnetic properties of high permeability silicon-iron," *IEEE Transactions on Magnetics*, vol. 15, no. 6, pp. 1575–1579, 1979.

[65] R. Perryman, "Effects of tensile and compressive stress on 3% grain-oriented silicon iron," *Journal of Physics D: Applied Physics*, vol. 8, no. 15, pp. 1901–1909, 1975.

[66] Joint Committee for Guides in Metrology / Working Group 1, "Evaluation of measurement data - Guide to the expression of uncertainty in measurement," September 2008.

[67] T. Tanzer, H. Pregartner, M. Riedenbauer, R. Labinsky, M. Witlatschil, A. Muetze, and K. Krischan, "Magnetostriction of electrical steel and its relation to the no-load noise of power transformers," *IEEE Transactions on Industry Applications*, 2018. Accepted for publication.

[68] F. Fahy, *Sound and Structural Vibration: Radiation, Transmission and Response.* Elsevier Science, 2012.

[69] A. Moses, "Measurement of magnetostriction and vibration with regard to transformer noise," *IEEE Transactions on Magnetics*, vol. 10, no. 2, pp. 154–156, 1974.

[70] *Electroacoustics - Sound level meters - Part 1: Specifications.* IEC 61672-1, 2013.

[71] H. Wu, Z. Pang, G. Yao, Y. Zhang, and Z. Liu, "Research into edge drop of cold rolled strip and its influencing factors," in *Second International Conference on Computer Modeling and Simulation*, vol. 1, pp. 151–154. 2010.